8-9-2014

# INSIGHTS INTO THE EVOLUTIONAL ADAPTATIONS AND FUNCTIONAL SWITCHING MECHANISM IN DUAL FUNCTION HEMOGLOBIN/ DEHALOPEROXIDASE (DHP) AND MODELING OF CYTOCHROME P450 ACTIVE SITE WITH H93G MYOGLOBIN CAVITY MUTANT

Shengfang Sun
*University of South Carolina - Columbia*

# INSIGHTS INTO THE EVOLUTIONAL ADAPTATIONS AND FUNCTIONAL SWITCHING MECHANISM IN DUAL FUNCTION HEMOGLOBIN/DEHALOPEROXIDASE (DHP)

AND

# MODELING OF CYTOCHROME P450 ACTIVE SITE WITH H93G MYOGLOBIN CAVITY MUTANT

by

Shengfang Sun

Bachelor of Bioengineering
Southwest Jiao-tong University, 2009

---

Submitted in Partial Fulfillment of the Requirements

For the Degree of Doctor of Philosophy in

Chemistry

College of Arts and Sciences

University of South Carolina

2014

Accepted by:

John H. Dawson, Major Professor

Lukasz Lebioda, Committee Member

F. Wayne Outten, Committee Member

Rekha C. Patel, Committee Member

Lacy Ford, Vice Provost and Dean of Graduate Studies

## DEDICATION

This dissertation is dedicated to my dear family.

## ACKNOWLEDGEMENTS

Five-year PhD study away from my family in China can be tough sometimes. But thanks to the people I met here in Columbia I've had a great time. So at the end my PhD study, I would like thank all of them and I can only hope that I do not leave anyone out. First of all, I thank my advisor Professor John H. Dawson, for taking me into the group and supporting my research. I'm grateful for his great efforts on encouraging the previous unconfident me. At that time I was even not sure how I could make to the end. But right now I am finishing up a two-hundred-pages dissertation, with much more confidence in myself. All these amazing transformations in myself are inspired by him. So thank you, Dr. Dawson. I also thank all my committee members, Dr. Lukasz Lebioda, Dr. Wayne Outten, Dr. Qian Wang and Dr. Rekha Patel, for their time and helpful advice on my research.

I've received a great deal of help from my lab members. Dr. Masanori Sono, who is involved in all my research projects, taught me how to conduct good research. He is one of the most intelligent people I've ever met, yet he is so humble and always willing to help. I thank my current lab mate, Anuja Modi, for taking the five-year journey along with me. I admire her amazing personality and wish I had her ability to cheer up other people. I also appreciate the support provided by our previous lab members Dr. Jing Du, Dr. Indika Bandara and Dr. Dan Collins.

In particular, I want to convey my gratitude to my collaborator Dr. Lukas Lebioda and Dr. Chunxue Wang. Most of my work would have been impossible without of their assistance and contribution. I have been also fortunate to work on several interesting projects with collaborators outside the department, Dr. Daping Fan, Dr. Rajagopalan Bhaskaran and Dr. Angela Wilks and I want to thank them for getting me involved.

I would like to say thank you to my boyfriend Guangzhi for understanding me and loving me as I am. Thanks to all my friends for trusting me and celebrating the wonderful life with me.

Last and foremost is my dear family. Mom and Dad, thanks for bringing me and Sunkey to this beautiful world and teaching us many great virtues that we could benefit for life. I feel so blessed to have Sunkey as my twin sister that with her I never felt lonely for a minute.

Columbia SC

June 1 2014

## ABSTRACT

The coelomic hemoglobin, dehaloperoxidase (DHP), from the sea worm *Amphitrite ornata,* is a dual function oxygen-binding heme protein that also possesses a significant peroxidase activity. As evolved from an ancient oxygen carrier globin, several structural adaptations have enabled DHP to evolutionally gain significantly enhanced peroxidase capability for self-protection while only minimally compromising its primary function as an $O_2$ carrier. To elucidate these adaptations, the peroxidase activities and $O_2$ affinities of several DHP and sperm whale myoglobin (Mb) mutants have been prepared. Several heme environmental structural factors that regulate the dual functions of DHP have been found, providing insight into how DHP has gained significantly enhanced enzymatic capability in an evolutional process for protection from its toxic living environment without compromising its primary function as an $O_2$ carrier. As to the question how DHP interconverts the different oxidation states of heme required for its hemoglobin ($Fe^{II}$) and peroxidase ($Fe^{III}$) functions, a functional switching mechanism of DHP has been proposed and carefully tested. Using stopped-flow methodology, the $H_2O_2$-mediated conversion of oxy-Fe(II) DHP to the ferric state triggered by both biologically relevant (TCP etc.) and non-relevant (ferrocyanide, etc.) compounds was examined. It has been found that ferric heme ligands and spin-trapping reagents can completely inhibit the TCP-triggered DHP functional switch, strongly supporting a proposed mechanism involving substrate radicals (TCP·).

To thoroughly study the structures and the functions of the diverse heme enzymes, numerous heme iron model systems have been developed. Using the H93G Mb cavity mutant, pioneered by Barrick, our laboratory has successfully prepared several model heme complexes of defined structure. However, previous attempts to generate H93G adducts with spectral properties resembling those of ferrous thiolate-ligated heme proteins such as cytochrome P450 (P450) and *C. fumago* chloroperoxidase (CPO), were not successful. In the second part of the dissertation, the first H93G Mb spectral models for ferrous P450 and CPO have been generated with phosphine as the axial ligand. The novel heme-phosphine complexes have been comprehensively characterized in their ferric, ferrous and ferryl states with UV-visible absorption and MCD spectroscopy. The data provide important insight into the unique spectral properties of thiolate-ligated heme iron systems and further expand our extensive H93G Mb spectral model library.

# TABLE OF CONTENTS

## LIST OF TABLES

## List of Figures

## List of Abbreviations

4-BP ..... 4-bromophenol

Abs ..... absorbance

CCP ..... chloroperoxidase

CCPO ..... C. Fumago chloroperoxidase

CooA ..... CO oxidation activator

Cpd I ..... Compound I

Cpd II ..... Compound II

Cpd ES ..... Compound ES

Cpd RH ..... Compound RH

DHP ..... dehaloperoxidase

DMPO ..... 5,5-dimethyl-1-pyrroline-N-oxide

DXQ ..... dihalobenzoquinone

Hb ..... dehaloperoxidase

HRP ..... horseradish peroxidase

Im ..... dehaloperoxidase

IPIC ..... isopropyl isocyanide

$k_{cat}$ ..... turnover number

$K_d$ ..... dissociation constants

$K_{O2}$ ..... $O_2$ equilibrium constants

Mb ..... myoglobin

MCD .....magnetic circular dichroism

MPO ..... myeloperoxidase

Oxy-DHP .....oxyferrous state

P450 ..... cytochrome P450

PDB.....protein data bank

SW..... sperm whale

TBIC .....*t*-butyl isocyanide

TBP ..... 2,4,6-tribromophenol

TCP .....2,4,6-trichlorophenol

THMP .....tris(hydroxymethyl)phosphine

UV-Vis.....UV-visible

PART I

CHAPTER 1

# Introduction to Part I:

# *Amphitrite ornata* dehaloperoxidase (DHP): a dual function hemoglobin/peroxidase

## Heme Proteins

About one quarter to one third of all proteins require metals to carry out their functions [1]. Such proteins are generally termed as "metalloproteins". Among them, the heme-containing proteins are an important class that carries out a diverse range of biological functions. One old and universal function of heme protein is the storage and transport of oxygen molecule carried out by hemoglobin (Hb)/myoglobin (Mb), the blood pigment. Some heme proteins are enzymes that catalyze the biological redox reactions such as cytochromes P450s. Other heme proteins play essential roles in electron transfer (e.g. cytochrome $b_5$ and c) and signal transduction (e.g. CooA).

Most native heme proteins contain an iron-protoporphyrin IX group (heme *b*) with the iron atom coordinated in the center by four pyrrole nitrogens and two vacant coordination positions available for additional ligands (Figure 1.1). In heme proteins, the heme prosthetic group is tethered to the protein backbone via a proximal amino acid ligand that covalently binds to the heme iron. The functions of heme proteins depend largely on the properties of the heme active site which is strongly influenced by three factors: the iron oxidation and spin states, the nature of axial ligands coordinated to the iron and the surrounding protein environment which affects the binding of the substrates.

## Peroxidases

The heme enzymes that catalyze oxidation of organic substrates can be generally dividend into two classes: oxygenases and peroxidases. The former uses $O_2$ to oxidize substrates (Eq. 1.1, showing reaction catalyzed by monooxygenase) and the latter uses $H_2O_2$ (Eq. 1.2).

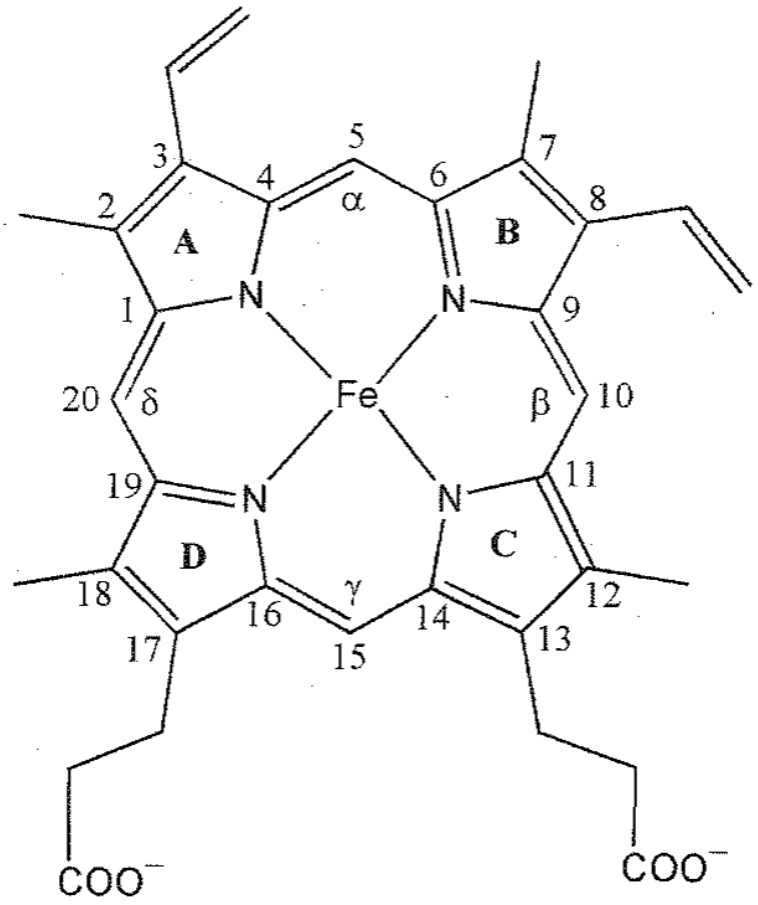


**Figure 1.1.** The structure of protoheme IX (iron protoporphyrin IX, heme b). The Greek letters α to δ identify the sites of four each methane bridges and the Roman letters A to D indicate the location of four pyrrole rings. An IUPAC numbering system is used here and thus the carbons at 2, 3, 7, 8, 12, 13, 17 and 18 positions correspond to those at 1, 2, 3, 4, 5, 6, 7 and 8 positions in the classic Fischer numbering system.

$$AH + O_2 + 2H^+ + 2e^- \rightarrow AOH + H_2O \quad (1.1)$$

$$AH_2 + H_2O_2 \rightarrow A + 2H_2O \quad (1.2)$$

Figure 1.2 elucidates the mechanism of action for peroxidases in comparison with oxygenases. For peroxidases like horseradish peroxidase (HRP), the addition of $H_2O_2$ to the ferric heme yields an unstable hydroperoxide adduct (commonly known as compound 0). Followed by heterolysis of the O-O bond, a high-valent oxidant intermediate called compound I (Cpd I) is formed. Cpd I is an $O=Fe^{IV}$ cation radical with an odd electron located on the porphyrin (porphyrin π cation radical). In some peroxidases, the Cpd I transforms to an equivalent oxidant traditionally called Cpd ES with the odd electron relocated to a nearby Trp or Tyr. The CpdI/CpdES oxidizes the organic substrate and returns to ferric state, which is a process consisting of two sequential one-electron steps for peroxidases involving another ferryl intermediate named Cpd II ($O=Fe^{IV}$) (not shown). The organic substrates were oxidized to radicals (AH•) that either disproportionate (Eq. 1.3) or dimerize (Eq. 1.4). By comparison, oxygenases like cytochrome P450 follow a more complicated catalytic mechanism involving an electron transfer system to generate Cpd I, which is again the active enzyme oxidant.

$$AH\bullet + AH\bullet \rightarrow AH_2 + A \quad (1.3)$$

$$AH\bullet + AH\bullet \rightarrow HA\text{-}AH \quad (1.4)$$

Typical peroxidases contains a single polypeptide of 30~50 kDa and a heme *b* prosthetic group. Based on the sequence homologies and crystal structures, peroxidases are generally divided into two classes: mammalian and nonmammalian types. Examples for mammalian peroxidases are myeloperoxidases (MPO) in human neutrophil,

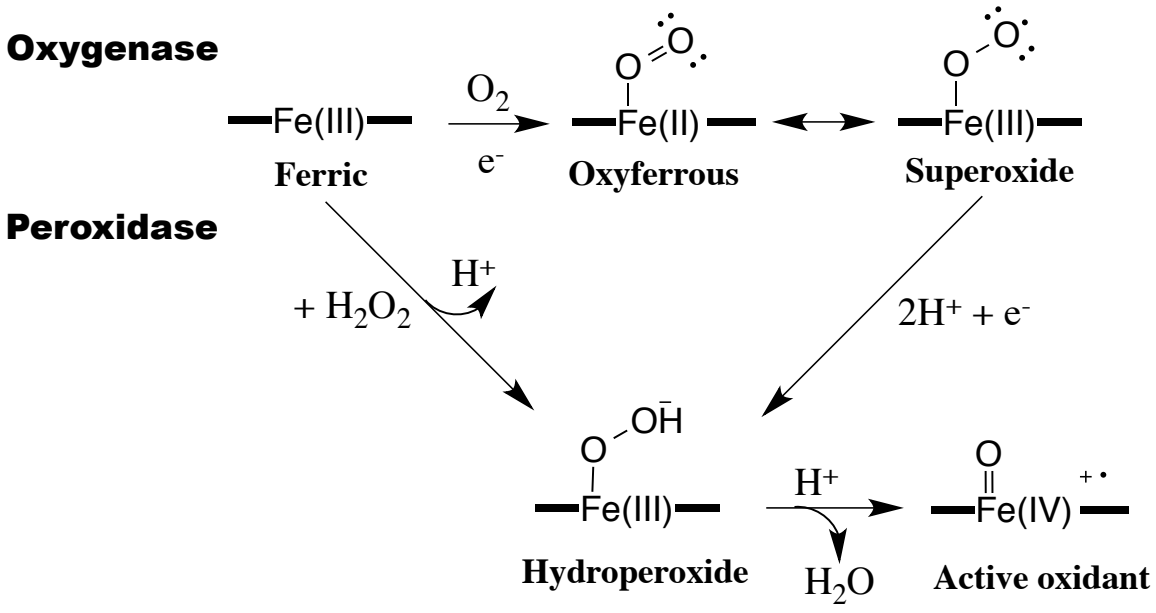


**Figure 1.2.** Activation of $O_2$ and $H_2O_2$ by monooxygenase and peroxidase, respectively, both results in active oxidant known as compound I (Adapted from reference [2]).

lactoperoxidase (LPO) in milk and thyroid peroxidase. The non-mamalian peroxidases have been found in yeast (e.g. cytochrome c peroxidase), fungi (e.g. lignin peroxidase) as well as plants (e.g. horseradish peroxidase). At present, over 700 peroxidase structures are available in the Protein Data Bank (PDB). The overall foldings and active site structures are well conserved (except for the two recently discovered globin peroxidases *Amphitrite ornata* dehaloperoxidase and *Notomastus lobatus* chloroperoidase).

The crystal structure of the yeast cytochrome c peroxidase (CCP) was the first heme peroxidase to be solved by X-ray crystallography (Figure 1.3) [3]. A close-up examination (Figure 1.3, right panel) reveals a charge relay network involving the proximal Asp/His and the distal His/Arg groups. Poulos and Kraut proposed a "push-pull" mechanism for the formation of peroxidase Cpd I, which is the most crucial step in the peroxidase catalytic path [4]. As shown in Figure 1.4, the proximal ligand $His^{175}$ forms a hydrogen bond with the nearby $Asp^{235}$ carboxylate group, which gives the proximal His partially deprotonated histidinate character. This provides an electron "push" to the heme iron. On the distal side, the cationic $Arg^{48}$ provides a "pull" effect by dispersing the developing negative charge on the outer O atom of the bound $H_2O_2$. The adjacent $His^{52}$ also contributes as a general acid/base catalyst, deprotonating the inner O and transferring the proton to the outer O. The "push" and "pull" machinery works together to heterolytically cleave the O-O bond in heme-bound $H_2O_2$, resulting in formation of Cpd I with release of a water molecule.

**Globins**

Globins are a group of heme proteins that reversibly bind dioxygen. The structure of

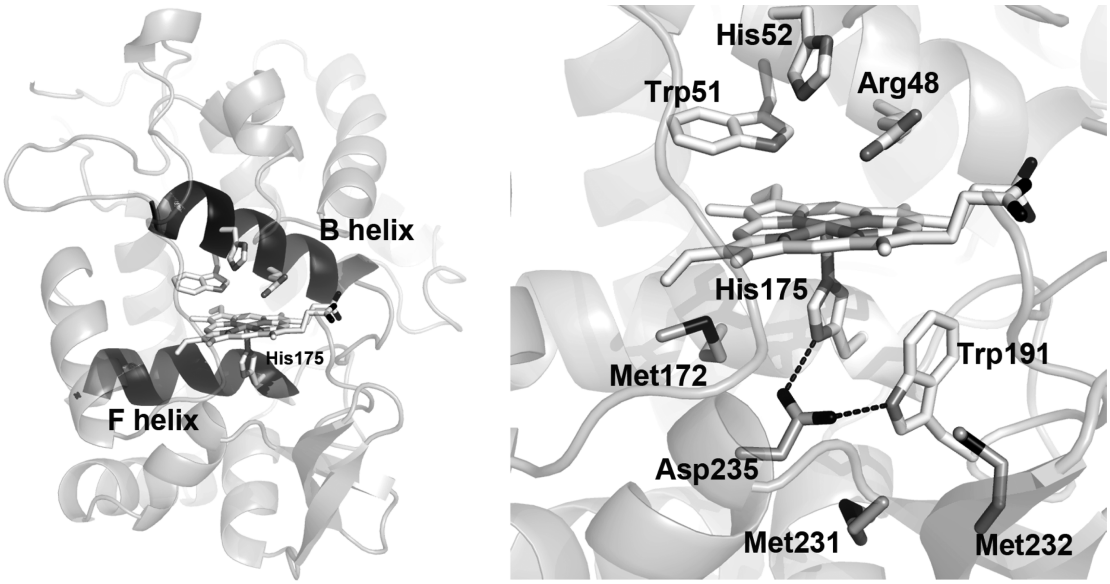


**Figure 1.3.** X-ray crystal structure of yeast CCP with the active site enlarged on the right (PDB 2CYP, also see reference [3]).

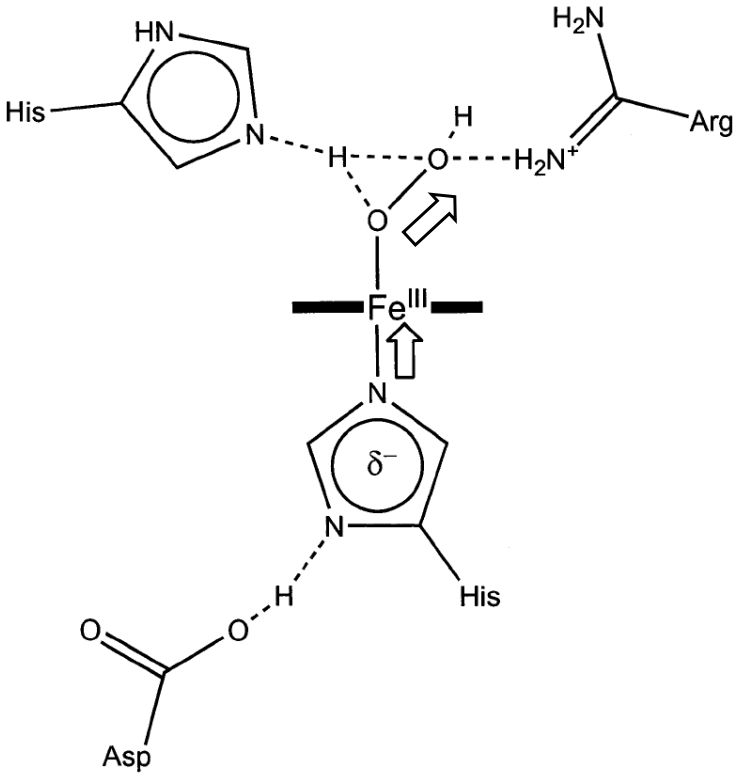


**Figure 1.4.** "Push-Pull" paradigm for heterolytic O-O bond cleavage in peroxidases (adapted from reference [5]).

a globin consists of several alpha helixes that form an overall globular shape and a heme cofactor whose center iron is where the $O_2$ binds. Myoglobins (Mb) are found in muscle cells and serve as an $O_2$ reservoir. Hemoglobins (Hb) circulate throughout the organisms, delivering $O_2$ to tissues for respiration. The first X-ray structure of globin was solved in 1958 by John Kendrew for sperm whale Mb [6]. It is a monomer consisting of 154 amino acids. Hb typically contains multiple subunits that may bind $O_2$ cooperatively, i.e. the $O_2$ affinity increases along with the saturation of $O_2$ due to the conformational changes upon ligand-binding and the dynamic correlations between subunits.

The globin function, i.e. reversible $O_2$ binding, is regulated by several factors such as heme iron oxidation state, reduction potential and the amino acids surrounding heme [7-12]. Only ferrous heme ($Fe^{II}$) binds $O_2$, ferric heme ($Fe^{III}$) does not. Therefore globins generally possess more positive redox potentials [100 ± 5 mV *vs.* standard hydrogen electrode (SHE) [13]] favoring the stable ferrous state. In contrast, the redox potential for peroxidases are typically negative [13]. Another important regulator of $O_2$ binding is the distal His that has been found to interact with the bound $O_2$ through an H-bond in most globins [7, 14].

Besides the major $O_2$ carrier function, some Mbs exhibit peroxidase-like activities under oxidative conditions when the heme iron is oxidized to theferric state [15, 16]. Ferric Mb reacts with $H_2O_2$ yielding high-valent heme species (Cpds I and II) that oxidize the biological molecules involved in oxidative stress reactions [17-20]. The peroxidase catalytic path of Mb is generally analogous to that of a typical peroxidase [21-23]. It has also been reported that Mb also has nitrate reductase activity in response to hypoxia in mammalian cells, which further broadens the functional versatility of globins [24].

**Dehaloperoxidase from *A. ornata***

In 1977, a coelomic Hb was discovered as the most abundant protein in the sea annelid *Amphitrite ornata* [25]. The worm was found buried in coastal mud with a reddish color throughout the body (Figure 1.5). Later in 1996, the same protein was rediscovered as a dehaloperoxidase enzyme that detoxifies halophenolic metabolites secreted by other marine cohabiters such as *Notamastus lubatus* (eq. 1.4) [26]. The dual functional Hb was then named as dehaloperoixdase (DHP) and was the first catalytically active globin [27]. Two genes (dphA and dphB) have been found encoding DHPA and DHPB respectively [28]. The two isomers only differ at five amino acids.

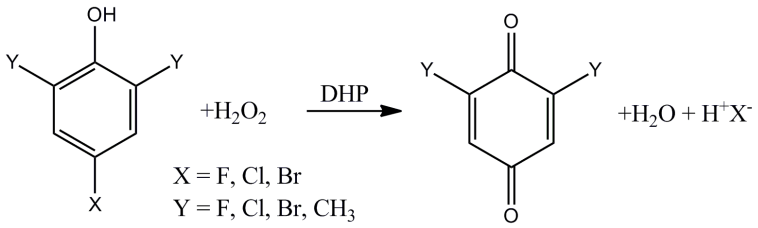


(1.4)

The crystal structure of DHP A was determined by Lebioda and coworkers in 2000 [29]. DHP is a dimer containing two identical, but functionally non-cooperative subunits ($M_r$ = 15,590). The typical globin-fold of DHP is analogous to that of SW Mb while distinct from those of traditional peroxidases such as HRP (Figure 1.6). HRP is twice as large as DHP and the two proteins have distinctly different heme environments: HRP has the heme buried inside the protein while the heme in DHP is more exposed to the solvent. Despite these differences, Mb, DHP and HRP all share a common heme active site construct consisting of a heme, a distal His and a proximal His (Figure 1.7). Close examination reveals subtle differences among the three. First of all, the distal His is much further (6.0 Å) from the heme iron in HRP than that in sperm whale Mb (4.6 Å). This longer distance favors $H_2O_2$ heterolysis over O2 biding. The DHP has an intermediate

**Figuer 1.5** The sea worm *Amphitrite ornata*

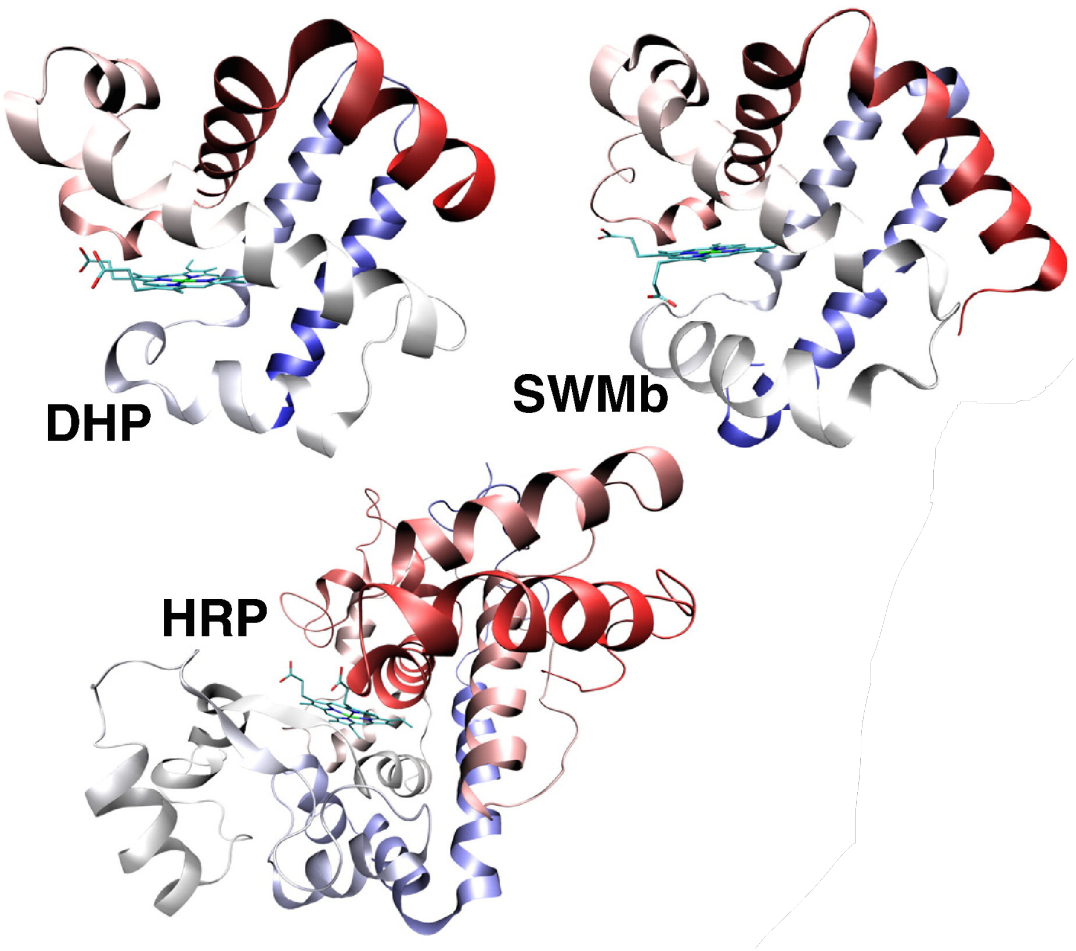


**Figure 1.6** Structural comparison of dehaloperoxidase hemoglobin (DHP, PDB 2QFK), sperm whale myoglobin (SWMb, PDB 1A6G) and horseradish peroxidase (HRP, PDB 2ATJ) [30].

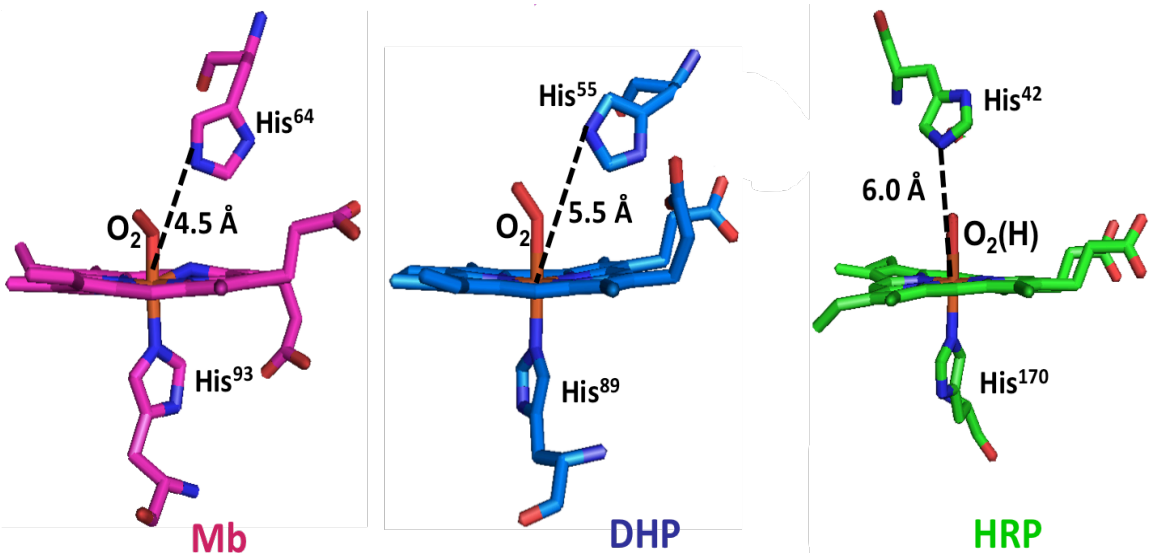


**Figure 1.7** A comparison of the active sites of sperm whale Mb (pink), DHP (blue) and horseradish peroxidase (green) (adapted from reference [31]).

distal His $N^{\varepsilon}$-Fe distance (5.4 Å) which to accomplish both $O_2$ binding and $H_2O_2$ heterolysis [27]. On the proximal side, the rotational angle of proximal His in DHP is about 60° rotated clockwise from that in Mb, resulting in new interaction of proximal His with peptide carbonyl group that provides a weak electron push [27]. Nevertheless, DHP lacks a strong proximal "push" effect that has been seen in typical peroxidases (see Figure 1.7) [32]. The proximal His in DHP is neutral like other globins as indicated by extensive spectroscopic data [33]. The significantly enhanced (> 250-fold) peroxidase activity of DHP compared with Mb is the outcome of both distal and proximal side heme environment adaptations during the evolution of DHP from an ancient $O_2$ carrier [27].

The DHP catalytic cycle involves two consecutive one-electron oxidations of the halophenolic substrates by Cpd ES/Cpd II, yielding halophenoxyl radicals (Figure 1.8). The radicals then undergo further oxidation and hydration to form the final quinone product [34, 35]. The substrate binding follows the traditional peroxidase order, i.e., $H_2O_2$ binds prior to organic substrate as suggested by extensive rapid-scan stopped flow spectroscopic studies [36].

A unique structural feature in DHP is the great flexibility of distal His, which has two conformations at room temperature. The "closed" conformation resembles that of sperm whale Mb while the "open" conformation has the distal His swung out and exposed to the solvent (Figure 1.9) [29]. The crystal structure also suggested that the "open" conformation associates with the absence of distal $H_2O$ while the "closed" His forms a hydrogen bond with a $H_2O$ molecule that coordinates to the heme iron. As the distal His is involved in the binding/activation of $H_2O_2$ as well as in the binding of $O_2$, it controls both peroxidase and globin functions of DHP. The halophenolic substrate

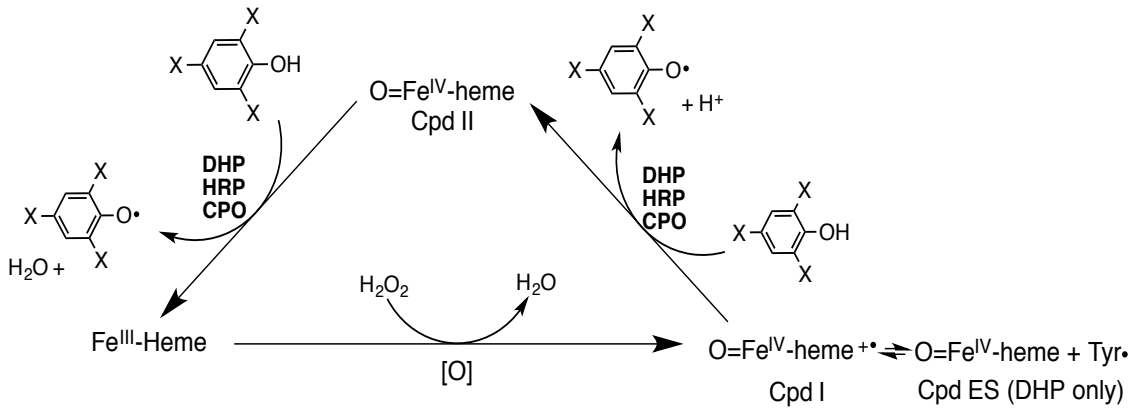


**Figure 1.8.** Proposed enzymatic mechanism for the dehalogenation reaction of trihalophenol catalyzed by three peroxidases: DHP, HRP and chloroperoxidase (CPO).

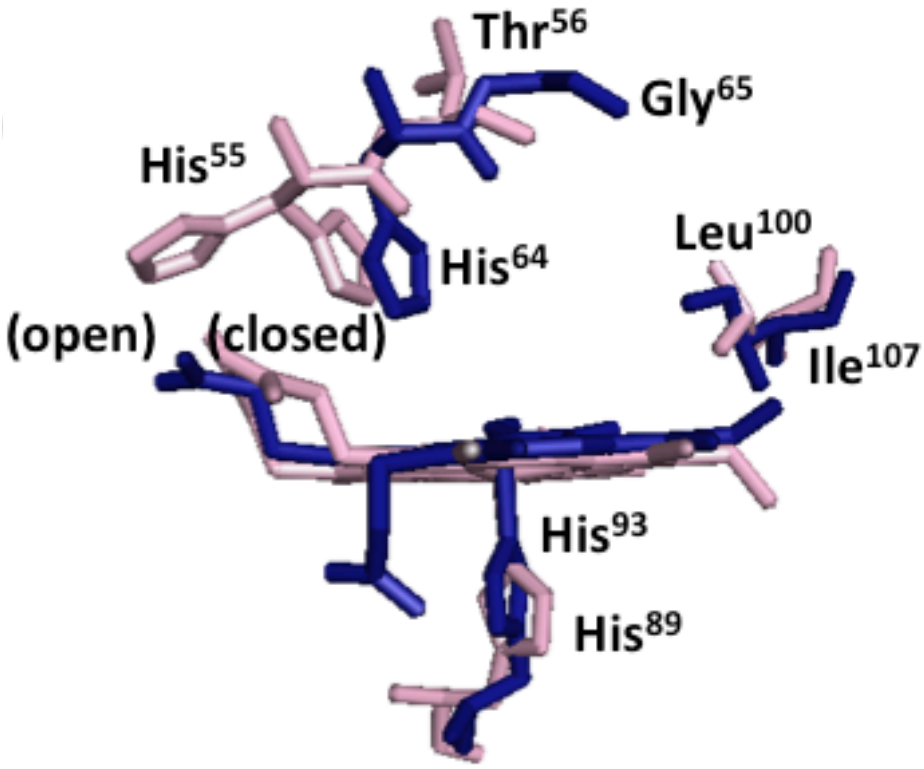


**Figure 1.9.** Superposition of heme active sites of Mb (blue) and DHP A (Pink) showing the two conformations of DHP distal His [31].

binding can modify the distal His conformation by binding internally inside the distal pocket or externally at the heme edge. As indicated by both X-ray crystallographic [29, 37] and resonance Raman spectroscopic [38] studies, small halophenols like 4-bromophenol (4-BP) bind internally, forcing the distal His to an "open" position and thus inhibiting the catalytic activity of DHP. Relatively bigger halophenols, such as 2,4,6-trichlorophenol (TCP), are found binding either deep inside or at the entrance of the distal pocket [39]. The latter is proposed as the binding site of substrate TCP to DHP Cpd I [39].

DHP has the highest reduction potential [~ 205 mV [40]] among the globins so its oxyferrous state is especially stable. However, this is not a favorable characteristic for a peroxidase because the catalytic cycle of peroxidases start from the ferric state and oxyferrous (also known as Cpd III) DHP is a catalytically inactive species. A paradoxical question as to how the $O_2$ carrier state of DHP switches to its enzymatically active ferric state needs to be addressed. There is evidence that substrate trihalophenol plays an important role in DHP functional switching [41, 42].

**REFERENCES**


[1] K.J. Waldron, N.J. Robinson, Nat. Rev. Microbiol. 7 (2009) 25-35.

[2] T.L. Poulos, Chem. Rev. 114 (2014) 3919-3962.

[3] T.L. Poulos, Arch. Biochem. Biophy. 500 (2010) 3-12.

[4] T.L. Poulos, J. Kraut, J. Biol. Chem. 255 (1980) 10322-10330.

[5] M. Sono, M.P. Roach, E.D. Coulter, J.H. Dawson, Chem. Rev. 96 (1996) 2841-2888.

[6] J.C. Kendrew, G. Bodo, H.M. Dintzis, R. Parrish, H. Wyckoff, D. Phillips, Nature 181 (1958) 662-666.

[7] J.S. Olson, G.N. Phillips Jr, Journal of Biological Inorganic Chemistry 2 (1997) 544-552.

[8] F. Cutruzzolà, C.T. Allocatelli, P. Ascenzi, M. Bolognesi, S.G. Sligar, M. Brunori, FEBS Lett. 282 (1991) 281-284.

[9] H. Ishikawa, T. Uchida, S. Takahashi, K. Ishimori, I. Morishima, Biophy. J. 80 (2001) 1507-1517.

[10] F. Draghi, A.E. Miele, C. Travaglini-Allocatelli, B. Vallone, M. Brunori, Q.H. Gibson, J.S. Olson, J. Biol. Chem. 277 (2002) 7509-7519.

[11] S.S. Narula, C. Dalvit, C.A. Appleby, P.E. Wright, Euro. J. Biochem. 178 (1988) 419-435.

[12] L. Capece, M.A. Marti, A. Crespo, F. Doctorovich, D.A. Estrin, J. Am. Chem. Soc. 128 (2006) 12455-12461.

[13] E.L. D'Antonio, E.F. Bowden, S. Franzen, J. Electro. Chem. 668 (2012) 37-43.

[14] J. Vojtěchovský, K. Chu, J. Berendzen, R.M. Sweet, I. Schlichting, Biophys. J. 77 (1999) 2153-2174.

[15] P. George, D. Irvine, Nature 168 (1951) 164-165.

[16] D. Keilin, E. Hartree, Proceedings of the Royal Society of London. Series B, Biol. Sci. 117 (1935) 1-15.

[17] A.I. Alayash, R.P. Patel, R.E. Cashon, Antiox. Redox Signal. 3 (2001) 313-327.

[18] U. Flögel, A. Gödecke, L.-O. Klotz, J. Schrader, FASEB J. 18 (2004) 1156-1158.

[19] D. Galaris, L. Eddy, A. Arduini, E. Cadenas, P. Hochstein, Biochem. Biophys. Res. Commun. 160 (1989) 1162-1168.

[20] R.L. Osborne, M.K. Coggins, M. Walla, J.H. Dawson, Biochemistry 46 (2007) 9823-9829.

[21] P.K. Witting, A.G. Mauk, P.A. Lay, Biochemistry 41 (2002) 11495-11503.

[22] C.D. Detweiler, O.M. Lardinois, L.J. Deterding, P.R. Ortiz de Montellano, K.B. Tomer, R.P. Mason, Free Rad. Biol. Med. 38 (2005) 969-976.

[23] D. Kelman, J. DeGray, R. Mason, J. Biol. Chem. 269 (1994) 7458-7463.

[24] U.B. Hendgen-Cotta, M.W. Merx, S. Shiva, J. Schmitz, S. Becher, J.P. Klare, H.-J. Steinhoff, A. Goedecke, J. Schrader, M.T. Gladwin, Proc. Natl. Acad. Sci. 105 (2008) 10256-10261.

[25] R.E. Weber, C. Mangum, H. Steinman, C. Bonaventura, B. Sullivan, J. Bonaventura, Comp. Biochem. Physiol. Part A 56 (1977) 179-187.

[26] Y.P. Chen, S.A. Woodin, D.E. Lincoln, C.R. Lovell, J. Biol. Chem. 271 (1996) 4609-4612.

[27] L. Lebioda, Cell. Mol. Life Sci. 57 (2000) 1817-1819.

[28] K. Han, S.A. Woodin, D.E. Lincoln, K.T. Fielman, B. Ely, Mar. Biotech. 3 (2001) 287-292.

[29] M.W. LaCount, E. Zhang, Y.P. Chen, K. Han, M.M. Whitton, D.E. Lincoln, S.A. Woodin, L. Lebioda, J. Biol. Chem. 275 (2000) 18712-18716.

[30] S. Franzen, M.K. Thompson, R.A. Ghiladi, Biochim. Biophys. Acta 1842 (2012) 578-588.

[31] S. Sun, M. Sono, C. Wang, J. Du, L. Lebioda, J.H. Dawson, Arch. Biochem. Biophys. (2014) *545, 108-145*.

[32] S. Franzen, M.P. Roach, Y.-P. Chen, R.B. Dyer, W.H. Woodruff, J.H. Dawson, J. Am. Chem. Soc. 120 (1998) 4658-4661.

[33] M.P. Roach, Y.P. Chen, S.A. Woodin, D.E. Lincoln, C.R. Lovell, J.H. Dawson, Biochemistry 36 (1997) 2197-2202.

[34] F. Wiese, H. Chang, R. Lloyd, J. Freeman, V. Samokyszyn, Arch. Environ. Contam. Toxicol. 34 (1998) 217-222.

[35] B.E. Sturgeon, B.J. Battenburg, B.J. Lyon, S. Franzen, Chem. Res. Toxicol. 24 (2011) 1862-1868.

[36] R.L. Osborne, M.K. Coggins, G.M. Raner, M. Walla, J.H. Dawson, Biochemistry 48 (2009) 4231-4238.

[37] C. Wang, L.L. Lovelace, S. Sun, J.H. Dawson, L. Lebioda, Biochemistry (2013).

[38] M.K. Thompson, M.F. Davis, V. De Serrano, F.P. Nicoletti, B.D. Howes, G. Smulevich, S. Franzen, Biophys. J. 99 (2010) 1586-1595.

[39] C. Wang, L.L. Lovelace, S. Sun, J.H. Dawson, L. Lebioda, Biochemistry 52 (2013) 6203-6210.

[40] J. D'Antonio, E.L. D'Antonio, M.K. Thompson, E.F. Bowden, S. Franzen, T. Smirnova, R.A. Ghiladi, Biochemistry 49 (2010) 6600-6616.

[41] J. Du, M. Sono, J.H. Dawson, Biochemistry 49 (2010) 6064-6069.

[42] J. D'Antonio, R.A. Ghiladi, Biochemistry 50 (2011) 5999-6011.

# CHAPTER 2

## Influence of Heme Environment Structure on Dioxygen Affinity for the Dual Function *Amphitrite ornata* Hemoglobin/Dehaloperoxidase. Insights into the Evolutional Structure-Function Adaptations[1]

[1] Sun, S., Sono, M., Wang, C., Du, J., Lebioda, L., and Dawson, J. H. (2014) *Arch. Biochem. Biophys.* 545: 108-115. Preprinted here with permission of publisher.

**ABSTRACT**

Sea worm, *Amphitrite ornata,* has evolved its globin (an $O_2$ carrier) also to serves as a dehaloperoxidase (DHP) to detoxify haloaromatic pollutants generated by competing species. A previous mutagenesis study by our groups on both DHP and sperm whale myoglobin (SW Mb) revealed some structural factors that influence the dehaloperoxidase activities (significantly lower for Mb) of both proteins. Using an isocyanide/$O_2$ partition constant measurement method in this study, we have examined the effects of these structural factors on the $O_2$ equilibrium constants ($K_{O2}$) of DHP, SW Mb, and their mutants. A clear trend of decreasing $O_2$ affinity and increasing catalytic activity along with the increase in the distal His $N^{\varepsilon}$–heme iron distance is observed. An H93K/T95H Mb double mutant mimicking the DHP proximal His positioning exhibited markedly enhanced $O_2$ affinity, confirming the essential effect of proximal His rotation on the globin function of DHP. For DHP, the L100F, T56G and M86E variants showed the effects of distal volume, distal His flexibility and proximal electronic push, respectively, on the $O_2$ affinity. This study provides insights into how DHP has evolved its heme environment to gain significantly enhanced peroxidase capability without compromising its primary function as an $O_2$ carrier.

**Keywords:** *Amphitrite ornata* dehaloperoxidase (DHP); sperm whale myoglobin (Mb); $O_2$ affinity; heme environment mutants; evolutional structure-function adaptations.

## INTRODUCTION

When the coelomic hemoglobin from the terebellid polychaete *Amphitrite ornata* was discovered in the 1970's [1], its peroxidase activity was unknown. In the 1990's, a dehaloperoxidase (DHP) enzyme was discovered in the same sea worm that detoxifies halophenols in the tidal sediments where it grows. It is the coelomic hemoglobin that carries out the DHP activity. Traditional heme-containing peroxidases [2] and globins [hemoglobins (Hbs) and myoglobins (Mbs)] [3] have distinct physiological functions: catalyzing the $H_2O_2$–dependent oxidation versus the reversible binding of dioxygen ($O_2$). These protein superfamilies have entirely different folds and are not evolutionally related. However, both contain a heme unit bound to the protein scaffold through a proximal histidine that serves as a coordinating ligand to the heme iron, leaving the distal side of the heme capable of binding peroxide (peroxidase) or $O_2$ (globin). DHP, which is the most abundant protein in *Amphitrite ornata*, carries out both functions as a globin that transports and stores $O_2$ and as a peroxidase that detoxifies trihalophenol substrates [2,4,6-TXP (X = F, Cl, Br)] (Scheme 1) [4]. Its structure (with very similar folds to Mb [5], Figure 2.1 A) and amino acid sequence indicate that DHP have evolved from an ancient oxygen carrier globin [6].

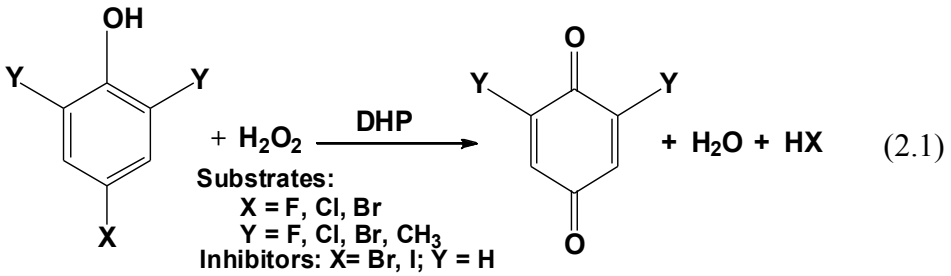


(2.1)

It has been a subject of intense investigations to probe what structural factors enable a globin to obtain peroxidase activity while still maintaining the $O_2$ carrier function [7-9].

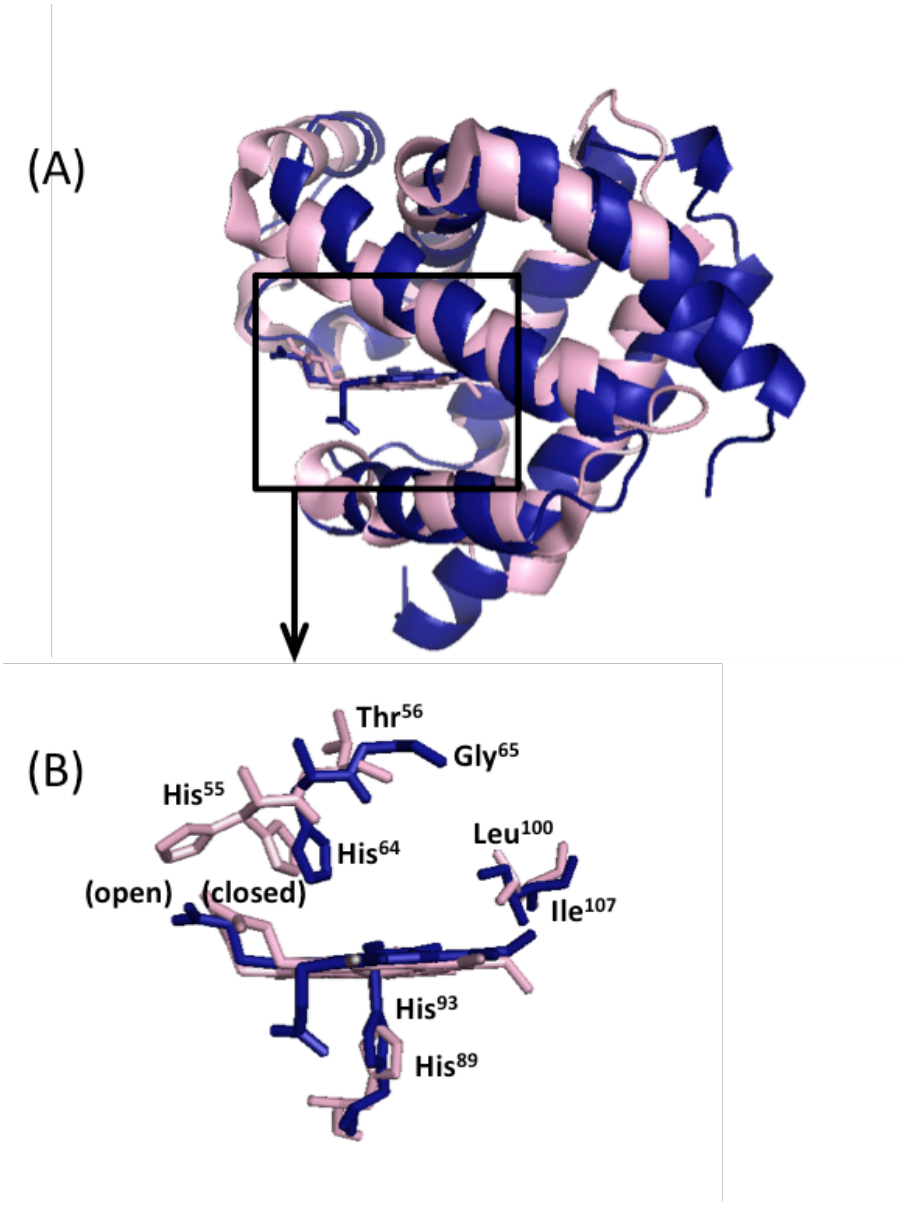


**Figure 2.1.** Ferric DHP (pink, lighter color) and sperm whale Mb (blue, darker color) X-ray structures alignments for entire peptide folds (A) and heme and its environmental amino acids that are subject of this study (B) created by superposing the common heme ring atoms. PDB accession codes are 1EW6 (DHP) and 1A6K (Mb). Note that, in panel A, amino acid side chains are omitted; in panel B, for the distal His-55 of DHP, two positions (open and closed) are shown. This figure was prepared using Pymol.

In a recent study by our group, a mutagenesis approach was utilized to investigate several structural factors that influence the peroxidase activity of DHP [10]. For example, the importance of the proper position of the distal His relative to the heme iron has been found crucial for the peroxidase activity of DHP [10]. DHP has an intermediate distal His $N^{\varepsilon}$-Fe distance (5.4 – 5.5 Å) compared to that in Mb (4.3 – 4.5 Å) and horseradish peroxidase (HRP) (~6.0 Å) and its dehaloperoxidase activity is also the intermediate of the three [10-12]. This position of the distal His in DHP appears to be convenient for carrying out both $O_2$ binding in the ferrous protein and acid-base catalysis for O-O bond cleavage of the heme iron-bound peroxide by ferric DHP. Several Mb mutants with an elongated distal His-Fe distance (G65T, G65I and F43H/H64L Mb) showed enhanced dehalogenation abilities [10]. The reversible $O_2$ binding property might also be affected by these mutations since the bound $O_2$ in Mb is stabilized by H-bonding to the distal His [13-15]. Another distal side factor that could regulate $O_2$ binding in Mb is the steric effect of Ile107 (Figure 2.1 B). Replacing I107 in both human and sperm whale (SW) Mbs with a bulky Phe has been shown to increase the $O_2$ affinity [16, 17]. In our previous mutagenesis study, a L100F DHP variant exhibited a dehaloperoxidase activity that is similar to that of the wild type [10].

Besides the distal effect, a charge relay mechanism from the proximal side may also affect the dual functions of DHP. A M86E mutation in DHP introduces a negatively charged residue nearby the originally neutral proximal His and expectedly enhances the peroxidase activity of DHP [10, 18]. This mutation could also modify the $O_2$ affinity since the charge relay system could stabilize ligand binding by enhancing the π-back-bonding from the iron to the ligand [19, 20]. Another proximal factor that is crucial for

the peroxidase activity of DHP (much higher than that of Mb) is a roughly 60° rotation of the proximal His imidazole ring compared with Mb [5, 10] (Figure 2.1 B). The Mb double mutant (H93K/T95H) that mimics the rotational position of the proximal His in DHP become a much better peroxidase than wild type Mb [10]. Since the rotation of proximal His has also been seen to significantly affect $O_2$ affinity in many other heme proteins [21, 22], similar effects of the proximal His rotation on the reversible $O_2$ binding property of DHP are expected.

In this study, the structural factors that influence the dehaloperoxidase acitivities of DHP (previous study [10]) have been examined for their influence on the $O_2$-binding function of DHP. Both heme distal and proximal side structural and electronic factors that influence the $O_2$-binding function of DHP have been examined to elucidate how DHP has altered its heme environment to evolutionally gain significantly enhanced peroxidase capability for self-protection without compromising its primary function as an $O_2$ carrier. In addition, the effects of substrate 2,4,6-trichlorophenol (TCP) and inhibitor 4-bromophenol (4-BP) binding on the $O_2$ affinities have also been evaluated for both wild type and a mutant DHP (T56G, designed with an increased flexibility of distal His) to probe their possible role(s) in functional switching of DHP from an $O_2$ carrier (ferrous state) to a peroxidase (ferric state).

## MATERIALS AND METHODS

*Materials.*

All reagents and biochemicals were purchased from Aldrich, ACROS, or Fisher and used without further purification except for potassium ferricyanide, which was

recrystallized from water. $H_2O_2$ stock (10 mM) in deionized water was prepared daily from a 30% commercial stock solution and the concentrations were routinely verified by UV-visible (UV-Vis) spectroscopic analysis at 240 nm ($\varepsilon_{240}$ = 39.4 $M^{-1}cm^{-1}$) [23]. Trichlorophenol (TCP) and 4-bromophenol (4-BP) stock solutions (100 mM) were freshly prepared in a 50/50 (v/v) ethanol/deionized water mixture.

*Mutagenesis and Sample Preparation.*

The expression vectors (pUC 19) for wild-type and F43H/H64L sperm whale Mb were gifts from Prof. Yoshihito Watanabe (Nagoya University). The procedures of expression and purification for sperm whale Mb mutants (pUC 19-G65T, -G65I and –H93K/T95H) and 6×His-taggged DHP A mutants (pET 16b-T56G and M86E) can be found in our previous mutagenesis study [10]. The isolated Mb and DHP proteins were completely oxidized to the ferric state by addition of a few crystals of potassium ferricyanide (Fluka) followed by gel-filtration column chromatography in 100 mM potassium phosphate (pH 5) at 4 °C. Protein concentrations were determined by the pyridine hemochromogen method ($\varepsilon_{555}$ = 34.4 $M^{-1}$ $cm^{-1}$) [24]. The oxyferrous protein was formed by addition of a slight excess of sodium dithionite to the ferric protein, followed by aerobic Bio-Gel P6DG (Bio-Rad) desalting column with 100 mM potassium phosphate buffer (pH 7) at 4 °C. Deoxyferrous protein samples were prepared in a rubber septum-sealed cuvette by addition of a small amount of solid sodium dithionite to a thoroughly degassed ferric sample in 100 mM potassium phosphate buffer (pH 7) at 4 °C.

*$O_2$ dissociation equilibrium constant ($K_{O2}$) determination.*

$O_2$ dissociation equilibrium constants ($K_{O2}$) of DHP (or Mb) were determined by the method used by Makino and Yamazaki [25] by first measuring a partition constants ($K_P$)

for the replacement of the bound $O_2$ in oxyferrous protein by isocyanide ligand (L) (Eq. 2.2) and then a dissociation constant ($K_L$) for an isocyanide bound deoxyferrous protein (Eq. 2.3).

$$\text{DHP-O}_2 + \text{L} \overset{K_p}{\rightleftharpoons} \text{DHP-L} + \text{O}_2 \qquad (2.2)$$

$K_P = [\text{DHP-L}]\,[\text{O}_2] / [\text{DHP-O}_2]\,[\text{L}]$

$= \{[\text{DHP}]\,[\text{O}_2] / [\text{DHP-O}_2]\} / \{[\text{DHP}]\,[\text{L}] / [\text{DHP-L}]\}$

$= K_{O2} / K_L$

$K_{O2}$ and $K_L$ are defined as follows:

$$\text{DHP} + \text{L} \overset{K_L}{\rightleftharpoons} \text{DHP-L} \qquad (2.3)$$

$$K_L = [\text{DHP}]\,[\text{L}] / [\text{DHP-L}] \qquad (2.4)$$

$$\text{DHP} + \text{O}_2 \overset{K_{O2}}{\rightleftharpoons} \text{DHP-O}_2 \qquad (2.5)$$

Thus, from Eq. (2)

$$K_{O2} = K_L \times K_p \qquad (2.6)$$

$K_p$ and $K_{L(O2)}$ were determined by step-wise isocyanide titration of oxyferrous (~ 10 μM) and deoxyferrous (~ 3 μM) DHP/Mb, respectively, in 100 mM potassium phosphate buffer (pH 7.0 or 9.0 for one particular case of a Mb mutant) at 4 $^{o}$C (or ~22 $^{o}$C for a few cases). Two kinds of isocyanide ligands were used in the titration experiments depending on proper affinity ranges between the values ($K_d$) for the $O_2$-bound ($K_d = 10^{-5} – 10^{-3}$ M) and deoxyferrous states bound ($K_d = \sim 10^{-6}$ M) of titrated proteins (if the isocyanide affinity is too high or too low, its accurate determination would be difficult or practically impossible because of large errors or ligand solubility limits, respectively): Isopropyl isocyanide (IPIC) was used for titrations of wt-Mb and H93K/T95H Mb; *t*-butyl isocyanide (TBIC) was used for titrations of other Mb mutants and all DHPs. For the

titration of oxyferrous proteins, 4 mM ascorbate (pH adjusted to a neutral value) and bovine liver catalase (0.1 – 0.5 μM based on heme) were added to the sample to prevent autoxidation of the heme and ascorbate-caused undesirable reactions [26]. To help maintain the $O_2$ concentration constant throughout the titration (< 3 h), the sample were bubbled with air through a Pasteur pipette after each addition of ligand. The titration of deoxyferrous proteins were carried out anaerobically in the presence of slight excess of sodium dithionite in a rubber septum-sealed cuvette and the isocyanide ligands were added in a step-wise manner using a gas-tight microliter syringe.

Titration spectra were analyzed using a simple biomolecular association scheme and the plots of absorbance change vs. ligand concentration were analyzed by a hyperbolic regression fit of a saturation plot (absorbance change vs. ligand concentration), giving the values of $K_p$ and $K_L$. Three or more sets of $K_p$ and $K_L$ were obtained for each titration to calculate the final $K_{O2}$ using Eq. 2.4. The $O_2$ concentrations were considered as 400 μM at 4 °C and 270 μM at room temperature (~22 °C) [27, 28].

*Peroxidase Activity Assay*

UV-Vis absorption spectroscopy was used to measure the peroxidase activity of DHP at 4 $^{o}$C in100 mM potassium phosphate buffer (pH 7.0). TCP were added to the ferric enzyme (~3 μM) before addition of hydrogen peroxide to initiate the reactions in a 0.5-cm cuvette. The turnover number ($k_{cat}$) can be measured by monitoring the change in absorbance at 272 nm for the appearance of quinone products ($\varepsilon_{272}$ = 14 $mM^{-1}cm^{-1}$) [29]. The $k_{cat}$ values were determined by calculating the velocity ($v_o$) from the initial linear portion of the trace at 272 nm as a function of $H_2O_2$ concentration with a fixed [TCP], followed by a graphical calculation (hyperbolic curve fitting) of a $v_o$ value at infinite

[$H_2O_2$] to obtain a $v_{max}$ value and then by dividing the $v_{max}$ by the enzyme concentration ($k_{cat} = v_{max}/[DHP]$). For each set of reaction conditions, 10 replicates were performed and then averaged to determine the velocity at the varying [$H_2O_2$] (typically 20 ~ 480 μM) and fixed [TCP] (500 μM).

*Spectroscopic Techniques.*

UV-Vis absorption spectra were recorded with a Cary 400 spectrophotometer interfaced to a Dell PC. Magnetic circular dichroism (MCD) spectra were measured with a magnetic field strength of 1.41 T by using a JASCO J815 spectropolarimeter equipped with a JASCO MCD-1B electromagnet and interfaced with a Gateway PC through a JASCO IF-815-2 interface unit. Data acquisition and manipulation were carried out as previously described [30].

*Crystallography.*

The L100F variant of DHP was crystallized in the oxyferrous form (as purified) using the vapor diffusion method in hanging-drop set-up. The protein dissolved in 20 mM sodium cacodylate pH 6.5 was concentrated to 10 mg/ml. The crystals were grown from solutions containing 0.2 M ammonium sulfate and 26-34% polyethylene glycol 4000, as previously reported for other DHP mutants [31]. The data set was collected at SERCAT 22ID beamline at the Advanced Photon Source (APS) in the Argonne National Laboratory. The data were indexed, integrated and scaled with the HKL2000 software package. Data collection and processing statistics are listed in Table 2.6. The structure of L100F•$O_2$ was determined using molecular replacement with the Phaser program from the CCP4 suite of program using the wt-DHP structure (PDB entry 1EW6) as the initial

model. Structure rebuilding was carried out using Coot and Turbo and structure refinement and map calculation were performed using Refmac5 from the CCP4 [31].

**RESULTS**

Representative TBIC titration spectra for oxyferrous and deoxyferrous DHP are shown in Figure 2.2, A and B, respectively. Analyses of these titrations (shown in the insets) yield $K_{L(O2)}$ (= $[O_2]$ / $K_p$) and $K_L$ values of 0.46 mM and 3.63 μM, respectively, at pH 7.0 and 4 °C (see Materials and Methods section). The $K_{O2}$ value of 3.23 μM (= $K_L$ × $K_p$) [3.23 ± 0.37 μM, Table 2.1] is calculated from these values (Eq. 2.6). To evaluate the accuracy of our isocyanide/$O_2$ partition constant measurements, we have also determined the $K_{O2}$ values of SW Mb and DHP at ~22 °C using this method (Table 2.5). The results for Mb agree with previously reported values [3, 25]. Our $K_{O2}$ value for DHP (7.70 ± 0.45 μM at ~22 °C) is somewhat larger than the one reported by Weber et al. at 20 °C [1] [$K_{O2}$ = 5.1 μM, converted from 2.8 mm Hg by $K_{O2}$ (μM) = 1.82 × $K_{O2}$ (mm Hg), (Section 7.4 in [3]). A probable reason for this difference may be that the $K_{O2}$ value reported by Weber et al. [1] was likely for a mixture of the two isozymes, DHP A and B while this $O_2$ affinity study is for DHP A as an extension of our previous investigations on DHP A and its mutants that we have prepared [10]. DHP A and DHP B encoded by two separate genes. They have very similar structures while only differing in five amino acids [4, 32]. DHP B has an almost two-fold higher $O_2$ affinity than DHP A (Sun, S., Wang, C., Sono, M., Lebioda, L., Dawson, J.H., unpublished result).

Tables 2.1-2.4 show the $K_{O2}$ values measured (in this study) as well as the dehaloperoxidase activities ($k_{cat}$) for Mb mutants (previous study [10]) and wt-DHP and

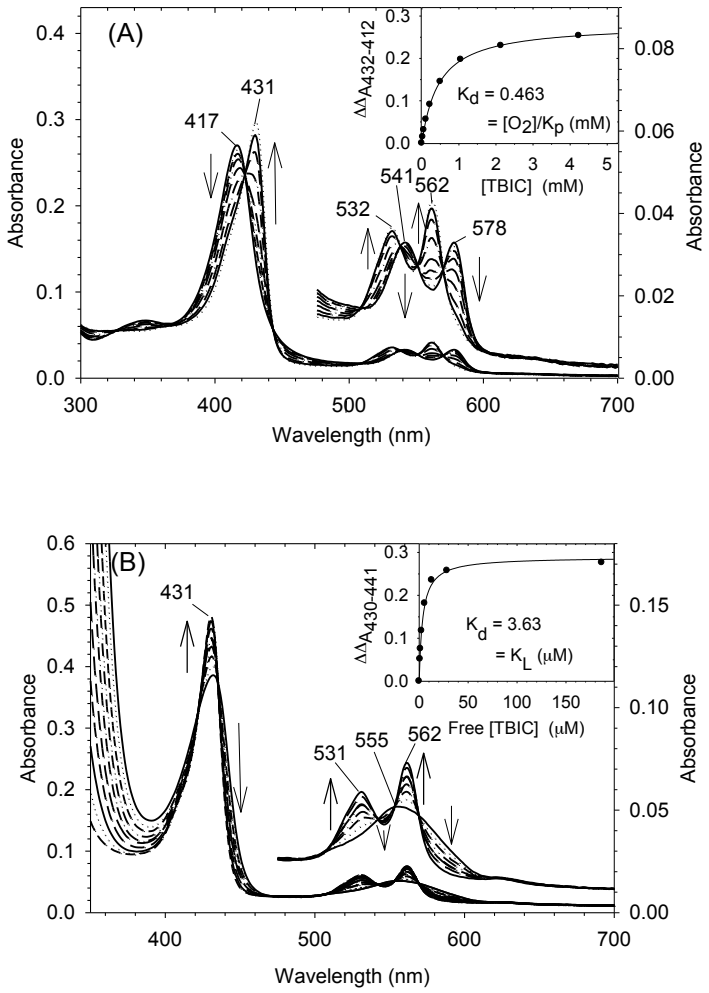


**Figure 2.2.** UV-visible absorption spectral changes on TBIC titrations of oxyferrous DHP (A) and deoxyferrous DHP (B) in 0.1 M potassium phosphate buffer, pH 7.0 at 4 °C. Oxyferrous DHP (2.31 mM) and deoxyferrous DHP (3.34 mM) were titrated by incremental additions of 0.03, 0.06, 0.11, 0.22, 0.50, 1.05, 2.14, 4.24 mM (oxyferrous DHP) and 0.80, 1.60, 2.40, 3.18, 3.98, 7.95, 15.90, 31.74, 190.14 mM TBIC (deoxyferrous DHP). Vertical arrows indicate the directions of absorbance change. Hyperbolic saturation plot (solid circle) and its regression fit (solid line) of the titration data are shown in the insets, where the peak-to-trough absorbance change in difference spectra (not shown) ($\Delta\Delta A_{432-412} = \Delta A_{432} - \Delta A_{412}$, $\Delta\Delta A_{430-414} = \Delta A_{430} - \Delta A_{414}$) are plotted as function of TBIC concentration ([TBIC]). In B, [TBIC] values used are [protein-free TBIC] (= [total TBIC] – [protein-bound TBIC]), while in A, [total TBIC] values are used since [protein-free TBIC] ≈ [total TBIC].

its mutants (new larger values by 1.1 – 3.1 times obtained in this study with higher [TCP] = 500 μM vs.150 μM in the previous study [10]). The resulting $k_{cat}$ values for G65T, G65I and F43H/H64L Mb mutants increased along with the distal His $N^{\varepsilon}$ – heme iron distance (Table 2.1) [10]. Conversely, the $K_{O2}$ values measured in this study show the opposite trend, i.e., their $O_2$ affinities decrease as the distal His $N^{\varepsilon}$ – heme iron distance increases.

The L100F DHP variant, in which the distal side Leu100 is replaced with a bulkier Phe group, has only a subtle effect in the turnover numbers [10], but exhibits a 3-fold higher $O_2$ affinity than the wild type (Table 2.2). The crystal structure of the L100F•$O_2$ complex was determined (Figure 2.3) and its parameters and refinement statistics are listed in Table 2.6. The structure of the L100F•$O_2$ complex shows that Phe100, which is located at the back of the cavity, does not form contacts with the bound dioxygen molecule nor with the distal histidine (Figure 2.3).

Two proximal side mutants, one for DHP and the other for Mb, have also been studied. The $O_2$ affinity of M86E DHP, in which a negatively-charged Glu group is introduced close to the proximal His89, shows a significant increase by about 5-fold while at the same time displacing an approximately three-fold increase in dehalogenase activity (Table 2.2), Table 2.3 lists the $K_{O2}$ value for H93K/T95H Mb, which is design to mimic the proximal His plane of DHP that is rotated by 60° compared with that of Mb (see Discussion), measured at pH 9.0 (to avoid enhanced autoxidation of its oxy-complex at pH 7.0). It should be noted that the $O_2$ affinities of both DHP [1] and Mb[3] are pH-independent (between pH 6 and 9), i.e., neither protein exhibits a Bohr effect. This Mb

**Table 2.1.** $O_2$ affinities of SW Mbs (wt and mutants) and wt-DHP (this study) in 100 mM potassium phosphate buffer (pH 7) at 4 °C and their turnover numbers ($k_{cat}$, previous study [10]) for the oxidative dechlorination with 150 μM TCP and varying $H_2O_2$ concentration in 50 mM sodium acetate buffer (pH 5.4) (Mbs) or 50 mM sodium citrate buffer (pH 5.4) (DHP) at 4 °C.

| Protein | $K_{O2}$ (μM) 4 °C, pH 7.0[a] | Fe-His55 $N^{\varepsilon}$ distance (Å)[b] | $k_{cat}$ ($min^{-1}$) 4 °C, pH 5.4[a,c] |
|---|---|---|---|
| wt-Mb | 0.27 ± 0.01 (1.0) | 4.3 | 19.0 ± 1.7 (1.0) |
| G65T Mb | 0.39 ± 0.05 (1.4) | 4.6 | 92.0 ± 7.0 (4.8) |
| G65I Mb | 1.34 ± 0.21 (5.0) | 5.1 | 138 ± 10 (7.3) |
| F43H/H64L Mb | 6.12 ± 0.60 (23) | 5.4 | 161 ± 9 (8.5) |
| wt-DHP | 3.23 ± 0.37 (12) | 5.4 | 243 ± 3 (13) |

[a] The values in parentheses are relative $K_{O2}$ or $k_{cat}$ vs. those of wt-Mb.
[b] PDB accession codes for metaqua ($H_2O$-ligated ferric heme) structures of proteins listed in this table: wt-Mb (1A6K), G65T Mb (3O89), G65I Mb (3SDN), F43H/H64L Mb (1OFK) and DHP (1EW6).
[c] From ref [10].

**Table 2.2.** $O_2$ affinities of DHPs and their turnover numbers for the oxidative dechlorination with 500 μM TCP and varying $H_2O_2$ concentration in 100 mM potassium phosphate buffer (pH 7) at 4 °C.

| Protein | $K_{O2}$ (μM) 4 °C, pH 7.0 [a] | $k_{cat}$ ($min^{-1}$) 4 °C, pH 7.0 [a, b] |
|---|---|---|
| wt-DHP | 3.23 ± 0.37 (1.0) | 25 ± 1.0 (1.0) |
| L100F DHP | 1.03 ± 0.07 (1/3.1) | 20 ± 1.7 (0.8) |
| M86E DHP | 0.64 ± 0.08 (1/5.1) | 78 ± 5.7 (3.1) |

[a] The values in parentheses are relative $K_{O2}$ or $k_{cat}$ vs. those of wt-DHP.

[b] The $k_{cat}$ values in this table that were obtained in this study using 500 μM TCP are larger than the corresponding values determined with 150 μM TCP in the previous study [10] by the factors of ~3.2 (wt-DHP), ~3.3 (L100F DHP) and ~1.1 (M86E DHP).

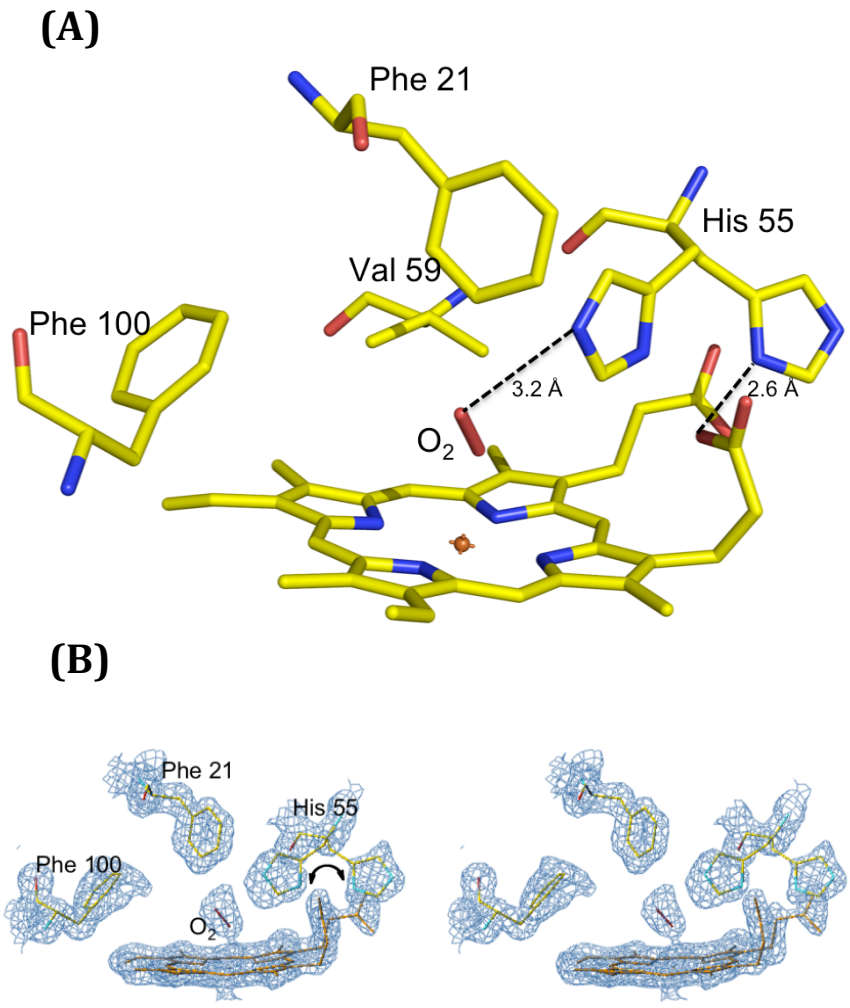


**Figure 2.3.** Stereoview of the structure (A) and electron densities (B) of the L100F DHP A•$O_2$ complex and its heme distal side environment. Phe100 is located deep in the distal pocket and does not form contacts with dioxygen or His55. Two positions of His55 are stabilized through hydrogen bonding with $O_2$ and a heme propionate. The final 2FoFc map is contoured at a 1 σ level. Somwhat broaden density of the distal $O_2$ atom of the dioxygen molecule may be relatedd to the disorder of His55. This figure was prepared using Pymol and Turbo.

**Table 2.3.** $O_2$ affinities of SW wt-Mb and its H93K/T95H mutant (this study) in 100 mM potassium phosphate (pH 9) at 4 °C and their turnover numbers (previous study [10]) for the oxidative dechlorination with 150 μM TCP and varying $H_2O_2$ concentration in 50 mM sodium acetate buffer (pH 5.4) at 4 °C.

| Protein | $K_{O2}$ (μM) 4 °C, pH 9.0[a] | $k_{cat}$ ($min^{-1}$) 4 °C, pH 5.4 [a,b] |
|---|---|---|
| wt-Mb | 0.33 ± 0.02 (1.0) | 19.0 ± 1.7 (1.0) |
| H93K/T95H Mb | 0.015 ± 0.003 (1/22) | 104 ± 13 (5.5) |

[a] The values in parentheses are relative $K_{O2}$ or $k_{cat}$ vs. those of wt-Mb. [b] From ref [10].

mutant exhibits ~ 20-fold higher $O_2$ affinity than that of wt-Mb, along with ~ 50-fold increase in peroxidase activity as reported previously [10].

For the T56G DHP mutant that designed to increase the flexibility of distal His, its $O_2$ affinity was measured both in the absence and presence of TCP/4BP. In the absence of TCP/4-BP, T56G DHP has ~ 3.4-fold higher $k_{cat}$ and ~2.4-fold lower $O_2$ affinity than the wt-DHP (Table 2.4). Upon addition of 2 mM TCP or 4BP, $O_2$ affinity of T56G DHP becomes almost two-fold higher and ~1.5-fold lower, respectively (Table 2.4). In contrast, addition of either 2 mM TCP or 4-BP barely altered the $K_{O2}$ of wt-DHP (Table 2.4). Note that none of the $K_L$ values in Table 2.4 for the affinity of isocyanide ligand used in the $O_2$ affinity measurements are significantly affected by added TCP or 4-BP. Figure 2.4 (plotted using data in Table 2.7) shows the concentration-dependency of the effect of TCP on the $O_2$ affinity of T56G DHP.

To understand the different effects of TCP on the $O_2$ affinity of T56G DHP vs. wt-DHP, the absorption and MCD spectra of TCP-bound ferric T56G DHP were recorded in this study (Figure 2.6, red solid line), which closely resemble those of the acetate complex of ferric wt-DHP (at pH 5.4, black dotted line in Figure 2.6) and Mb (at pH 7, blue dashed line in Figure 2.6), both reported previously [10].

**DISCUSSION**

Here, we consider several steric and electronic factors that influence the $O_2$ affinities of DHP as well as Mb using the wild-type proteins and several mutants in the context of evolutional heme environment structural adaptations of DHP to its dual functions. Since we can only see the consequence (outcome) of evolutions in the functions and structure

**Table 2.4.** $O_2$ affinities ($K_{O2}$) of wt-DHP and T56G DHP and turnover numbers ($k_{cat}$) for the oxidative dechlorination with 500 μM TCP and varying $H_2O_2$ concentration (100 mM potassium phosphate buffer, pH 7.0, 4 °C). All the values were determined in this study. See text for the definitions of $K_L$ (isocyanide equilibrium dissociation constant) and $K_P$ ($O_2$/isocyanide partition constant) for deoxyferrous DHP.

| Protein | $k_{cat}$ ($min^{-1}$) | | $K_{O2}$ (μM) | $K_L$ (μM) and $K_p$ | |
|---|---|---|---|---|---|
| wt-DHP | 25.0 ± 1.0 | w/o TCP | 3.23 ± 0.37 | $K_L$ | 3.47 ± 0.48 |
| | | | | $K_p$ | 0.93 ± 0.06 |
| | | + TCP (2 mM) | 3.53 ± 0.24 | $K_L$ | 3.60 ± 0.19 |
| | | | | $K_p$ | 0.98 ± 0.02 |
| | | + 4-BP (2 mM) | 2.95 ± 0.04 | $K_L$ | 3.17 ± 0.32 |
| | | | | $K_p$ | 0.93 ± 0.15 |
| T56G DHP | 86.4 ± 6.5 | w/o TCP / 4-BP | 7.83 ± 0.83 | $K_L$ | 0.45 ± 0.03 |
| | | | | $K_p$ | 17.40 ± 0.92 |
| | | + TCP (2 mM) | 4.23 ± 0.52 | $K_L$ | 0.43 ± 0.04 |
| | | | | $K_p$ | 9.83 ± 0.82 |
| | | + 4-BP (2 mM) | 11.73 ± 0.89 | $K_L$ | 0.47 ± 0.05 |
| | | | | $K_p$ | 25.00 ± 2.83 |

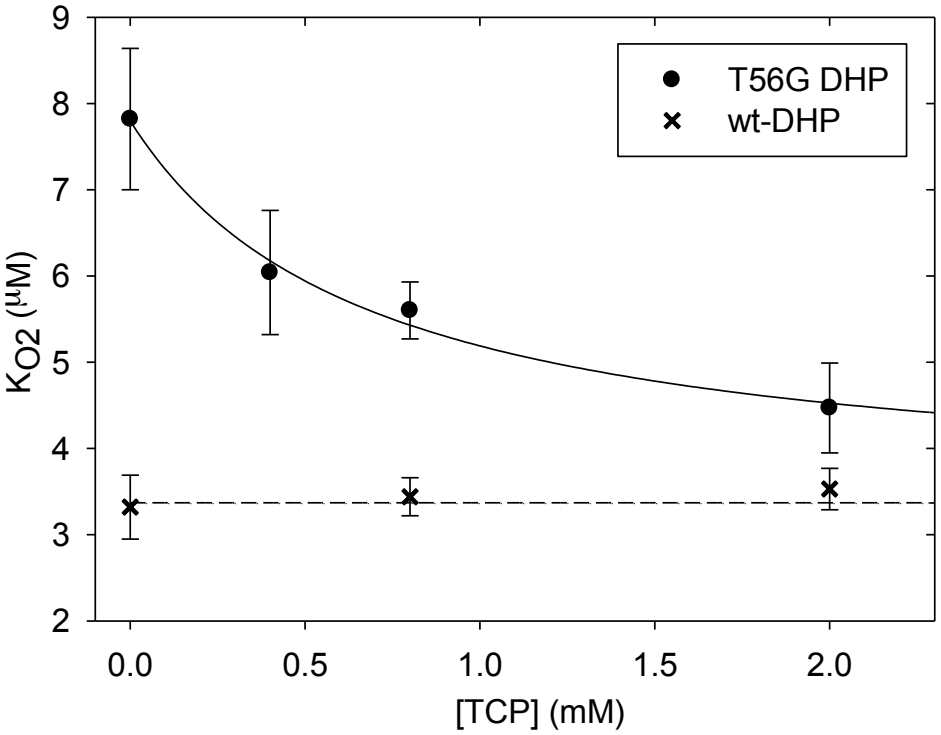


**Figure 2.4.** Effects of TCP concentration (0 – 2 mM) on the $O_2$ affinities ($K_{O2}$ in μM) of T56G DHP vs. wt-DHP in 100 mM potassium phosphate buffer (pH 7.0) at 4 °C. The solid line for T56G DHP is drawn by fitting the four data points to a hyperbolic regression curve that yields $K_{O2}$ = 3.4 μM at infinite [TCP] and [TCP] = 0.68 mM for a half maximum change in $K_{O2}$ value. The dashed line for wt-DHP is drawn as a straight horizontal line at $K_{O2}$ = 3.4 μM.

of wt-DHP, we use here Mb, and in some cases, DHP itself and their heme environmental mutants in an effort to trace back and interpret likely function-related structural evolutions in DHP. We note although the effects of such mutations within a given system (Mb or DHP) may be applicable to the other system, the actual $K_{O2}$ values of the two systems may not necessarily be directly comparable.

*Effects of Fe-Distal His55 $N^{\varepsilon}$ Distance*

DHPA has an almost 10- (or 6-) fold lower $O_2$ affinity (i.e., higher $K_{O2}$ value) than that of SW Mb [3, 25] (or horse heart Mb [3, 33]). This is likely the result of a compromise involved in obtaining the peroxidase activity during the evolution of DHP while maintaining a functional requirement as Hb. In addition, other physiological factors likely also play a role given that human hemoglobin (a tetrameric and allosteric heme protein [3]) has approximately 10-fold lower $O_2$ affinity than DHP at about neutral pH. Note that Mb itself has a dehaloperoxidase activity that is much lower (~ 8% that of DHP at pH 5.4, with TCP as substrate [8]) than that of DHP.

One structural factor that contributes to the lower $O_2$ affinity of DHP is almost certainly the longer distal His $N^{\varepsilon}$ – heme iron distance in DHP compared to that in Mb. In our previous study, the dehaloperoxidase activities of G65T, G65I and F43H/H64L Mb mutants, all of which have elongated distances (by 0.3 – 1.1 Å) between distal His and heme iron, were examined. The resulting $k_{cat}$ values for these mutants increased along with the distal His $N^{\varepsilon}$ – heme iron distance (Table 2.1) [10]. This is consistent with the significantly (× ~6) enhanced peroxidase activity of the F43H/H64L Mb mutants over that of wt-Mb and may be true within a certain distance limit (< 6.6 Å, estimated based on L29H/H64L Mb, PDB: 10FJ) as found by Watanabe and co-workers [34]. Conversely,

the $K_{O2}$ values measured in this study show the opposite trend. As shown in Table 2.1, their $O_2$ affinities decrease as the distal His $N^{\varepsilon}$ – heme iron distance increases, This is reasonable considering the H-bond formed between the distal His and dioxygen in the wt-Mb might be weakened in the mutants with the distal His located further from the heme center [13-15]. Thus, based on the present results with Mbs, we propose that "the longer the heme iron-distal His $N^{\varepsilon}$ distance, the weaker the $O_2$ affinity" co-relation exists in general for $O_2$-binding heme proteins when other structural and electronic factors are kept similar. This finding (Table 2.1) in turn strongly suggests that the longer heme iron-distal His $N^{\varepsilon}$ distance in DHP than in wt-Mb must have a considerable $O_2$ affinity lowering effect even by a factor of an order of magnitude (Table 2.1). However, to maintain its primary function as an $O_2$ carrier, such an unfavorable effect may need to be compensated for DHP by altering other structural/electronic factors such as those described below. Any such adaptations that also involve further enhancement of the peroxidase activity would certainly be even more beneficial for DHP.

*Steric Effects in the Distal Pocket*

The L100F DHP variant, with the volume of the distal cavity reduced by a larger side chain amino acid residue, was designed in our previous study as a probe of the TXP (X = Br, Cl) substrate binding site of DHP [10]. The structure of this mutant in the ferric state has been reported by Plummer et al. [35]. The structure of the L100F•$O_2$ complex shows that Phe100, which is located at the back of the cavity, does not form contacts with the bound dioxygen molecule nor with the distal histidine (Figure 2.3 A). The increased affinity is likely due to entropic factors resulting from the cavity volume reduction meaning that fewer disordered water molecules need to be displaced upon $O_2$ binding.

Similar conclusions, based on a modeled position of dioxygen, were reached for the I107F mutant of human and sperm whale Mbs [16, 17]. Only the subtle difference in the turnover numbers for this mutant compared to that for the wild type enzyme suggested that the productive binding site of substrate halophenol is not in the distal pocket [31]. It is also interesting to test the $O_2$ affinity of this mutant since the analogous I107F Mb mutant has been studied as a part of unsuccessful effort to engineer high $O_2$ affinity Mb using *Ascaris suum* globin [16]. As found in this study, the effect is similar, albeit stronger, I107F Mb has 1.4-fold higher $O_2$ affinity than wt-Mb while L100F DHP exhibits a 3-fold higher $O_2$ affinity than wt-DHP (Table 2.2). Apparently, this type of mutation would not be effective in enhancing higher $O_2$ affinity or peroxidase activity for DHP.

*Effects of the Electronic "push" from the Proximal His89*

Dioxygen affinity has been shown to positively correlate with electron density on the heme iron [25, 33, 36] and negatively correlated with reduction potential [37]. An electronic "push" from the proximal side toward the heme center could promote the formation of an $Fe^{3+}$-$O_2^-$ -like species and thus hinder the dissociation of $O_2$ from the $Fe^{2+}$-$O_2$ complex. The M86E DHP mutant designed in our previous study has a negative charge inserted near the neutral proximal His in the wt-DHP. Subsequently, Franzen and coworkers have shown that its redox potential is considerably lowered [from 202 mV to 112 mV (vs. SHE)] compared to the wild type, confirming the increased electron density on the heme iron of this mutant [18]. As expected, the $O_2$ affinity for this DHP mutant shows a significant increase by about five-fold while at the same time displaying an approximately three-fold increase in dehalogenase activity (Table 2.2). However, DHP

did not use this mutational strategy for its functional adaptation, presumably because the gains by this alteration may still not be beneficial enough. However, in making such an interpretation it should be considered that this mutation was done on DHP, which has already an adapted $O_2$ affinity.

*Effect of the Rotational Position of the Proximal His89*

Comparing the heme coordination structures of DHP and Mb, a roughly 60° rotation of the proximal His imidazole ring (Figure 2.5) has been found and is believed to play an essential role in the peroxidase function of DHP [5, 10]. This factor might also influence the $O_2$ binding ability of DHP as the rotation of the proximal His has also been seen to affect $O_2$ affinity in heme proteins [21, 22]. One example is soybean leghemoglobin-a (Lba) which exhibits ~20-fold higher $O_2$ affinity than SW Mb. The proximal His of Lba is in the "staggered" conformation in which the His plane aligns with a line that goes through the center of the two perpendicular intersecting lines going through two sets of diagonal pyrrole nitrogen-nitrogen. (Figure 2.7, B). In contrast, the proximal His of SW Mb is in "eclipsed" conformation (with the His plane aligning with a line that goes through two opposite pyrrole nitrogens) [41]. The "staggered" conformation favors ligand binding with higher affinity than the eclipsed one via an electronic effect [38, 39]. Therefore this 45° rotation of the proximal His in Lba compared to that in Mb is mainly responsible for its much higher $O_2$ affinity [21, 40-42].

H93K/T95H Mb was prepared in our previous study for the purpose of mimicking the positioning of the proximal His in DHP (*vide supra*) [10]. Although its crystal structure is not presently available, a model based on the DHP structure indicates that the

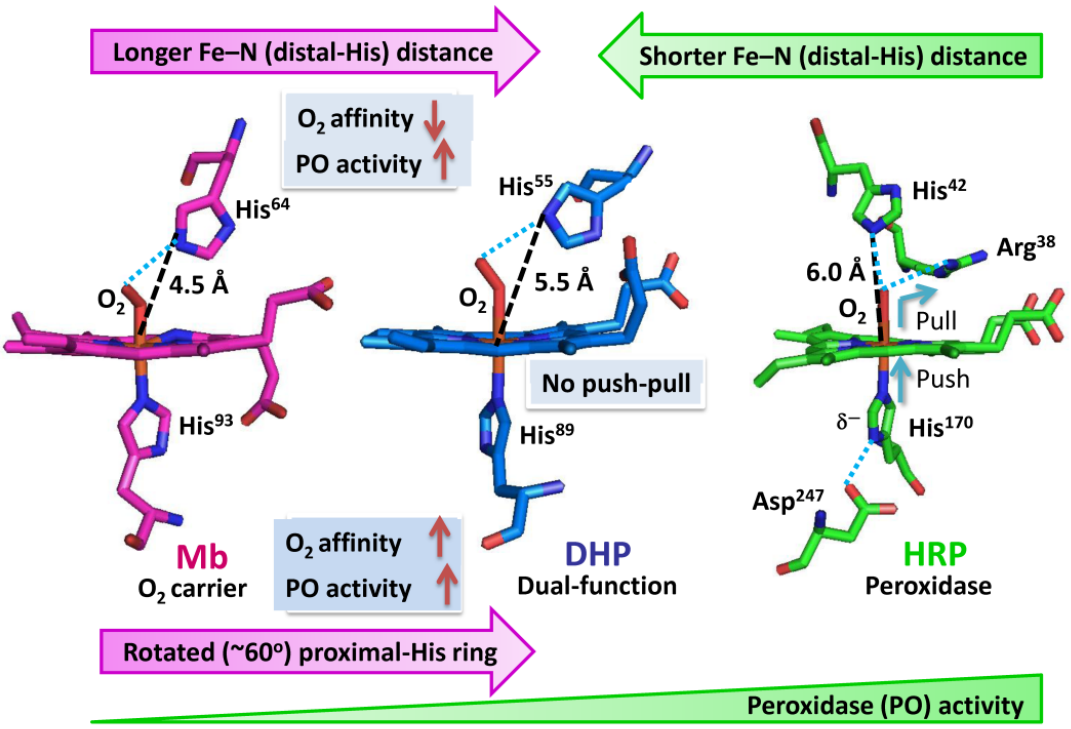


**Figure 2.5.** Schematic illustration showing the heme environmental structural differences between SW-Mb (left), DHP (middle) and HRP (right) in their $O_2$ complexes. In this illustration, the differences in their $O_2$ affinities (Mb vs. DHP) and in peroxidase activities (Mb, DHP and HRP) are shown to be correlated to the distal His to heme iron distances (black dashed lines), proximal His plane rotations relative to the porphyrin plane (Mb vs. DHP) and the absence (DHP)/presence (HRP) of the electron ‘‘push’’ (proximal His→heme iron) and ‘‘pull’’ (from heme iron toward distal Arg) mechanism. Cyan dotted lines indicate hydrogen bonds. Note that the Fe-O-O bond angle in the HRP-$O_2$ [47] complex is similar to that in the Mb or DHP complex, but looks linear (180°) in this illustration due to the projection angle chosen. Also note that $O_2$ binding to ferrous HRP is essentially irreversible, i.e., HRP heme-bound dioxygen is not dissociable presumably because of its interaction with the positively charged distal Arg38 [48]. The PDB access codes for the structures of oxy-Mb, -DHP and HRP are 1a6m, 4kjt (this paper) and 1h57 [47], respectively.

proximal His in this mutant is rotated about 60° from the eclipsed conformation (Figure 2.7, C vs. A). This is a conformation that favors ligand binding with high affinity. Indeed, this mutant exhibits ~ 20-fold higher $O_2$ affinity than that of wt-Mb (Table 2.4), which in turn supports the structural model for the mutant, along with ~ 50-fold increase in peroxidase activity as reported previously [10] (see also Table 2.4). These remarkable increases in both $O_2$ affinity and dehaloperoxidase activity by the H93K/T95H double mutation in Mb explain reasonably well why DHP has adapted its proximal His plane to a position that is rotated about 60° from the eclipsed conformation (Figure 2.7, C). The $K_{O2}$ data obtained in this study give more importance to this rotation, which not only markedly increases peroxidase function but also helps maintain moderate $O_2$ binding affinity by sufficiently compensating for the weakened $O_2$ affinity as a consequence of the longer distal His $N^{\varepsilon}$ – heme iron distance.

*Effects of Distal His-55 Flexibility: Oxygen Affinity of T56G DHP and Effects of the Substrate TCP and Inhibitor 4-BP*

As discussed above, the flexibility and location of the distal His55 in DHP are key determinants for both $O_2$ binding and enzymatic activity. The Thr56 adjacent to the distal His55 is likely to affect the flexibility of the distal His, and thus we would expect to see significant effects on the functions of DHP by changing this residue. By replacing Thr56 in DHP with much smaller-sized Gly that is found in Mb next to the distal His-64 (Figure 2.1 B), the distal His55 is expected to gain more mobility. Although we could not crystallize this mutant and thus its crystal structure is not available, the analysis of the molecular dynamics simulations very recently reported indicates that in T56G DHP, the distal His is further away from the heme iron and much more flexible than in the wild

type [43]. This might explain the ~ 3.4-fold higher $k_{cat}$ for this mutant than wt-DHP (Table 2.4). With respect to the $O_2$ affinity for this mutant, the $K_{O2}$ value is ~2.4-fold larger (i.e., the $O_2$ affinity is lower) than that for the wild type (Table 2.4). These results are consistent with the trend that "the longer the Fe-$N^{\varepsilon}$ distance, the greater the peroxidase activity [10] and the lower the $O_2$ affinity (this study)".

Recently, D'Antonio and Ghiladi proposed an mechanism for TCP-triggered DHP functional switching from oxy-ferrous globin to ferric peroxidase by $H_2O_2$ [9]. In this study, an assumption was made that TCP triggers the functional switching by destabilizing the bound $O_2$ in the oxy-ferrous DHP. To test this assumption, we examined the effect of substrate (TCP) or inhibitor (4-BP) on the $O_2$ affinity of the wt- and T56G DHP. As shown in Table 2.4, the addition of either 2 mM TCP or 4-BP barely altered the $K_{O2}$ of wt-DHP. However, the $O_2$ affinity of T56G DHP becomes almost two-fold higher and about 1.5-fold lower on addition of 2 mM TCP and 2 mM 4-BP, respectively.

The different effects of TCP/4-BP on $O_2$ affinity of these two proteins can be partially explained by the following spectrophotometric study probing the TCP binding mode to ferric T56G DHP. Firstly, the binding affinity for ferric T56G DHP (pH 7.0, 4 ˚C) is almost 20-fold higher than that of wt-DHP ($K_d$ = ~ 3 μM vs. 58 μM, this study), suggesting a different TCP binding mode in T56G DHP than in the wild type. Secondly, while TCP binding barely affects the bound distal water ligand of the ferric wt-DHP [10], the UV-Vis and MCD spectra of the TCP-bound T56G DHP closely resembles those of wt-DHP•acetate complex in the ferric state (Figure 2.6), indicating an anionic oxygen ligand instead of water. Since no carboxylate-containing amino acid groups are available in the DHP heme vicinity as a candidate to become a heme ligand (distal side Asp54 is

located > 10 Å away from the wt-DHP heme iron), the distal ligand in the TCP-bound T56G DHP is perhaps the hydroxide ion stabilized by the interaction with the TCP hydroxyl group. Such interaction between TCP and heme ligand has also been seen in the ferric L100F DHP•TCP complex where a water molecule bound to the heme Fe is also found hydrogen bonded to the TCP hydroxyl group [31]. Based on the above findings, we propose that the higher $O_2$ affinity of T65G DHP•TCP than T65G DHP observed in this study is likely due to the hydrogen bond formed between the TCP hydroxyl group and $O_2$ ligand, while such a hydrogen bond is absent in the wild type. Further discussion about the likely binding modes in the substrate TCP and inhibitor 4-BP complexes of oxy- and ferric T56G DHP and L100F DHP mutants vs. wt-DHP is found in the Supplementary Information.

*Implications of the Effects of TCP on the $O_2$ Affinity of DHP for the Functional Switch Mechanism*

Our group previously proposed a functional switching mechanism for the conversion of DHP from an $O_2$ carrier to a peroxidase that is mediated by TCP radical generated by $H_2O_2$ and a trace amount of ferric DHP in the oxy-DHP sample [7]. Subsequently, D'Antonio and Ghiladi proposed an alternative mechanism [9], in which substrate (2,4,6-TXP) binding causes a tautomerization of the distal H55 that destabilizes the bound dioxygen and thus shifts the equilibrium towards deoxyferrous DHP. Deoxyferrous DHP then reacts with $H_2O_2$ to form the catalytically active ferryl species Cpd II [9]. Such reactions of ferrous heme proteins with $H_2O_2$ to yield ferryl species are known [44-46]. However, the results demonstrated in this study indicate that the binding of TCP to DHP barely affects its dioxygen affinity, suggesting an alternative role of TCP in the functional

switching such as a reductant. In fact, we have very recently obtained evidence that supports our previous proposal that TCP radicals are indeed involved in the DHP functional switching mechanism [7] (S. Sun, M. Sono, J. Du, J. H. Dawson, manuscript in preparation).

## CONCLUSIONS

Since the major Hb in the terebellid polychaete *Amphitrite ornata* was discovered to also have a physiological peroxidase activity, studies of the mechanism of this globin-catalyzed oxidative reaction have been the focus of much attention [8]. As determined in this study, DHP has much lower $O_2$ affinity than SW Mb ($K_{O2(DHP)}$ = 3.23 μM vs. $K_{O2(Mb)}$ = 0.27 μM at 4˚C), which is reasonable because Mb functions in $O_2$ storage while DHP transports $O_2$ as a coelomic Hb [1]. As schematically illustrated in Figure 2.5, we found a trend of "the longer the distal His Fe-$N^{\varepsilon}$ distance, the greater the peroxidase activity (previous study [10]) and weaker the dioxygen binding ability" (this study) for Mb. These trends help explain the intermediate globin and peroxidase function of DHP compared to HRP and Mb. On the proximal side of DHP, our results suggest that the rotational position of the proximal His89 are quite essential to maintain a proper $O_2$ affinity for its Hb function. These results demonstrate how DHP has gained significantly enhanced enzymic (peroxidase) capability in its evolutional process for protection from toxic living environment without compromising its primary function as an $O_2$ carrier.

On another aspect, destabilization of the $O_2$ complex of ferrous wt-DHP (i.e., weakening of the $O_2$ affinity) was not seen in the presence of even at millimolar concentrations (up to 2 mM) of TCP. These results challenge the newly proposed

peroxidase cycle for DHP by D'Antonio and Ghiladi [9] in which the oxyferrous derivative is the starting state and the release of $O_2$ is the trigger to activate peroxidase activity.

**ACKNOWLEDGMENTS**

We thank Professor Yoshihito Watanabe (Nagoya University) for the sperm whale F43H/H64L Mb plasmid.

**REFERENCES**


[1] R.E. Weber, C. Mangum, H. Steinman, C. Bonaventura, B. Sullivan, J. Bonaventura, J., Comp. Biochem. Physiol. A: Physiology 56 (1977) 179-187.

[2] H.B. Dunford, Heme peroxidases, John Wiley New York:, 1999.

[3] E. Antonini, M. Brunori, Hemoglobin and Myoglobin in their Reactions with Ligands, North-Holland Publishing Company Amsterdam, 1971.

[4] K. Han, S.A. Woodin, D.E. Lincoln, K.T. Fielman, B. Ely, Mar. Biol. 3 (2001) 287-292.

[5] L. Lebioda, Cell. Mol. Life Sci. 57 (2000) 1817-1819.

[6] M.W. LaCount, E. Zhang, Y.P. Chen, K. Han, M.M. Whitton, D.E. Lincoln, S.A. Woodin, L. Lebioda, J. Biol. Chem. 275 (2000) 18712-18716.

[7] J. Du, M. Sono, J.H. Dawson, Biochemistry 49 (2010) 6064-6069.

[8] S. Franzen, M.K. Thompson, R.A. Ghiladi, Biochim. Biophys. Acta 1842 (2012) 578-588.

[9] J. D'Antonio, R.A. Ghiladi, Biochemistry 50 (2011) 5999-6011.

[10] J. Du, X. Huang, S. Sun, C. Wang, L. Lebioda, J.H. Dawson, Biochemistry 50 (2011) 8172-8180.

[11] R.L. Osborne, G.M. Raner, L.P. Hager, J.H. Dawson, J. Am. Chem. Soc. 128 (2006) 1036-1037.

[12] S. Sumithran, M. Sono, G.M. Raner, J.H. Dawson, J. Inorg. Biochem. 117 (2012) 316-321.

[13] J.S. Olson, G.N. Phillips Jr, J. Biol. Inorg. Chem. 2 (1997) 544-552.

[14] F. Cutruzzolà, C.T. Allocatelli, P. Ascenzi, M. Bolognesi, S.G. Sligar, M. Brunori, FEBS Lett. 282 (1991) 281-284.

[15] W. Tian, J. Sage, P. Champion, J. Mol. Biol. 233 (1993) 155-166.

[16] H. Ishikawa, T. Uchida, S. Takahashi, K. Ishimori, I. Morishima, Biophys. J. 80 (2001) 1507-1517.

[17] F. Draghi, A.E. Miele, C. Travaglini-Allocatelli, B. Vallone, M. Brunori, Q.H. Gibson, J.S. Olson, J. Biol. Chem. 277 (2002) 7509-7519.

[18] E.L. D'Antonio, J. D'Antonio, V. de Serrano, H. Gracz, M.K. Thompson, R.A. Ghiladi, E.F. Bowden, S. Franzen, Biochemistry 50 (2011) 9664-9680.

[19] S. Franzen, J. Am. Chem. Soc. 123 (2001) 12578-12589.

[20] D.B. Goodin, D.E. McRee, Biochemistry 32 (1993) 3313-3324.

[21] S.S. Narula, C. Dalvit, C.A. Appleby, P.E. Wright, Eur. J. Biochem. 178 (1988) 419-435.

[22] L. Capece, M.A. Marti, A. Crespo, F. Doctorovich, D.A. Estrin, J. Am. Chem. Soc. 128 (2006) 12455-12461.

[23] D.P. Nelson, L.A. Kiesow, Enthalpy of decomposition of hydrogen peroxide by catalase at 25°C (with molar extinction coefficients of H2O2 solutions in the UV), DTIC Document, 1972.

[24] K.G. Paul, H. Theorell, A. Akeson, Acta Chem. Scand. 7 (1953) 1284-1287.

[25] R. Makino, I. Yamazaki, Arch. Biochem. Biophys. 165 (1974) 485-493.

[26] C. Giulivi, E. Cadenas, FEBS Lett. 332 (1993) 287-290.

[27] F.J. Millero, F. Huang, A.L. Laferiere, Marine. Chem. 78 (2002) 217-230.

[28] J. Robinson, J.M. Cooper, Anal. Biochem. 33 (1970) 390.

[29] L.G. Oberg, K.G. Paul, Biochim Biophys Acta 842 (1985) 30-38.

[30] A.M. Huff, C.K. Chang, D.K. Cooper, K.M. Smith, J.H. Dawson, Inorg. Chem. 32 (1993) 1460-1466.

[31] C. Wang, L.L. Lovelace, S. Sun, J.H. Dawson, L. Lebioda, Biochemistry 52 (2013) 6203-6210.

[32] V. de Serrano, J. D'Antonio, S. Franzen, R.A. Ghiladi, Acta Crystallogr. D Biol Crystallogr. 66 (2010) 529-538.

[33] M. Sono, T. Asakura, J. Biol. Chem**.** 250 (1975) 5227-5232.

[34] T. Matsui, S. Ozaki, Y. Watanabe, J. Biol. Chem**.** 121 (1999) 9952-9957.

[35] A. Plummer, M.K. Thompson, S. Franzen, Biochemistry 52 (2013) 2218-2227.

[36] T. Shibata, D. Matsumoto, R. Nishimura, H. Tai, A. Matsuoka, S. Nagao, T. Matsuo, S. Hirota, K. Imai, S. Neya, Inorg. Chem. 51 (2012) 11955-11960.

[37] M.J. Carter, D.P. Rillema, F. Basolo, J. Am. Chem. Soc. 96 (1974) 392-400.

[38] D. Barrick, Biochemistry 33 (1994) 6546-6554.

[39] W.R. Scheidt, D.M. Chipman, J. Am. Chem. Soc. 108 (1986) 1163-1167.

[40] S.J. Smerdon, S. Krzywda, A.J. Wilkinson, R.E. Brantley Jr, T.E. Carver, M.S. Hargrove, J.S. Olson, Biochemistry 32 (1993) 5132-5138.

[41] S. Kundu, B. Snyder, K. Das, P. Chowdhury, J. Park, J.W. Petrich, M.S. Hargrove, Proteins 46 (2002) 268-277.

[42] E. Harutyunyan, T. Safonova, I. Kuranova, A. Popov, A. Teplyakov, G. Obmolova, A. Rusakov, B. Vainshtein, G. Dodson, J. Wilson, J. Mol. Biol. 251 (1995) 104-115.

[43] S. Jiang, I. Wright, P. Swartz, S. Franzen, Biochim. Biophys. Acta 1834 (2013) 2020-2029.

[44] K.D. Whitburn, Arch. Biochem. Biophys. 253 (1987) 419-430.

[45] A.I. Alayash, B.A.B. Ryan, R.F. Eich, J.S. Olson, R.E. Cashon, J. Biol. Chem. 274 (1999) 2029-2037.

[46] A.E. Pond, G.S. Bruce, A.M. English, M. Sono, J.H. Dawson, Inorg. Chim. Acta 275 (1998) 250-255.

[47] G.I. Berglund, G.H. Carlsson, A.T. Smith, H. Szöke, A. Henriksen, J. Hajdu, Nature 417 (2002) 463-468.

[48] J. N. Rodriguez-Lopez, A. T. Smith, R. N. F. Thorneley, J. Biol. Chem. 272 (1997) 389-395.

**SUPPORTING INFORMATION**

***Binding modes for the substrate TCP and inhibitor 4-BP complexes of oxy- and ferric T56G DHP and L100F DHP mutants vs. wt-DHP***

Spectrophotometric titrations for TCP binding to ferric T56G DHP (not shown) and wt-DHP (see [S1] for a similar titration) and spectral (UV-Vis and MCD) characterizations of the resulting complexes suggest that the two proteins have distinct binding modes (positions and locations) for TCP (Figure 2.6). The resulting absorption and MCD spectra of TCP-bound ferric T56G DHP (Figure 2.6, red solid line) closely resemble those of the acetate complex of ferric wt-DHP (at pH 5.4, black dotted line in Figure S1) and Mb (at pH 7, blue dashed line in Figure S1), both reported previously [S1]. Furthermore, the binding affinity for the TCP complex of T56G DHP (pH 7.0, 4 ˚C) is found to be extremely high ($K_d$ = ~ 3 μM, this study).

Previously, two modes of TCP binding were observed in crystallographic studies: one "internal", deep within the distal cavity, the other "external" with a TCP molecule blocking access to the distal cavity and hindering ligand binding to the heme iron [S3]. Both TCP binding modes are different from the 4-XP binding mode [S4]. The TCP binding mode observed in crystals depended on DHP mutant studied and even in some cases was different in the subunits of the DHP dimer. On the other hand the very high TCP concentration used, 200 mM (in 50/50 v/v water/ethanol), makes it unlikely that another TCP binding site in the studied proteins (DHP, Y34N, Y34N/S95G and L100F) exists [S3]. At lower concentrations, such as 2 mM, TCP binding in crystals was below the observation threshold. TCP functions as a substrate with a $K_M$ of about 0.5 mM because its affinity for Compound I is higher than for DHP [S3]. Similar conclusion was

reached for Mb based on inhibition studies of its dehaloperoxidase activity by phenol [S5]. Ferric T65G DHP has TCP affinity much higher than any other DHP variant studied so far. It is highly unlikely that the TCP mode of binding is external because this mode locks the dioxygen binding site while T65G oxygen affinity in the presence of TCP is higher than in its absence. Much more plausible is that T65G DHP•TCP complex resembles L100F DHP•TCP and wt DHP•TBP complexes in which the internal binding mode is observed [S3, S6].

The L100F•TCP structure allows more in depth mechanistic analysis because the TCP occupancy is high while in the reported DHP•TBP structure it is low, only 10%. In the L100F DHP•TCP complex there is a water molecule bound to the heme Fe and hydrogen bonded to the TCP hydroxyl. Although there is some overlap of the TCP hydroxyl positions in L100F DHP•TCP and the position of the distal atom of the dioxygen molecule in the reported here L100F DHP•$O_2$ structure (Figure 2.5), only a minor adjustment of the TCP position or tilting the $O_2$ molecule is needed to eliminate the hindrance. Also, the likely hydrogen bond between the hydroxyl and dioxygen can explain the higher $O_2$ affinity of T65G DHP•TCP than T65G DHP as observed in this study, the assumption that the T65G•TCP complex is similar to the L100F DHP•TCP complex would suggest a water molecule as the distal ligand in the ferric state.

[S1] J. Du, X. Huang, S. Sun, C. Wang, L. Lebioda, J.H. Dawson, Biochemistry 50 (2011) 8172-8180.

[S2] J. Vojtěchovský, K. Chu, J. Berendzen, R.M. Sweet, I. Schlichting, Biophys. J. 77 (1999) 2153-2174.

[S3] C. Wang, L.L. Lovelace, S. Sun, J.H. Dawson, L. Lebioda, Biochemistry 52 (2013) 6203-6210.

[S4] M.W. LaCount, E. Zhang, Y.P. Chen, K. Han, M.M. Whitton, D.E. Lincoln, S.A. Woodin, L. Lebioda, J. Biol. Chem. 275 (2000) 18712-18716.

[S5] X. Huang, C. Wang, L.R. Celeste, L.L. Lovelace, S. Sun, J.H. Dawson, L. Lebioda, Acta Crystallogr. F Struct. Biol. Cryst. Commun. 68 (2012) 1465-1471.

[S6] J. Zhao, V. de Serrano, J. Zhao, P. Le, S. Franzen, Biochemistry 52 (2013) 2427-2439.

**Table 2.5.** $O_2$ affinities of wild-type Sperm Whale Mb and DHP in 100 mM potassium phosphate buffer (pH 7.0) at 4 °C and ~ 22 °C.

| Protein | $K_{O2}$ (μM) 4 °C, pH 7.0 | $K_{O2}$ (μM) ~ 22 °C, pH 7.0 |
|---|---|---|
| WT Mb | 0.27 ± 0.01 | 0.83 ± 0.06 |
| DHP | 3.23 ± 0.37 | 7.70 ± 0.45 |

**Table 2.6** Crystallographic data and refinement statistics for L100F DHP A-$O_2$ complex.

| | | |
|---|---|---|
| DHP complex<br>PDB code | | L100F•$O_2$<br>4kjt |
| X-ray source | | APS ID 22 |
| Wavelength (Å) | | 1.000 |
| Number of Frames | | 180 |
| Oscillation Range (degree) | | 1.0 |
| Temperature (K) | | 100 |
| Space group | | $P2_12_12_1$ |
| Unit cell dimensions | a (Å) | 59.128 |
| | b (Å) | 67.782 |
| | c (Å) | 68.132 |
| Volume (Å$^3$) | | 273061 |
| Mosaicity (deg.) | | 0.45 |
| Resolution range (Å)<br>(highest shell)[a] | | 47.8-1.44<br>(1.46-1.44) |
| Redundancy (highest shell) | | 6.9 (4.7) |
| Average I/σ(*I*) | | 15.0 |
| Total number of reflections | | 342270 |
| Number of unique reflections | | 47333 |
| Completeness (%) (hi. shell) | | 98.3 (68.9) |
| Total linear R-merge (hi. shell) | | 6.4 (33.2) |
| R-value (%) (highest shell) | | 13.3 (19.0) |
| $R_{free}$ -value (%) (highest shell) | | 18.0 (26.7) |
| *Ramachandran statistics*<br>*% of residues* | | |
| In most favored regions | | 94.0 |
| In additional allowed | | 6.0 |
| In generously allowed | | 0 |
| Average B factor for protein<br>Average B factor for solvent | | 19.0<br>36.3 |

**Table 2.7** Effects of TCP on $O_2$ affinity of T56G DHP in 100 mM potassium phosphate buffer (pH 7.0) at 4 °C. See the main text for the definitions of $K_L$ (isocyanide equilibrium dissociation constant) and $K_P$ ($O_2$/isocyanide partition constant).

| [TCP], mM | $K_{O2}$ (μM) 4 °C, pH 7.0 | $K_L$ (μM) and $K_p$ 4 °C, pH 7.0 | |
|---|---|---|---|
| 0.0 | 7.83 ± 0.83 | $K_L$ | 0.45 ± 0.03 |
| | | $K_p$ | 17.40 ± 0.92 |
| 0.4 | 6.17 ± 0.72 | $K_L$ | 0.46 ± 0.02 |
| | | $K_p$ | 13.42 ± 0.77 |
| 0.8 | 5.60 ± 0.33 | $K_L$ | 0.47 ± 0.02 |
| | | $K_p$ | 11.92 ± 0.98 |
| 2.0 | 4.23 ± 0.52 | $K_L$ | 0.43 ± 0.04 |
| | | $K_p$ | 9.83 ± 0.82 |

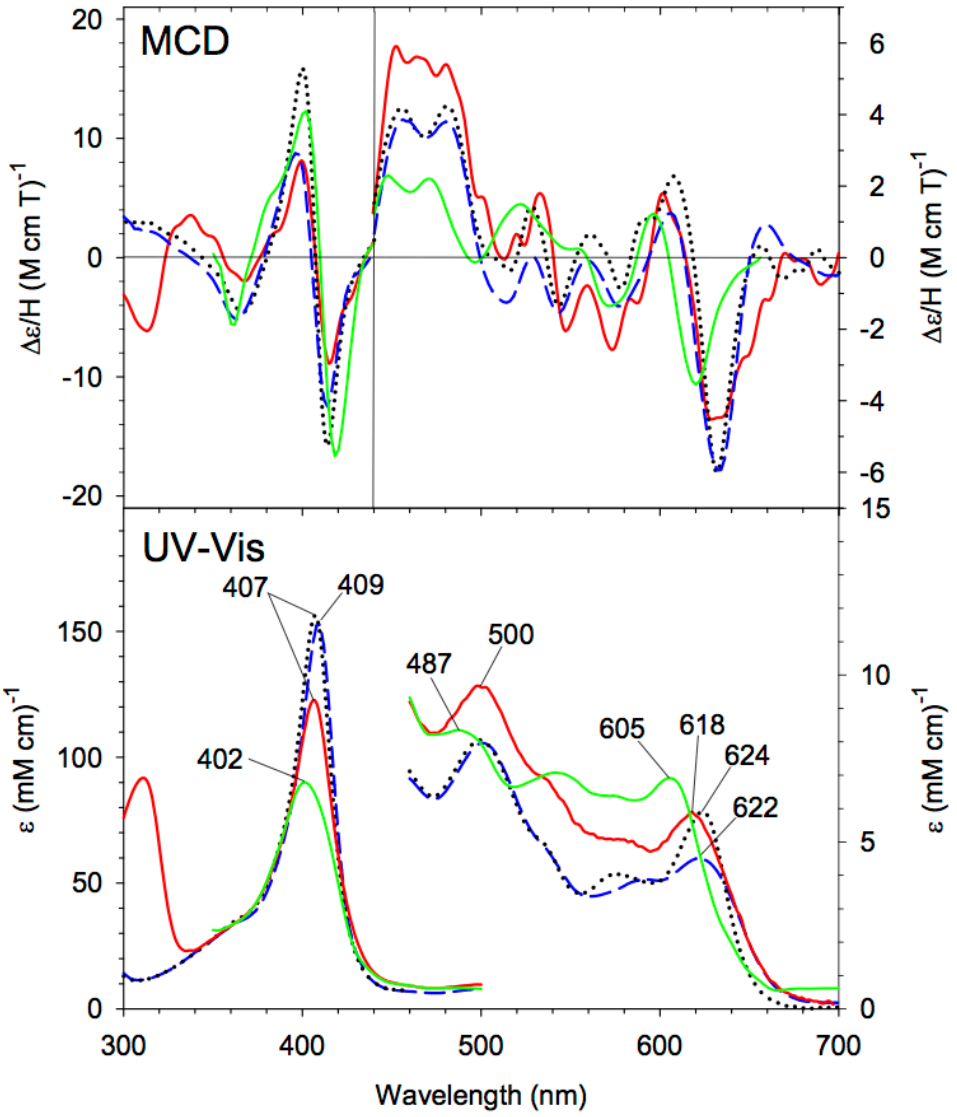


**Figure 2.6** MCD (top) and UV-Vis (bottom) absorption spectral of TCP-bound ferric T56G DHP (red solid line, 0.8 mM TCP) in 0.1 M potassium phosphate buffer pH 7.0, acetate-bound ferric DHP (black dotted line, 82 mM acetate) in 50 mM sodium citrate buffer pH 5.4 (re-plotted from [S1]), acetate-bound ferric Mb (blue dashed line, 6 M sodium acetate) in 0.1 M potassium phosphate buffer pH 7.0 (re-plotted from [S1]) and phenol-bound ferric Lba (green solid line) (replotted from [S2]). All spectra were recorded at 4°C.

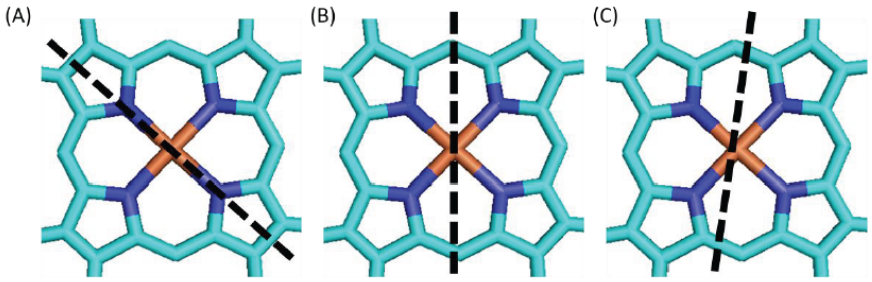


**Figure 2.7** Proximal histidine rotational positions in (A) SW Mb, (B) Soybean leghemoglobin (Lba) and (C) DHP. The dashed line is parallel to the plane of His ring (which is positioned perpendicular to the porphyrin plane, i.e., the plane of this paper), showing eclipsed (A) and staggered (B) conformations.

# CHAPTER 3

## Evidence for Direct Involvement of Substrate TCP Radical in Functional Switching from Oxyferrous $O_2$ Carrier to Ferric Peroxidase in the Dual Function Hemoglobin/dehaloperoxidase from *Amphitrite ornata*[2]

[2] Sun, S., Sono, M., Du, J. and Dawson, J. H. Submitted to *Biochemistry*, 03/06/2014.

**ABSTRACT**

The coelomic dioxygen binding hemoglobin dehaloperoxidase (DHP) from the sea worm *Amphitrite ornata* is a dual function heme protein that also possesses a peroxidase activity. Two different starting oxidation states are required for reversible $O_2$ binding (ferrous) and peroxidase (ferric) activity bringing into question how DHP manages the two functions. In our previous study, the co-presence of substrate 2,4,6-trichorophenol (TCP) along with $H_2O_2$ was found to be essential for activation of the enzymatically inactive oxyferrous DHP (oxy-DHP) state. Based on that study, a functional switching mechanism involving substrate radicals (TCP•) was proposed. To further support this mechanism, herein we report details of our investigations into the $H_2O_2$-mediated conversion of oxy-DHP to the ferric state triggered by both biologically relevant [TCP, 4-bromophenol (4-BP)] and non-relevant (ferrocyanide) compounds. We also find that all of these conversion reactions are completely inhibited by the presence of ferric heme ligands (KCN, imidazole), indicating an involvement of the ferric oxidation state. Furthermore, the spin-trapping reagent 5,5-dimethyl-1-pyrroline-N-oxide (DMPO) effectively inhibits the TCP/4-BP (but not ferrocyanide)-triggered oxy- to ferric conversion of DHP. Taken together, the results demonstrate that substrate TCP triggers the activation of oxy-DHP into a catalytically active peroxidase through direct oxidation by TCP radicals that are generated and start to accumulate upon $H_2O_2$-oxidation of TCP catalyzed by trace amounts of ferric DHP initially present in the oxy-DHP sample. The data presented herein further address the mechanism of how the halophenolic substrate triggers the activation of hemoglobin DHP into a peroxidase.

## INTRODUCTION

Dehaloperoxidase (DHP) from the terebellid polychaete *Amphitrite Ornata* is a dual-functional dioxygen-binding hemoglobin that also exhibits peroxidase activity. As the most abundant protein in this worm [1], DHP mainly functions as an $O_2$ carrier globin. It is isolated in the oxyferrous state [1] and has a moderate $O_2$ affinity ($K_{O2}$) at 5.1~7.7 μM (22 °C) [2, 3]. As a peroxidase, ferric DHP catalyzes the $H_2O_2$-dependent oxidative dehalogenation of 2,4,6-trihalophenol (TXP) substrates to the corresponding 2,6-dihaloquinone (DXQ) (where X = Cl and Br), providing *A. ornata* with protection against toxic halophenols that are excreted by another inhabitant, *Notomastus lobatus*, in its living environment [4, 5]. The dehaloperoxidase reaction mechanism is similar to that of horseradish peroxidase (HRP)- or chloroperoxidase (CPO)-catalyzed oxidation that involves two consecutive one-electron oxidations of TXP to TXP radical by two high-valent (ferryl) oxidants Cpd I/ Cpd ES and Cpd II (Scheme 3.1) [6-12]. The TXP radicals generated in the catalytic cycle then form the final product DXQ, possibly by either disproportionation or further enzymatic one-electron oxidation of the radicals, followed by hydration [13, 14]. Kinetic studies have shown that at pH 5.4, DHP catalyzes dechlorination of 2,4,6-trichlorophenol (TCP) at rates ($k_{cat}$) ~33 times slower than HRP but ~13 times faster than myoglobin (Mb) [4, 15]. The moderate peroxidase activity of DHP arises from several structural adaptations it has acquired during its evolution from an ancient $O_2$ carrier with its proximal neutral histidine conserved [3, 16-18]. Besides TXP, the much less toxic monohalophenols (4-XP) are co-present in the *A. ornata* ecosystem [19, 20]. Although 4-bromophenol (4-BP) is apparently a competitive inhibitor

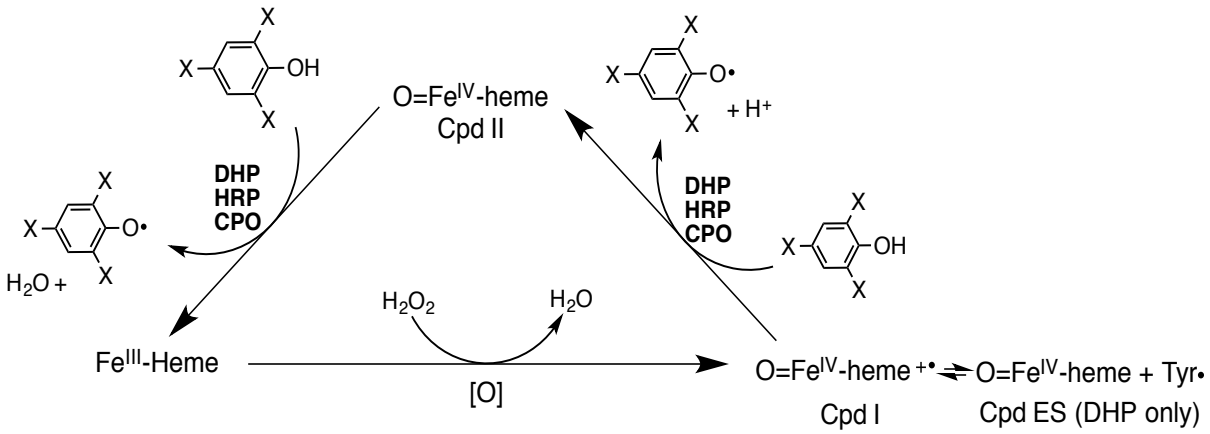


**Scheme 3.1.** Catalytic cycle for the peroxidase-catalyzed oxidative dehalogenation of 2,4,6-trihalophenol (TXP), adapted from[6].

for substrate TCP catalysis [21], it has been recently shown that 4-BP itself is also oxidized by DHP with slow yet measurable turnover [22]. DHP has two isozyme forms, DHP A and DHP B, encoded by two separate genes. They have very similar structures while only differing in five amino acids [1, 23, 24]. This study will focus on DHP A.

A major question arises as to how DHP will interconvert the different oxidation states of the heme required by these two functions, i.e., the ferrous state for the $O_2$ carrier role vs. the ferric state for the peroxidase activity. It has been shown that DHP can switch from the oxyferrous state to the ferric state via $H_2O_2$-oxidation, but this only occurs when substrate trihalophenol is present [25, 26]. The triggering mechanism has been disputed by two research groups. Our lab has proposed a direct oxidation of the oxyferrous heme to the ferric state by substrate TCP radicals (TCP•) that are initially generated via oxidation of TCP by the peroxidase reaction of $H_2O_2$ in the presence of trace amounts of ferric DHP that exist in the oxyferrous protein sample [25]. Analogous results and mechanistic interpretations have been previously reported for the role of substrate radicals in the conversion of lignin peroxidase compound III (non-physiological oxyferrous state) to the active ferric enzyme [27, 28] On the other hand, Ghiladi and co-workers subsequently proposed that conversion of the ferrous state to the catalytically active species Cpd II initiated by $H_2O_2$ replacing the bound-$O_2$ upon substrate binding [26]. The latter mechanism is built on the experimental observation that Cpd II can be formed directly from deoxyferrous DHP by reaction with $H_2O_2$ alone [26]. However, such a reaction has only been demonstrated under anaerobic conditions. With $O_2$ bound to the ferrous heme, Cpd II DHP can not be formed upon addition of $H_2O_2$ [25, 26]. The lack of reactivity of oxy-ferrous DHP towards $H_2O_2$ in the absence of TXP may have

physiological significance since DHP primarily functions as an oxygen transport protein. The hypothesis of Ghiladi and co-workers that TCP binding triggers the formation of Cpd II by promoting the replacement of bound $O_2$ with $H_2O_2$ has been challenged by our recent $O_2$ affinity ($K_{O2}$) study of DHP in which we reported that the $K_{O2}$ value of DHP is barely affected by the presence of TCP [3].

To clarify the unsettled functional switching mechanism of DHP, i.e., the $H_2O_2$-mediated oxidation of oxyferrous to ferric DHP, we have further probed the role of TCP in activating the peroxidase function from the $O_2$-carrying ferrous state of DHP. We have found that not only the substrate TCP and inhibitor/substrate 4-BP, but also a structurally totally unrelated redox compound ferrocyanide, a known peroxidase substrate [29]. can trigger the functional switch. Furthermore, we have demonstrated that the ferric heme ligands imidazole (Im) and cyanide ($CN^-$) as well as a spin-trapping reagent 5,5-dimethyl-1-pyrroline-N-oxide (DMPO) each alone can completely inhibit the TCP-triggered conversion of oxyferrous to ferric DHP. These and additional data shown in this study are consistent with a direct oxidation of oxy-DHP to the ferric state by TCP radicals as the initial step in the activation of oxy-DHP for peroxidase function.

## MATERIALS AND METHODS

**Materials.** Reagent-grade chemicals (Aldrich, ACROS, Cayman, or Fisher) were used without further purification. HRP (type VI, Rz 2.7) was purchased from Sigma-Aldrich. Wild-type six-His-tagged DHP was expressed and purified as previously described [30]. Protein concentrations were determined by the pyridine hemochromogen method ($\varepsilon_{555}$ = 34.4 $M^{-1}$ $cm^{-1}$) and are the concentrations of the heme component. Homogeneous oxyferrous DHP was generated by addition of a slight excess of sodium

dithionite to isolated DHP followed by Biogel P6DG (BioRad) desalting column chromatography with 0.1 M potassium phosphate buffer (pH 7) at 4 °C [25].

All stock solutions of chemicals were freshly made before experiments. Concentration of $H_2O_2$ diluted from a 30% stock solution was confirmed spectrophotometrically ($\varepsilon_{240}$ = 39.4 $M^{-1}$ $cm^{-1}$) [31]. TCP and 4-BP stocks (10 mM) were made in a 50/50 (v/v) ethanol/deionized water mixture.

**Stopped-Flow UV-visible Spectrophotometric Studies.** Transient reactions and the detection of enzyme intermediates were performed on a stopped-flow spectrophotometer (1.0 cm path length, model SF-61 DX2; Hi-Tech Scientific, Salisbury, U.K.) at 4 °C in 100 mM potassium phosphate buffer (pH 7.0) in the single-mixing mode. The double-mixing mode has also been used only for generation of Cpd ES DHP and its reaction with substrates: Fe(III) DHP is first mixed with 1.2 equiv. $H_2O_2$ allowing for Cpd ES to be fully formed (age time, 15 s) and then mixed with substrates. Oxyferrous DHP at a final concentration of 5 μM alone or containing TCP, 4-BP or ferrocyanide was mixed with 1 or 5 equiv. of $H_2O_2$. Global analysis was performed using the Specfit Global Analysis software and fit to exponential functions as a two-step, three species irreversible mechanism.

**Bench-top Mixing Kinetics Assays.** The inhibition reactions were monitored using a Cary 400 UV-visible spectrophotometer in a 1.0 cm path length cuvette at 4 °C. The oxy-DHP concentration in each sample was 5 μM in 100 mM potassium phosphate buffer (pH 7.0). The substrates (TCP, 4-BP or potassium ferrocyanide) and inhibitors (Im or $CN^-$) were first mixed with oxy-DHP in phosphate buffer (total volume 0.7 ml) and incubated for 3 min in the cuvette. Subsequently, $H_2O_2$ solution (a few μl) was added to

the cuvette to initiate the reaction.

**GC-MS Analyses.** A HP-5890 Restek RTX-5 GC capillary column (30 m × 0.32 mm) was used for detection of the products extracted from aqueous solution by ethyl acetate. The initial temperature of the column was set at 50 °C for 2 min, and the temperature was subsequently increased at a rate of 10 °C/min up to a final temperature of 300 °C and held for 10 min. MS detection was in the electron impact (EI) ionization mode, and a VG70S mass spectrometer scanning from 50 to 450 amu was used for product identification.

## RESULTS

**TCP/$H_2O_2$-triggered conversion of oxy-DHP to the ferric state.** In our previous study, we demonstrated that conversion of oxy-DHP (5 μM) to the ferric enzyme requires co-presence of the substrates TCP and $H_2O_2$ using excess TCP (150 μM, 30 equiv.) and 1 or 0.5 equiv. of $H_2O_2$ [25]. During the conversion, an absorption spectral change with a single set of isosbestic points (412, 528, 592 nm) was observed, suggesting that no detectable intermediates are involved. To further probe the conversion mechanism, we have performed more detailed investigations in this study on the activation reaction with [oxy-DHP]:[$H_2O_2$]:[substrate] = 1 : 1 : 1. Figure 3.1A shows that in the presence of 1 equiv. of TCP, 1 equiv. of $H_2O_2$ readily converts oxy-DHP [417 (Soret), 542 and 578 nm] to the ferric state [407 (Soret), 503 and 635 nm] within 450 s reaction time. Under these conditions, the spectral changes exhibit three sets of isosbestic points indicating that another enzyme species is involved as an intermediate during the conversion.

The three sets of isosbestic point in Figure 3.1A are nearly identical to those for oxy-DHP/Cpd ES (394, 586 nm), Cpd ES/ferric (414, 611 nm) and oxy-DHP/ferric DHP

(412, 591 nm) based on overlaid normalized absorption spectra of these three DHP species (Figure 3.6A), indicating that ferryl DHP is formed as an intermediate in the reaction. The difference between the isosbestic point seen at 394 nm for oxy-DHP/Cpd ES in Figure 3.6A and the actual isosbestic point at 404 nm in the time-dependent spectral changes (Figure 3.1A) can be explained by simulated spectral changes for the three DHP forms (Figure 3.7B) that yield a shifted (394 to 404 nm) position for this particular isosbestic point. This shift is probably observed because of the less than stoichiometric formation of ferryl DHP. The formation of the ferryl intermediate is also supported by the global analysis result for the above reaction as shown in Figure 3.1B [absorption peaks at 420 (Soret), 545 and 583 nm, green solid line], whose maximum amount reaches only ~45% of the total DHP concentration.

Based on the above assignment, the time-dependent absorption changes at two observed Soret isosbestic points (at 414 nm for Cpd ES/ferric DHP and 405 nm for oxy-DHP/Cpd ES) could represent the time-dependent disappearance of oxy-DHP (green diamond) and the appearance of ferric species (black circles), respectively, as shown in the Figure 3.1A, left panel inset. These spectral changes are coupled with the rise (absorption decrease) and decay (absorption increase) of the ferryl intermediate as indicated by the absorption changes at 412 nm, an isosbestic point for oxy-DHP/ferric DHP as a function of time (blue triangles in Figure 3.1A, left panel inset). A similar result in the visible region at 591 nm was also observed for the appearance (first phase) and disappearance (second phase) of the ferryl intermediate (blue triangles) as well as at 586 nm for the rise (absorption decrease) of ferric DHP (Figure 3.1A, right panel inset, black circles). We have calculated the apparent rate constant ($k_{obs}$) from the exponential

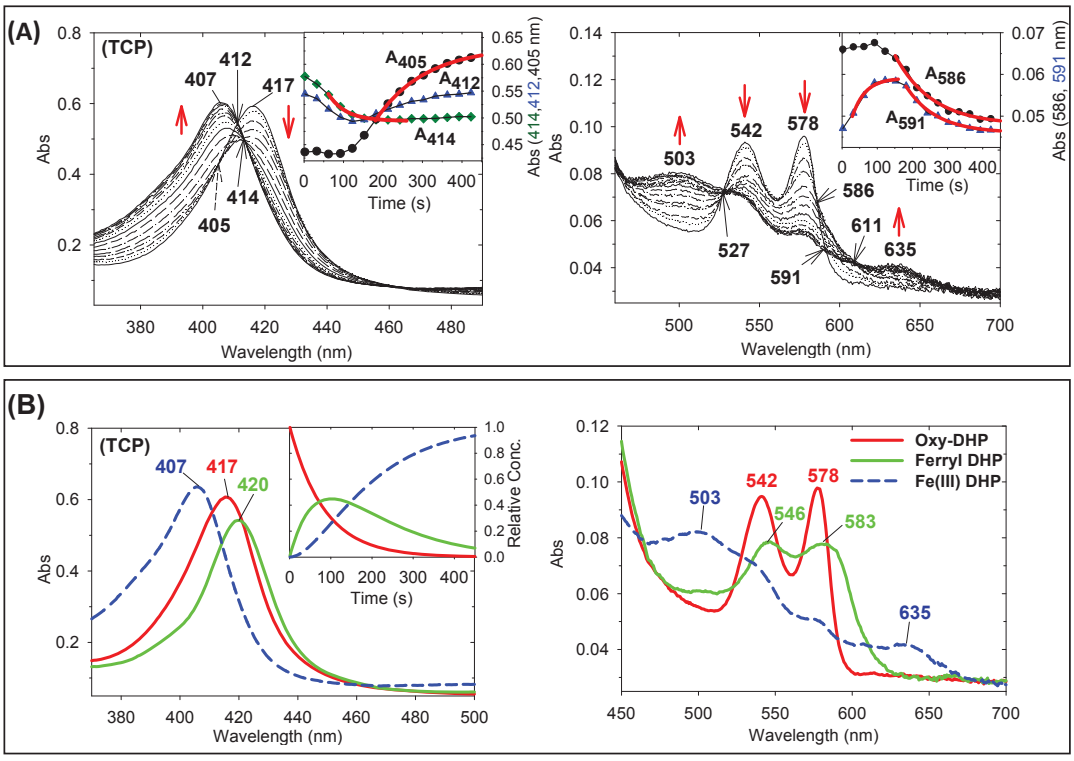


**Figure 3.1.** (A) Spectral change upon addition of 5 μM $H_2O_2$ to 5 μM oxyferrous DHP in the presence of 5 μM TCP. The insets in panel A show time-dependent absorbance changes at particular isosbestic points indicated to monitor disappearance of oxy-DHP (green diamonds), appearance of ferric DHP (black circles) and rise and decays of ferryl (Cpd ES) DHP (blue triangles). The red bold lines on the traces show exponential fits for the indicated time ranges and calculated apparent first-order rate constants. (B) UV-visible spectra of oxyferrous (red solid line), ferryl (green solid line) and ferric (blue dashed line) DHP obtained from global analysis of the data in panel A. The inset in panel B shows the relative concentration profile determined by the global analysis.

part (bold red lines) of these absorption changes for oxy-DHP disappearance [(2.3 ± 0.1) × $10^{-2}$ $s^{-1}$ ($A_{414}$)], ferric DHP appearance [(8.4 ± 0.1) × $10^{-3}$ $s^{-1}$ ($A_{405}$) or (9.4 ± 0.2) × $10^{-3}$ $s^{-1}$ ($A_{586}$), both considered practically identical], ferryl DHP appearance [(2.7 ± 0.1) × $10^{-2}$ $s^{-1}$ ($A_{591}$)] and ferryl DHP disappearance [(1.2 ± 0.1) × $10^{-2}$ $s^{-1}$ at ($A_{591}$)]. Even though these $k_{obs}$ values were obtained under the non-pseudo-first-order reaction conditions, the reaction traces nicely fit exponential decays or emergences of the three species and thus these values can provide a convenient way to estimate the true second-order rate constants ($k$) based on $k_{obs} = \sim k[TCP]_o$ or $\sim k[H_2O_2]_o$, where $[TCP]_o$ and $[H_2O_2]_o$ are the initial concentrations of TCP and $H_2O_2$, respectively [32]. The $k_{obs}$ values thus obtained may be useful, in evaluating the relative rates among different reactions in order to interpret the reaction mechanisms as done in this study. Note that the rise of the ferryl DHP species starts slowly with an apparent lag time period before its formation rate reaches a maximum (see Figure 3.1A insets, blue triangles) suggesting that there is yet another species is being formed prior to the formation of ferry l DHP (vide infra).

**$H_2O_2$-mediated conversion of oxy-DHP to ferric DHP triggered by 4-BP or ferrocyanide / ferricyanide.** Reactions of oxy-DHP with $H_2O_2$ in the presence of 4-BP are shown in Figure 3.2A. The maximum activation rate in the presence of excess 4-BP (150 μM) is (2.3 ± 0.1) × $10^{-2}$ $s^{-1}$, which is as fast as the conversion triggered by 1 equiv. of TCP [(2.3 ± 0.1) × $10^{-2}$ $s^{-1}$, Figure 3.1A]. In the presence of only 1 equiv. of 4-BP, the rate is considerably slower [(6.9 ± 0.5) × $10^{-3}$ $s^{-1}$, Figure 3.7A] compared with TCP by ~3.4-fold. Underivatized phenol is also able to induce the $H_2O_2$-oxidation of oxy-DHP at a comparable rate [(3.1± 0.1) × $10^{-2}$ $s^{-1}$, at 150 μM, Figure 3.7B].

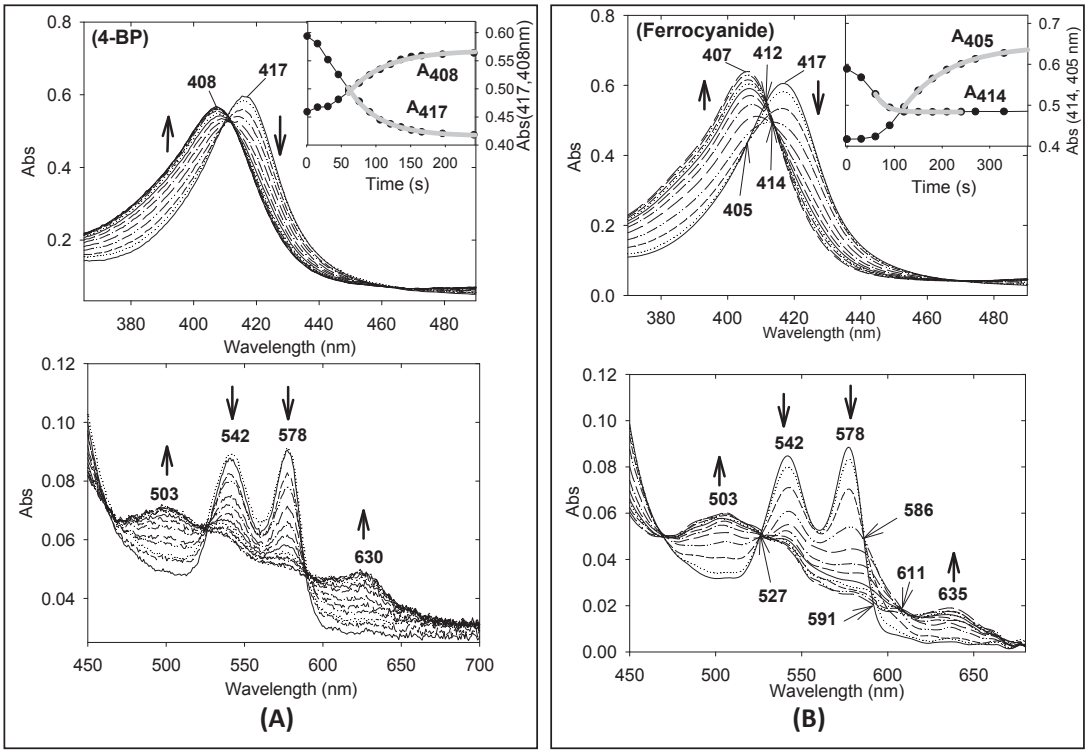


**Figure 3.2.** Spectral change upon addition of 5 μM $H_2O_2$ to 5 μM oxyferrous DHP in the presence of (A) 150 μM 4-BP or (B) 5 μM potassium ferrocyanide. The insets in the top part of both panels show the time-dependent absorbance changes at selected isosbestic points to monitor the disappearance of oxy-DHP [417 nm (A) and 414 nm (B)], or the appearance of ferric DHP [408 nm (A) and 405 nm (B)]. The gray bold lines on the traces show exponential fits for the indicated time ranges. Apparent first-order rate constants ($k_{obs}$) obtained from the fits are $2.3 \times 10^{-2}$ $s^{-1}$ ($A_{417}$) and $1.9 \times 10^{-2}$ $s^{-1}$ ($A_{408}$) in panel A and $4.8 \times 10^{-2}$ $s^{-1}$ ($A_{414}$) and $1.0 \times 10^{-2}$ $s^{-1}$ ($A_{405}$) in panel B.

Surprisingly, ferrocyanide, a known peroxidase substrate[29] with a structure that is totally different from DHP substrates, can also trigger the functional switch of oxy-DHP. Figure 3.2 B shows that in the presence of 1 equiv. of ferrocyanide, oxy-DHP quickly switches to the ferric state upon reaction with 1 equiv. $H_2O_2$. The spectral change for ferrocyanide-triggered conversion of oxy-DHP is not significantly different from that for TCP-triggered one, except that the rate is about twice greater [$(4.8 \pm 0.2) \times 10^{-2}$ $s^{-1}$ vs. $(2.3 \pm 0.1) \times 10^{-2}$ $s^{-1}$] under the same conditions. A similar conversion has also been seen in the presence of another structurally unrelated compound, potassium iodide (KI), but only at acidic pH (data not shown). In fact, iodide is known to be a reductant (substrate) for HRP Cpd I preferably at acidic pH values [12]. The apparent conversion rates, $k_{obs}$ values, of oxy-DHP triggered by various substrates discussed here are listed in Table 3.1.

TCP and ferrocyanide presumably trigger the switch of oxy-DHP to the ferric state by serving as peroxidase substrates for the trace amount of ferric DHP in the oxy-DHP sample in the presence of $H_2O_2$. This would then generate TCP radical (TCP•) and ferricyanide, respectively, which, in turn, would serve as an oxidant to convert oxy-DHP to the ferric state. Thus, ferricyanide would serve the same role as TCP• in the switching mechanism. To directly test this hypothesis, we have monitored the spectral change for the reaction of oxy-DHP with 1.0 equiv. ferricyanide (in place of ferrocyanide) and 1.0 equiv. $H_2O_2$ as shown in Figure 3. Similar to the cases with TCP (Figure 3.1A) and ferrocyanide (Figure 3.2B), three sets of isosbestic points are observed as shown in Figure 3A and assigned to those for oxy-DHP/Cpd ES (586 nm), Cpd ES/ferric (414, 611 nm) and oxy-DHP/ferric DHP (412, 591 nm). Thus the change of oxy-, ferryl and ferric DHP species can be represented by the time course traces for 611, 591 and 586 nm,

**Table 3.1.** Apparent first-order reaction rate constants ($k_{obs}$) for conversion of oxy-DHP to ferric DHP triggered by various peroxidase substrates at pH 7.0, 4 °C. All rates are determined by analyzing the time-dependent absorbance changes at 414 (TCP and ferrocyanide) or 417 nm (4-BP and phenol) for the disappearance of oxy-DHP. Concentrations for oxy-DHP, $H_2O_2$ and substrates are all 5 μM.

| Substrate | $k_{obs}$ ($s^{-1}$) |
|---|---|
| TCP | $(2.3 \pm 0.1) \times 10^{-2}$ |
| 4-BP | $(6.9 \pm 0.5) \times 10^{-3}$ |
| Phenol | $(3.1 \pm 0.1) \times 10^{-2}$ |
| Ferrocyanide | $(4.8 \pm 0.2) \times 10^{-2}$ |

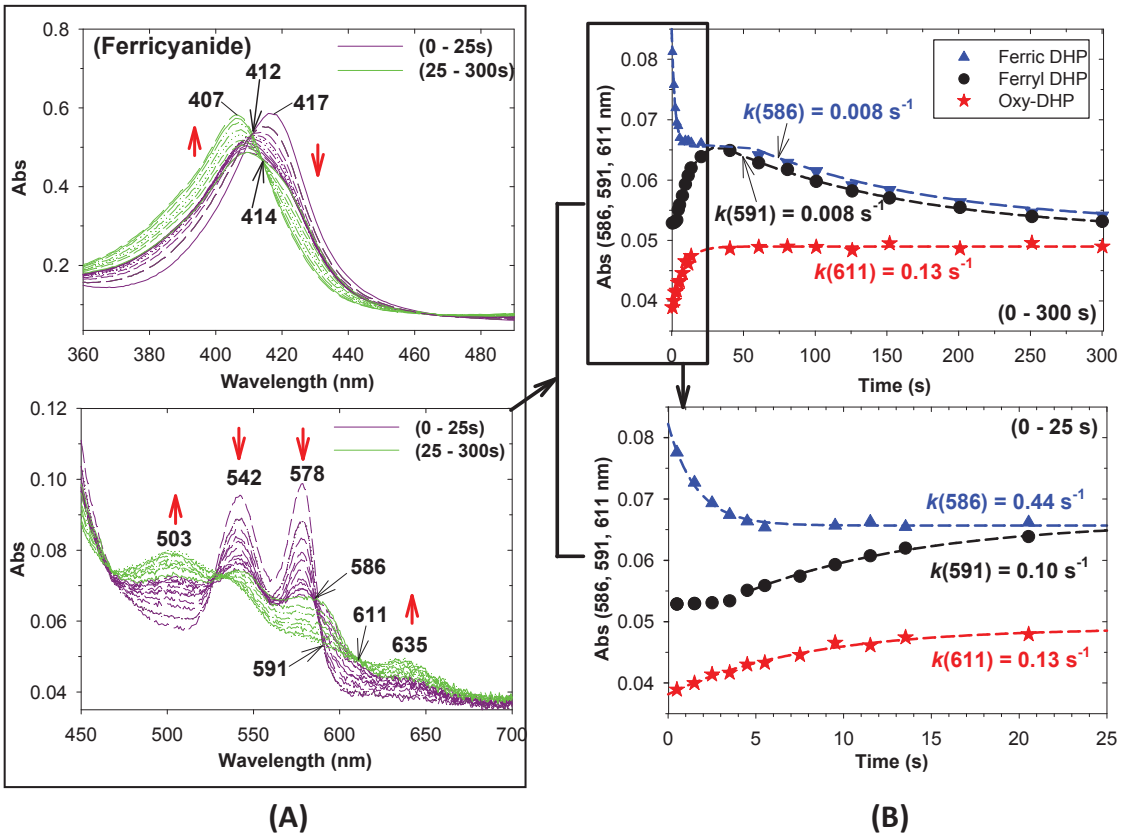


**Figure 3.3.** (A) Spectral change upon addition of a mixed solution of 5 μM $H_2O_2$ and 5 μM potassium ferricyanide to 5 μM oxyferrous DHP for time periods of 0 – 25 s (dark pink) and 25 – 300 s (green). (B) Time-dependent absorbance changes at particular isosbestic points in panel A to monitor disappearance of oxy-DHP ($A_{611}$, red stars), appearance of ferric DHP ($A_{586}$, blue triangles) and rise and decays of ferryl ($A_{591}$, Cpd ES) DHP (black circles). The dashed lines on the plots show exponential fits for the indicated time ranges and calculated apparent first-order rate constants.

respectively, as shown in Figure 3B. Different from the conversion reaction with ferrocyanide, the reaction with ferricyanide (blue triangles) consists of a fast phase (0 - 25 s, enlarged in the bottom panel of Figure 3B), followed by a slow phase (75 - 300 s, Figure 3B, top). In the fast phase (Figure 3B, bottom), ferric DHP is formed before formation of ferryl DHP as indicated by the decrease of $Abs_{586}$ to the nearly constant value (blue triangles) vs. the little change of $Abs_{591}$ (black circles for ferryl DHP) for the first ~5 s. After ferric species stops accumulating, ferryl DHP starts to arise until it reaches its maximum amount at the end of the fast phase (~25 s). At a later stage (75 - 300 s), ferryl DHP decays (black circles) concomitant with further formation of ferric DHP (blue triangles) at a rate of ~0.008 $s^{-1}$. The bimolecular rate constants for the step of ferricyanide oxidizing oxy-DHP to the ferric state as well as for other steps involved in the reaction above have been separately determined using a stopped-flow technique in this study and are listed in Table 3.2 (see Discussion section).

**Inhibitory effects of ferric heme protein ligands and spin trap reagent DMPO on the functional switching of oxy-DHP.** In our previously proposed functional switching mechanism for DHP, it was speculated that the peroxidase activity of a trace amount of Fe(III) enzyme is critical in initiating the conversion by generating TCP• as an oxy-DHP oxidant. To further test this proposed mechanism, reagents that bind to and thereby inhibit the activity of the ferric enzyme or that trap the TCP radicals were added to the oxy- to ferric DHP conversion reaction. Cyanide (KCN) and imidazole (Im) are both ferric heme ligands ($K_d$ values for their complexes with ferric DHP at pH 7.0 and 4 °C were ~0.5 μM for cyanide and ~0.2 mM for Im, this study) and they have much weaker affinities for the ferrous heme proteins [e.g., $K_d = 10^{-1} – 10^{0}$ M (cyanide) [33] and $10^{-1}$ -

**Table 3.2.** Bimolecular rate constants for the reactions indicated in Scheme 3.2; $k_1$, $k_2$ and $k_4$ are for the reactions of oxy-DHP with ferricyanide ($k_1$), ferric DHP with $H_2O_2$ ($k_2$), and DHP Cpd II with TCP, 4-BP or ferrocyanide ($k_4$). Apparent first-order reaction rate constants ($k_{obs}$) obtained from the time-dependence spectral change of DHP upon reacting with various concentrations of substrates or oxidants (from 1 up to 10 equiv.) were plotted vs. [substrate/oxidant] and the bimolecular rate constants ($k_1 - k_4$) were calculated from the linear correlations (see Figure 3.11 for representative examples).

| Substrate/oxidant | Rate constants ($M^{-1}s^{-1}$) pH 7.0, 4 °C | |
|---|---|---|
| Ferricyanide | $k_1$ | $(4.6 \pm 0.4) \times 10^4$ |
| $H_2O_2$ | $k_2$ | $(3.5 \pm 0.1) \times 10^4$ |
| TCP | $k_4$ | $(9.4 \pm 0.3) \times 10^2$ |
| 4-BP | $k_4$ | $(9.7 \pm 0.9) \times 10^2$ |
| Ferrocyanide | $k_4$ | $(4.4 \pm 0.4) \times 10^2$ |

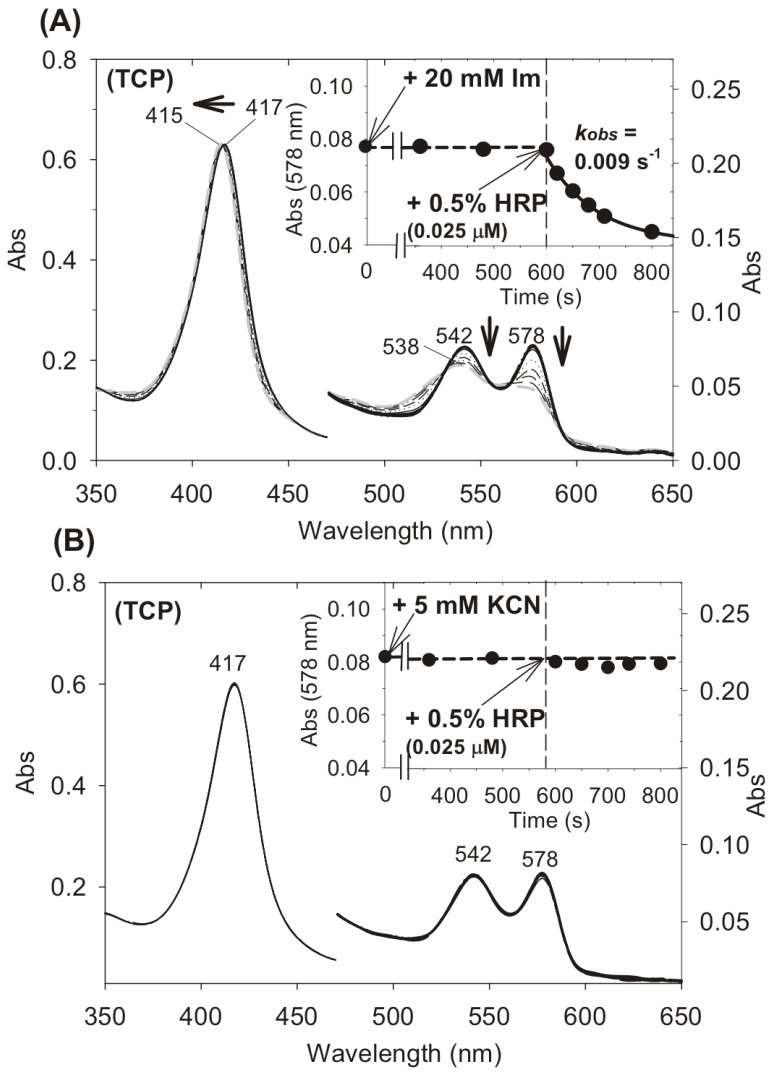


**Figure 3.4.** UV-visible spectroscopic monitoring upon addition of 5 μM $H_2O_2$ to a mixture of 5 μM oxy-DHP and (A) 20 mM Im or (B) 5 mM KCN in the presence of 5 μM TCP during a period of 0 - 600 s and upon subsequent addition of 25 nM HRP at time 600 s (0.005 equiv., 0.5%) during a period of 600 to 800 s. The black circles in the insets show the plots of absorbance at 578 nm ($A_{578}$) as a function of time. The black dashed lines are straight lines drawn through the black circles and the solid line (600 – 800 s in panel A) is the fit to an exponential decay curve which yield an apparent first-order rate constant ($k_{obs}$) of 0.009 $s^{-1}$.

$10^{1}$ M (Im) [34] or deoxyferrous Mb at pH 7.0]. As shown in Figure 3.4, both Im (20 mM, panel A) and KCN (5 mM, panel B) are able to totally inhibit the TCP-triggered conversion of oxy-DHP, as indicated by the absence of absorption changes at 417 nm (Soret peak) upon addition of $H_2O_2$ and TCP to oxy-DHP (0 - 600 s). Inhibition by $CN^-$ or Im was also observed in the ferrocyanide-triggered conversion of oxy-DHP (Figure 3.8). In addition, inhibition by Im can be reversed by adding a small amount of HRP (0.5%, 25 nM), which generates TCP radicals by catalyzing the TCP oxidation by $H_2O_2$.[4, 13] As shown in Figure 3.4A (600 - 800 s), addition of HRP results in the transformation of oxy-DHP [417 (Soret), 542, 578 nm (red solid line)] to Fe(III)-Im DHP complex [415 (Soret), 538 nm (red solid line)] ($k$ = 0.009 $s^{-1}$). On the other hand, addition of HRP (0.5%, at 600 s) to the $CN^-$-inhibited oxy- to ferric DHP conversion had little effect (Figure 3.2.4B). This is due to the fact that ferric HRP has a very low affinity for Im (negligible binding at 20 mM, this study), but has a high affinity for cyanide [tight binding with $K_d$ = (2.5 – 3.0) × $10^{-6}$ M at pH 7] [35] and thus the peroxidase activity of HRP was completely inhibited in the presence of $CN^-$ (5 mM).

Next, to directly prove the involvement of TCP radicals in the functional switch of oxy-DHP, the spin-trapping reagent DMPO (see Supporting Information for its structure) that potentially traps TCP radicals was introduced to the switching process. A complete inhibition of the TCP- or 4-BP-triggered conversion of oxy- to ferric DHP by 10 mM DMPO was observed as shown in Figure 5. Such inhibition was also observed with increased [$H_2O_2$] to 5 equiv. (25 μM), but more DMPO (50 mM) was needed to achieve the complete inhibition (Figure 3.9). Attempts to detect and identify the trapped product (DMPO-TCP radical) by GC-MS were not successful, probably due to the likely low

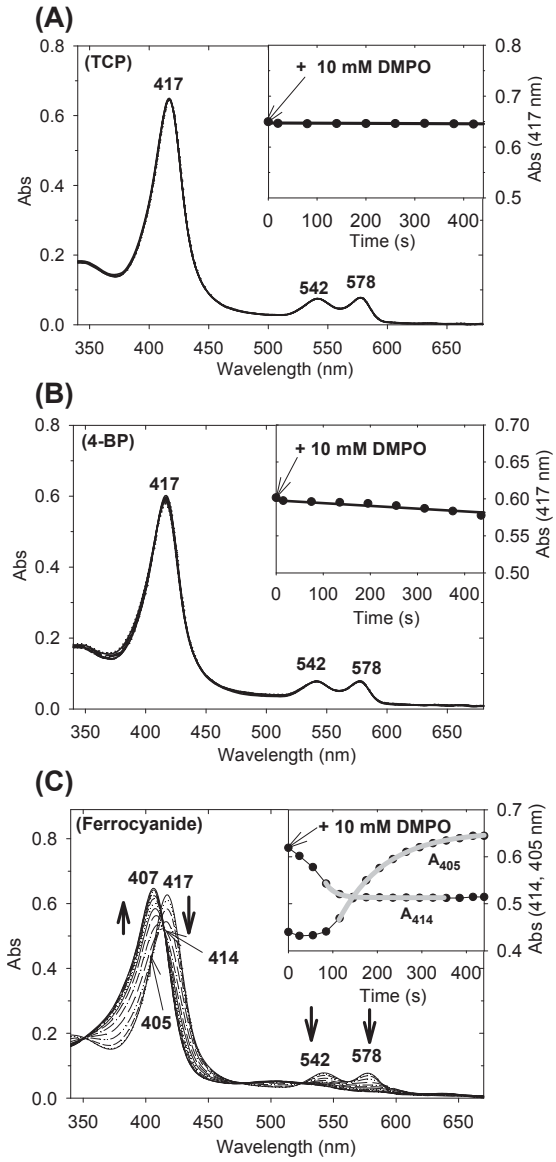


**Figure 3.5.** UV-visible spectroscopic monitoring upon addition of 5 μM $H_2O_2$ to the mixture of 5 μM oxy-DHP and 10 mM DMPO in the presence of (A) 5 μM TCP, (B) 150 μM 4-BP or (C) 5 μM potassium ferrocyanide for a period of 0 - 420 s. The insets in panels A and B show plots of absorbance at 417 nm ($A_{417}$) as a function of time. The inset in panel C follows the $A_{414}$ and $A_{405}$ as a function of time to monitor the decay of oxy-DHP and rise of ferric DHP, respectively. The gray bold lines on the traces show exponential fits for the indicated time ranges, which yield calculated apparent first-order rate constants of $4.7 \times 10^{-2}$ $s^{-1}$ from $A_{414}$ and $1.0 \times 10^{-2}$ $s^{-1}$ from $A_{405}$.

stability of this adduct. However, we have been able to detect a DMPO adduct of 4-BP (m/z = 285) formed in the DHP-catalyzed $H_2O_2$-oxidation of 4-BP in the presence of DMPO (Figure 3.10). Significantly, DMPO (10 mM) has no effect on the ferrocyanide-triggered conversion of oxy- to ferric DHP [$k_{obs}$: (4.7 ± 0.1) × $10^{-2}$ $s^{-1}$ (Figure 5 C) vs. (4.8 ± 0.2) × $10^{-2}$ $s^{-1}$ (Figure 3.2 B)], indicating that the DMPO inhibition on the functional switch can be only through trapping the halophenolic radicals.

**DISCUSSION**

In this study, we have found that not only TCP, but also 4-BP, phenol, ferrocyanide and KI can all trigger the $H_2O_2$-dependent activation of oxy-DHP [apparent activation rates ($k_{obs}$) listed in Table 3.1]. Since these five compounds have different structures (especially the first three phenol derivatives vs. ferrocyanide and KI), yet all are peroxidase substrates, i.e., electron donors, it is quite likely that rather than substrate (TCP) binding, substrate oxidation is involved in the conversion mechanism. In agreement with this supposition, we recently showed that addition of TCP or 4-BP (up to 2 mM, cf. $K_m$ = ~0.3 mM for TCP[36]) does not affect the $K_{O2}$ values for DHP [3], thus ruling out the possibility that TCP triggers the functional switch by binding and modulating the $O_2$ affinity [26]. In addition, we have shown clear evidence that blocking the catalytic activity of the ferric component in the oxy-DHP sample (using ferric heme ligands, Im and cyanide) also blocks the functional switch and such blockage by Im can be reversed by HRP (Figure 3.4A) that catalyzes the oxidation of the substrate TCP to its radical [4]. Previously, a spin-trapping reagent DIPPMO (5-diisopropoxy-phosphoryl-5-methyl-1-pyrroline-N-oxide) has been reported to trap the TCP• generated from the reaction of ferric or oxy-DHP with $H_2O_2$ in the presence of TCP as demonstrated by $^{31}P$

NMR [26]. However, the identity of the compound formed by the trapping was not established and the possible inhibition of the oxy- to ferric DHP or ferryl DHP conversion by DIPPMO was not examined in that study. In the present study, we have used DMPO as the TCP radical trap to probe the role of TCP in triggering the DHP functional switch. The complete inhibition of the TCP/4-BP-triggered (but not the ferrocyanide-triggered) activation of oxy-DHP by DMPO confirms the involvement of TCP radicals in the DHP functional switch.

Based on the results from the present study on the activation of oxy-DHP as well as our previous findings [25]. Scheme 3.2 illustrates the mechanism for the $H_2O_2$-mediated oxidation of oxy-DHP to the ferric state in the presence of substrate TCP (as proposed previously [25]) or ferrocyanide (newly found in this study). In the first phase, oxyferrous DHP is oxidized to ferric DHP by TCP• or ferricyanide (with bimolecular rate constant $k_1$), both of which are the oxidative products gradually generated from the normal peroxidase catalytic cycle mediated by the initial trace amount of ferric DHP present in the oxy-DHP sample. It is most likely that TCP radical directly oxidizes oxy-DHP as previously proposed for lignin peroxidase Cpd III (oxy-peroxidase) [28] while the oxidation by ferricyanide occurs via the deoxyferrous form as has been shown for oxy-Mb [37]. During this phase, TCP• or ferricyanide oxidize oxy-DHP to the ferric state, which subsequently forms ferryl DHP upon reacting with $H_2O_2$ in the second phase (with bimolecular rate constant $k_2$). In the following third/fourth phases, the ferryl DHP species (Cpd ES and Cpd II) decay to Cpd II and ferric DHP, respectively, with bimolecular rate constants $k_3$ and $k_4$. This is the stage when TCP or ferrocyanide (the product of oxidation of oxy-DHP by TCP• or ferricyanide) reduces the ferryl DHP back to ferric state. The

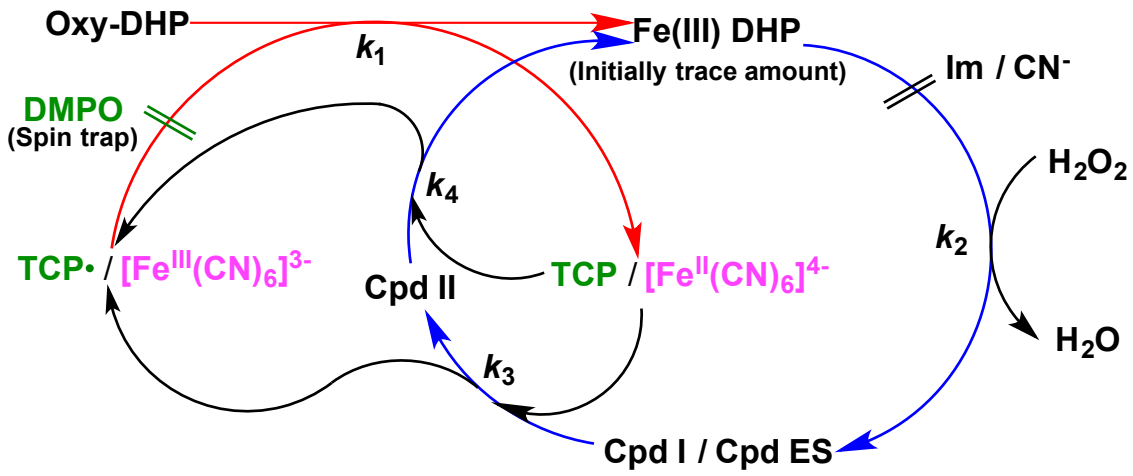


**Scheme 3.2.** Reaction mechanism for $H_2O_2$ converting oxy-DHP to ferric state in the presence of TCP (green) or ferrocyanide (pink).

values of the bimolecular rate constants $k_1$ (for ferricyanide only), $k_2$ and $k_4$ have been determined in this study using stopped-flow technique and are listed in Table 3.2. Determination of $k_3$ is not technically feasible because DHP Cpd ES and Cpd II are spectrally indistinguishable. Assuming $k_3 > k_4$, the rate constants that have been determined in this study for Cpd ES + TCP/ferrocyanide reflect the $k_4$ instead of $k_3$ value. D'Antonio and Ghiladi have reported the bimolecular rate constant for the reaction of ferryl DHP B (prepared from the oxy-form in a similar way as shown in Figure 3.9A) with TCP to be $4.1 \times 10^2$ $M^{-1}$ $s^{-1}$ at pH 8 and 25 $^oC$ [26]. This value is on the same order of magnitude as the $k$ value (presumably $k_4$) obtained in this study for DHP A (Cpd ES + TCP) at pH 7 and 4 $^oC$ (Table 3.2). In the case of HRP, we have shown in a previous study that $k_3 = \sim 3 \times 10^7$ $M^{-1}$ $s^{-1}$ >> $k_4 = \sim 1.5 \times 10^5$ $M^{-1}$ $s^{-1}$ for ferryl HRP-oxidation of TCP at pH 5 [32].

As shown in Scheme 3.2, ferric DHP ligands ($Im/CN^-$) effectively inhibit the functional switch by blocking the formation of Cpd ES and thus the generation of subsequent oxidative products, TCP• or $[Fe^{III}(CN)_6]^{3-}$. DMPO inhibits the functional conversion (TCP-triggered only) by trapping the TCP• that oxidizes oxy-DHP to ferric state. In the absence of these inhibitors, this reaction cycle continues in an accelerated fashion after the initial stage using progressively accumulated ferric DHP and regenerated TCP/ferrocyanide.

In the proposed mechanism described above, oxy-DHP directly switches to the ferric state without formation of any intermediate. However, in the present study on oxy- to ferric DHP conversion (with [oxy-DHP] : [$H_2O_2$] : [substrate] = 1 : 1 : 1), a ferryl intermediate is formed before the appearance of ferric DHP (Figures 3.1 and 3.2B). The

apparent inconsistency can be explained using Scheme 3.2. In the beginning of the activation reaction, TCP• (or ferricyanide) is gradually generated by the peroxidase reaction of $H_2O_2$ (initially 1 equiv.) and ferric DHP (initially trace amount). Under such conditions, the concentration of TCP• (or ferricyanide) is much less than [$H_2O_2$]. Consequently, the apparent rate of the initial (oxy- → ferric DHP) phase ($k_{obs} = k_1$[TCP•] or $k_1$[ferricyanide]) is considerably slower than that of the following (ferric DHP → Cpd ES) phase ($k_{obs} = k_2[H_2O_2] = 3.5 \times 10^4\ M^{-1}s^{-1} \times 5\ \mu M = 1.8 \times 10^{-1}\ s^{-1}$, Table 3.2). When the (oxy-DHP → ferric DHP) phase becomes progressively faster until it reaches the maximum rate [$2.3 \times 10^{-2}\ s^{-1}$ (TCP) or $4.8 \times 10^{-2}\ s^{-1}$ (ferrocyanide), Table 3.1], more than a half of the initially $H_2O_2$ remains since 1 equiv. of oxy- to ferric DHP conversion requires 1 equiv. of TCP• generated by consuming only 0.5 equiv. of $H_2O_2$. Therefore, the (ferric DHP → Cpd ES) phase ($k_{obs} = k_2[H_2O_2] \geq 3.5 \times 10^4\ M^{-1}s^{-1} \times 0.5$ equiv. $\times 5\ \mu M = 8.8 \times 10^{-2}\ s^{-1}$) is still faster than the first (oxy-DHP → ferric DHP) phase ($k_{obs} = 2.3 \times 10^{-2}\ s^{-1}$, Table 3.1 ).

This explains why it is not easy to detect the first phase under the conditions we employed in this study. Actually, what we have observed is a combination of two sequential phases, i.e. oxy- →ferric → Cpd ES DHP, with the former phase the rate-limiting step. As the consumption of $H_2O_2$ continues while TCP•/TCP (or ferricyanide/ferrocyanide) keeps recycling, the third/fourth phase (ferryl → ferric DHP, $k_{obs} = k_4$[substrate]) become dominant over the second phase (ferric DHP → Cpd ES, $k_{obs} = k_2[H_2O_2]$) and the ferryl intermediate starts to be reduced back to the ferric state. Thus, ferric DHP produced in the first phase is partially converted to ferryl DHP (~45% as

shown by the global analysis in Figure 3.1B) and then generated to a ~100% stoichiometric amount at the end of the reaction.

However, when excess [TCP] is used as in our previous study [25] ([oxy-DHP] : $[H_2O_2]$ : [TCP] = 1 : 1 : 30), the rate of the third/fourth phases (ferryl → ferric DHP, $k_{obs} = k_4[TCP] = 9.4 \times 10^2\ M^{-1}s^{-1} \times 150\ \mu M = 1.4 \times 10^{-1}\ s^{-1}$) exceeds the apparent ferryl DHP formation rate ($k_{obs} = 2.3 \times 10^{-2}\ s^{-1}$, Table 3.1). As a result, the ferryl species was not detectable and only two species, oxy-DHP and Fe(III) DHP, were observed during the activation reaction with a single set of isosbestic points.

The first step (oxy- → ferric DHP) in the activation reaction was not detectable in either of the above cases. However, it could be detected when sufficiently high concentrations of oxidant (TCP• or ferricyanide) of oxy-DHP are available. In fact, such a situation was observed in the reaction of oxy-DHP with equal equiv. of the oxidant ferricyanide and $H_2O_2$ (Figure 3.3), in which the $k_{obs}$ of the first step slightly exceeds that of the second step theoretically (0. 23 vs. 0.18 $s^{-1}$, calculated from the bimolecular rate constants $k_1$ and $k_2$ in Table 3.2 under the conditions employed). We have observed a fast phase (0 - 5 s, Figure 3.2B bottom panel) during which ferricyanide first oxidizes oxy-DHP to the ferric state (0.44 $s^{-1}$, blue triangles) which subsequently forms ferryl DHP upon reacting with $H_2O_2$ (0.10 $s^{-1}$, black circles) in the second phase (5 – 25 s). In the following phase (25 - 300 s, Figure 3.2B top panel), ferryl DHP slowly decays (0.008 $s^{-1}$, black circles) along with an increase (absorption decrease) of ferric DHP (0.008 $s^{-1}$, blue triangles). This is a process indicated in Scheme 3.2 as the third/fourth phases when ferrocyanide (recycled from oxy-DHP reducing ferricyanide) is reducing ferryl DHP to the ferric state.

As already mentioned earlier, a "lag" (slow-phase) time for ~25 s has been found before the ferryl DHP formation rate reaches its maximum (right panel inset, Figure 3.1A). This observation is reasonable if we consider that the conversion reaction starts from a trace amount of Fe(III) DHP catalyzing the formation of TCP• and gets accelerated until it becomes maximum. On the other hand, direct oxidation of deoxyferrous DHP (in equilibrium with the oxy form) by $H_2O_2$, as proposed by Ghiladi and co-workers, will not explain such a "lag" period, in contrast to the case of the reaction of oxy-Mb with $H_2O_2$, where no such lag phase is obserbed [38]. Furthermore, such direct oxidation of deoxyferrous DHP to the ferryl state by $H_2O_2$ would not be inhibited by the ferric heme ligands, Im or $CN^-$. Taken together, the ferryl intermediate observed in the $H_2O_2$-mediated oxy- to ferric DHP conversion is more likely derived from $H_2O_2$ subsequently reacting with the initially generated ferric DHP, not from $H_2O_2$ directly reacting with ferrous DHP.

**CONCLUSIONS**

In this report, we have shown that the DHP functional switch from the oxyferrous state to the ferric peroxidase active state as a peroxidase, triggered by the co-presence of the substrate TCP and $H_2O_2$, is inhibited by the ferric heme ligands Im or cyanide as well as by the radical trap DMPO. The present results strongly support our previous proposal that the oxyferrous enzyme is directly oxidized to the ferric state by TCP radicals that are generated by the peroxidase reaction of ferric DHP (initially present in a trace amount in the oxy-DHP sample and progressively accumulating), not simply through a TCP-induced displacement of bound $O_2$ followed by $H_2O_2$ binding. The present report further

clarifies how this bifunctional $O_2$ carrier hemoglobin switches to its enzymatically active ferric state as a defensive response to the presence of toxic trihalophenol substrates.

**ACKKNOWLEDGEMENTS**

We thank Prof. Lukasz Lebioda and Dr. Mike Walla (University of South Carolina, Department of Chemistry and Biochemistry) for helpful discussions and Prof. Stefan Franzen (North Carolina State University) for the six-His-tagged DHP plasmid.

**ABBREVIATIONS**

DHP, dehaloperoxidase; Mb, myoglobin; HRP, horseradish peroxidase; CPO, *C. fumago* chloroperoxidase; TXP, 2,4,6-trihalophenol; DXQ: 2,6-dihaloquinone; TCP, 2,4,6-trichlorophenol; TCP•, TCP radical or one-electron oxidized TCP; 4-BP: 4-bromophenol; Cpd I, Compound I; Cpd II, Compound II; Cpd ES, Compound ES (common name for Cpd II/Tyr radical); Cpd III, Compound III; DMPO, 5,5-dimethyl-1-pyrroline-N-oxide.

**REFERENCES**


[1] Han, K., Woodin, S. A., Lincoln, D. E., Fielman, K. T., and Ely, B. (2001) *Amphitrite ornata*, a marine worm, contains two dehaloperoxidase genes, *Mar. Biotechnol. 3*, 287-292.

[2] Weber, R. E., Mangum, C., Steinman, H., Bonaventura, C., Sullivan, B., and Bonaventura, J. (1977) Hemoglobins of two terebellid polychaetes: *Enoplobranchus sanguineus* and *Amphitrite ornata*, *Comparative Biochemistry and Physiol. Part A: Physiology 56*, 179-187.

[3] Sun, S., Sono, M., Wang, C., Du, J., Lebioda, L., and Dawson, J. H. (2014) Influence of heme environment structure on dioxygen affinity for the dual function *Amphitrite ornata* hemoglobin/dehaloperoxidase. Insights into the evolutional structure-function adaptations, *Arch. Biochem. Biophys. 545, 108-145*.

[4] Osborne, R. L., Taylor, L. O., Han, K. P., Ely, B., and Dawson, J. H. (2004) *Amphitrite ornata* dehaloperoxidase: enhanced activity for the catalytically active globin using MCPBA, *Biochem. Biophys. Res. Commun. 324*, 1194-1198.

[5] Chen, Y. P., Woodin, S. A., Lincoln, D. E., and Lovell, C. R. (1996) An unusual dehalogenating peroxidase from the marine terebellid polychaete *Amphitrite ornata*, *J. Biol. Chem. 271*, 4609-4612.

[6] Osborne, R. L., Coggins, M. K., Raner, G. M., Walla, M., and Dawson, J. H. (2009) The mechanism of oxidative halophenol dehalogenation by *Amphitrite ornata* dehaloperoxidase is initiated by $H_2O_2$ binding and involves two consecutive one-electron steps: role of ferryl intermediates, *Biochemistry 48*, 4231-4238.

[7] Davydov, R., Osborne, R. L., Kim, S. H., Dawson, J. H., and Hoffman, B. M. (2008) EPR and ENDOR studies of cryoreduced compounds II of peroxidases and myoglobin. proton-coupled electron transfer and protonation status of ferryl hemes, *Biochemistry 47*, 5147-5155.

[8] Davydov, R., Osborne, R. L., Shanmugam, M., Du, J., Dawson, J. H., and Hoffman, B. M. (2010) Probing the oxyferrous and catalytically active ferryl states of *Amphitrite ornata* dehaloperoxidase by cryoreduction and EPR/ENDOR spectroscopy. Detection of compound I, *J. Am. Chem. Soc.132*, 14995-15004.

[9] Osborne, R. L., Raner, G. M., Hager, L. P., and Dawson, J. H. (2006) *C. fumago* chloroperoxidase is also a dehaloperoxidase: oxidative dehalogenation of halophenols, *J. Am. Chem. Soc. 128*, 1036-1037.

[10] Osborne, R. L., Coggins, M. K., Terner, J., and Dawson, J. H. (2007) *Caldariomyces fumago* chloroperoxidase catalyzes the oxidative dehalogenation of chlorophenols by a mechanism involving two one-electron steps, *J. Am. Chem. Soc. 129*, 14838-14839.

[11] Kim, S. H., Perera, R., Hager, L. P., Dawson, J. H., and Hoffman, B. M. (2006) Rapid freeze-quench ENDOR study of chloroperoxidase compound I: the site of the radical, *J. Am. Chem. Soc. 128*, 5598-5599.

[12] Roman, R., and Dunford, H. (1972) pH dependence of the oxidation of iodide by compound I of horseradish peroxidase, *Biochemistry 11*, 2076-2082.

[13] Wiese, F., Chang, H., Lloyd, R., Freeman, J., and Samokyszyn, V. (1998) Peroxidase-catalyzed oxidation of 2, 4, 6-trichlorophenol, *Arch. Environ. Contam. Toxicol. 34*, 217-222.

[14] Sturgeon, B. E., Battenburg, B. J., Lyon, B. J., and Franzen, S. (2011) Revisiting the peroxidase oxidation of 2, 4, 6-trihalophenols: ESR detection of radical intermediates, *Chem. Res. Toxicol. 24*, 1862-1868.

[15] Osborne, R. L., Coggins, M. K., Walla, M., and Dawson, J. H. (2007) Horse heart myoglobin catalyzes the $H_2O_2$-dependent oxidative dehalogenation of chlorophenols to DNA-binding radicals and quinones, *Biochemistry 46*, 9823-9829.

[16] Du, J., Huang, X., Sun, S., Wang, C., Lebioda, L., and Dawson, J. H. (2011) *Amphitrite ornata* dehaloperoxidase (DHP): Investigations of structural factors that influence the mechanism of halophenol dehalogenation using "peroxidase-like" myoglobin mutants and "Myoglobin-like" DHP Mutants, *Biochemistry 50*, 8172-8180.

[17] Roach, M. P., Chen, Y. P., Woodin, S. A., Lincoln, D. E., Lovell, C. R., and Dawson, J. H. (1997) *Notomastus lobatus* chloroperoxidase and *Amphitrite ornata* dehaloperoxidase both contain histidine as their proximal heme iron ligand, *Biochemistry 36*, 2197-2202.

[18] Franzen, S., Roach, M. P., Chen, Y.-P., Dyer, R. B., Woodruff, W. H., and Dawson, J. H. (1998) The unusual reactivities of *Amphitrite ornata* dehaloperoxidase and *Notomastus lobatus* chloroperoxidase do not arise from a

histidine imidazolate proximal heme iron ligand, *J. Am. Chem. Soc. 120*, 4658-4661.

[19] Lincoln, D. E., Fielman, K. T., Marinelli, R. L., and Woodin, S. A. (2005) Bromophenol accumulation and sediment contamination by the marine annelids *Notomastus lobatus* and *Thelepus crispus, Biochem. System. Ecol. 33*, 559-570.

[20] Lovell, C. R., Steward, C. C., and Phillips, T. (1999) Activity of marine sediment bacterial communities exposed to 4-bromophenol, a polychaete secondary metabolite, *Mar. Ecol. Prog. Ser. 179*, 241-246.

[21] Thompson, M. K., Davis, M. F., De Serrano, V., Nicoletti, F. P., Howes, B. D., Smulevich, G., and Franzen, S. (2010) Internal binding of halogenated phenols in dehaloperoxidase-hemoglobin inhibits peroxidase function, *Biophys. J. 99*, 1586-1595.

[22] Plummer, A., Thompson, M. K., and Franzen, S. (2013) The role of polarity of the distal pocket in the control of inhibitor binding in dehaloperoxidase-hemoglobin, *Biochemistry 52, 2218-2227*.

[23] De Serrano, V., D'Antonio, J., Franzen, S., and Ghiladi, R. A. (2010) Structure of dehaloperoxidase B at 1.58 A resolution and structural characterization of the AB dimer from Amphitrite ornata, *Acta Crystallogr. D: Biol. Crystallogr. 66*, 529-538.

[24] LaCount, M. W., Zhang, E., Chen, Y. P., Han, K., Whitton, M. M., Lincoln, D. E., Woodin, S. A., and Lebioda, L. (2000) The crystal structure and amino acid

sequence of dehaloperoxidase from *Amphitrite ornata* indicate common ancestry with globins, *J. Biol. Chem. 275*, 18712-18716.

[25] Du, J., Sono, M., and Dawson, J. H. (2010) Functional switching of *Amphitrite ornata* dehaloperoxidase from $O_2$-binding globin to peroxidase enzyme facilitated by halophenol substrate and $H_2O_2$, *Biochemistry 49*, 6064-6069.

[26] D'Antonio, J., and Ghiladi, R. A. (2011) Reactivity of deoxy- and oxyferrous dehaloperoxidase B from *Amphitrite ornata*: Identification of compound II and its ferrous–hydroperoxide precursor, *Biochemistry 50*, 5999-6011.

[27] Cai, D., and Tien, M. (1992) Kinetic studies on the formation and decomposition of compounds II and III. Reactions of lignin peroxidase with $H_2O_2$, *J. Biol. Chem. 267*, 11149-11155.

[28] Barr, D. P., and Aust, S. D. (1994) Conversion of lignin peroxidase compound III to active enzyme by cation radicals, *Arch. Biochem. Biophys. 312*, 511-515.

[29] H.B. Dunford (1999) Heme peroxidases, John Wiley, New York.

[30] Belyea, J., Gilvey, L. B., Davis, M. F., Godek, M., Sit, T. L., Lommel, S. A., and Franzen, S. (2005) Enzyme function of the globin dehaloperoxidase from *Amphitrite ornata is* activated by substrate binding, *Biochemistry 44*, 15637-15644.

[31] Nelson, D. P., and Kiesow, L. A. (1972) Enthalpy of decomposition of hydrogen peroxide by catalase at 25 °C (with molar extinction coefficients of $H_2O_2$ solutions in the UV), Anal. Biochem. 49, 474-478.

[32] Sumithran, S., Sono, M., Raner, G. M., and Dawson, J. H. (2012) Single turnover studies of oxidative halophenol dehalogenation by horseradish peroxidase reveal a mechanism involving two consecutive one electron steps: Toward a functional halophenol bioremediation catalyst, *J. Inorg. Biochem*. 117, 316-327.

[33] Antonini, E., and Brunori, M. (1971) Hemoglobin and myoglobin in their reactions with ligands, Vol. 21, North-Holland Publishing Company, Amsterdam. Chapter 2.

[34] Du, J., Sono, M., and Dawson, J. H. (2008) The proximal and distal pockets of the H93G myoglobin cavity mutant bind identical ligands with different affinities: Quantitative analysis of imidazole and pyridine binding, *Spectroscopy 22*, 123-141.

[35] Ellis, W. D., and Dunford, H. B. (1968) The kinetics of cyanide and fluoride binding by ferric horse-radish peroxidase, *Biochemistry 7*, 2054-2062.

[36] Wang, C., Lovelace, L. L., Sun, S., Dawson, J. H., and Lebioda, L. (2013) Complexes of dual-function hemoglobin/dehaloperoxidase with substrate 2,4,6-trichlorophenol are inhibitory and indicate binding of halophenol to compound I, *Biochemistry* 52, 6203-6210.

[37] Antonini, E., Brunori, M., and Wyman, J. (1965) Studies on the oxidation-reduction potentials of heme proteins. IV. The kinetics of oxidation of hemoglobin and myoglobin by ferricyanide, *Biochemistry 4*, 545-551.

[38] Whitburn, K. D. (1987) The interaction of oxymyoglobin with hydrogen peroxide: the formation of ferrylmyoglobin at moderate excesses of hydrogen peroxide, *Arch. Biochem. Biophys. 253*, 419-430.

**Supporting Information**

**Figure 3.6**: Overlaid spectra of oxyferrous DHP/ferric DHP/Cpd ES DHP and simulated spectra for mixture of the three using the global analysis data for their time-dependent relative popurations in Figure 1B; **Figure 3.7**: Spectroscopic monitoring of the oxy-DHP reacting with 1 eq. $H_2O_2$ in the presence of 4-BP or phenol; **Figure 3.8**: The KCN/Im inhibition on the reaction of oxy-DHP with 1 eq. $H_2O_2$ in the presence of ferrocyanide; **Figure 3.9**: The DMPO (50 mM) inhibition on the reaction of oxy-DHP with 5 eq. $H_2O_2$ in the presence of TCP; **Figure 3.10**: Mass spectrum of the 4-BP-DMPO adduct product; **Figure 3.11**: Measurements for the bimolecular rate constants $k_1$ and $k_2$ in Table 2.

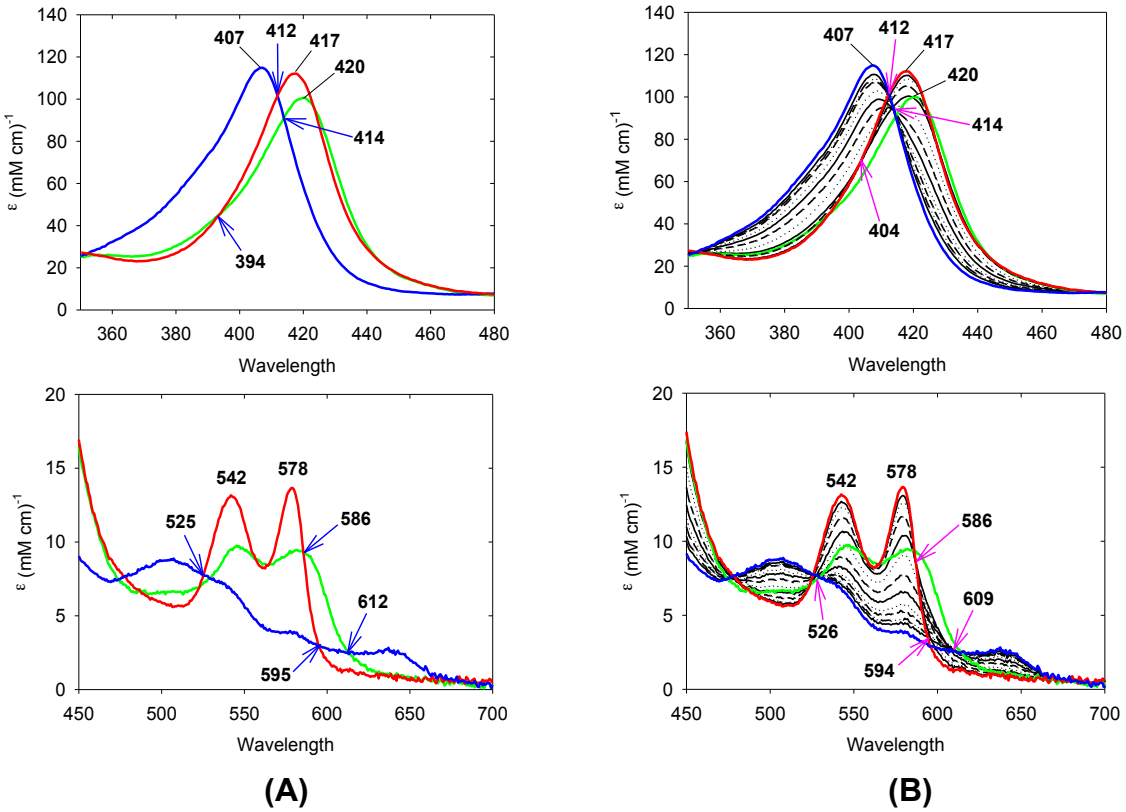


**Figure 3.6.** (A) Overlaid normalized spectra of oxyferrous DHP (red), ferric DHP (blue) and Cpd ES DHP (green). Cpd ES DHP is obtained from the reaction of 5 μM ferric DHP with 50 μM $H_2O_2$. Arrows indicate isosbestic points. (B) Simulated time-dependent spectra (black lines) of the mixture of the three species (shown in color, which are re-plotted from panel A) using the normalized relative concentrations (0 – 1.00) at various time points for a period of 0 - 450 s in Figure 1B. Arrows indicate isosbestic points.

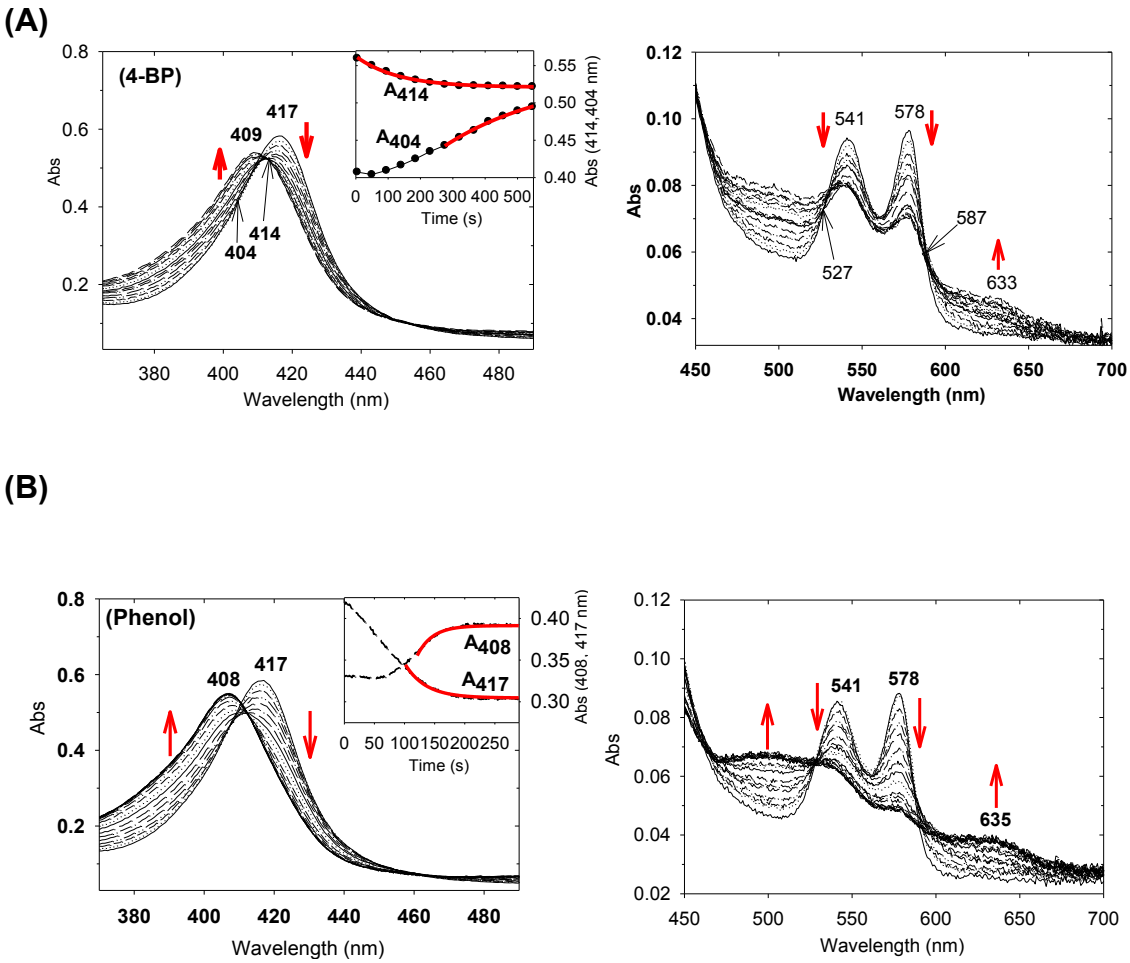


**Figure 3.7.** Spectral change upon addition of 5 μM $H_2O_2$ to 5 μM oxyferrous DHP in the presence of (A) 5 μM 4-BP or (B) 150 μM phenol. The insets show the time-dependent absorbance changes monitoring disappearance of oxy-DHP [414 nm (A), 417 nm (B)] and appearance of ferric DHP [404 nm (A) and 408 nm (B)].

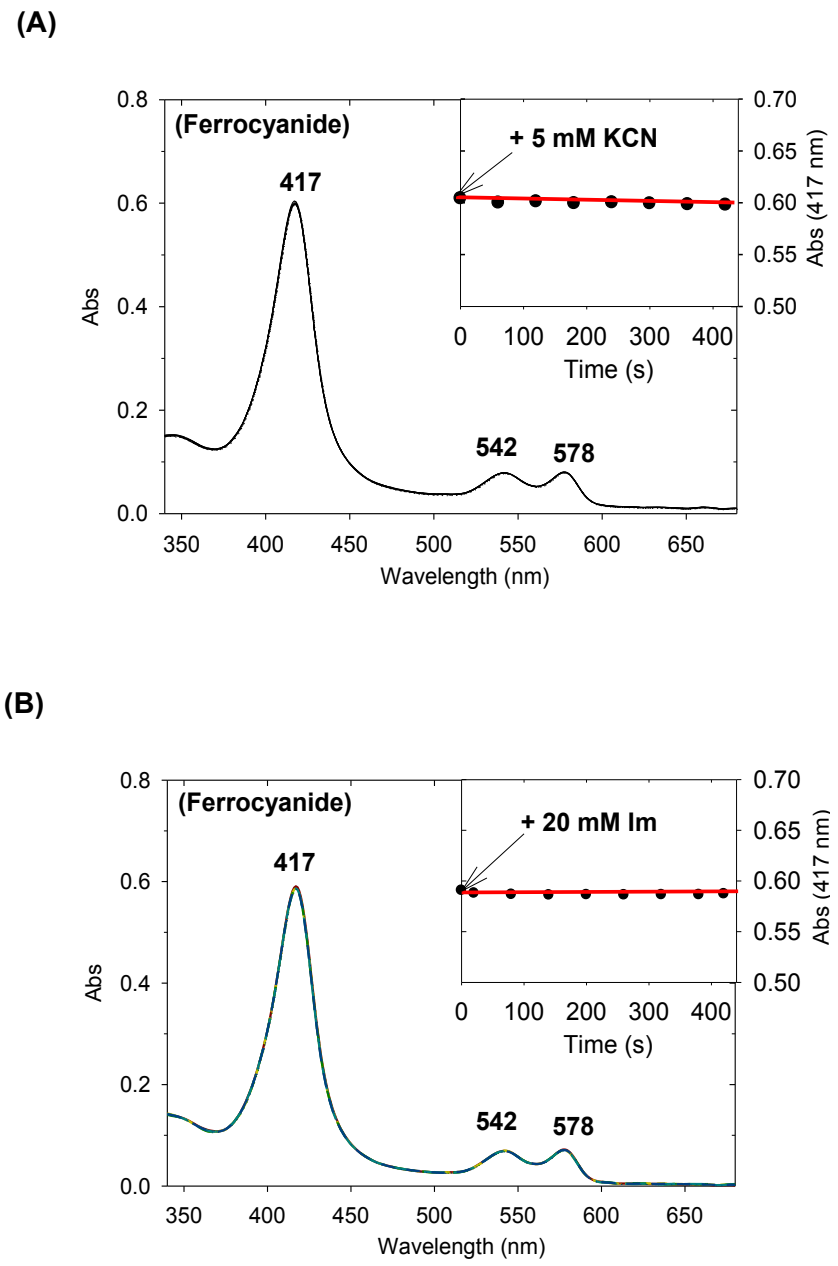


**Figure 3.8.** UV-visible spectroscopic monitoring upon addition of 5 μM $H_2O_2$ to the mixture of 5 μM oxy-DHP and (A) 5 mM KCN or (B) 20 mM Im in the presence of 5 mM potassium ferrocyanide (0 - 420 s). The insets show the plots of absorbance change at 417 nm as a function of time with a straight red solid line drawn over the data points.

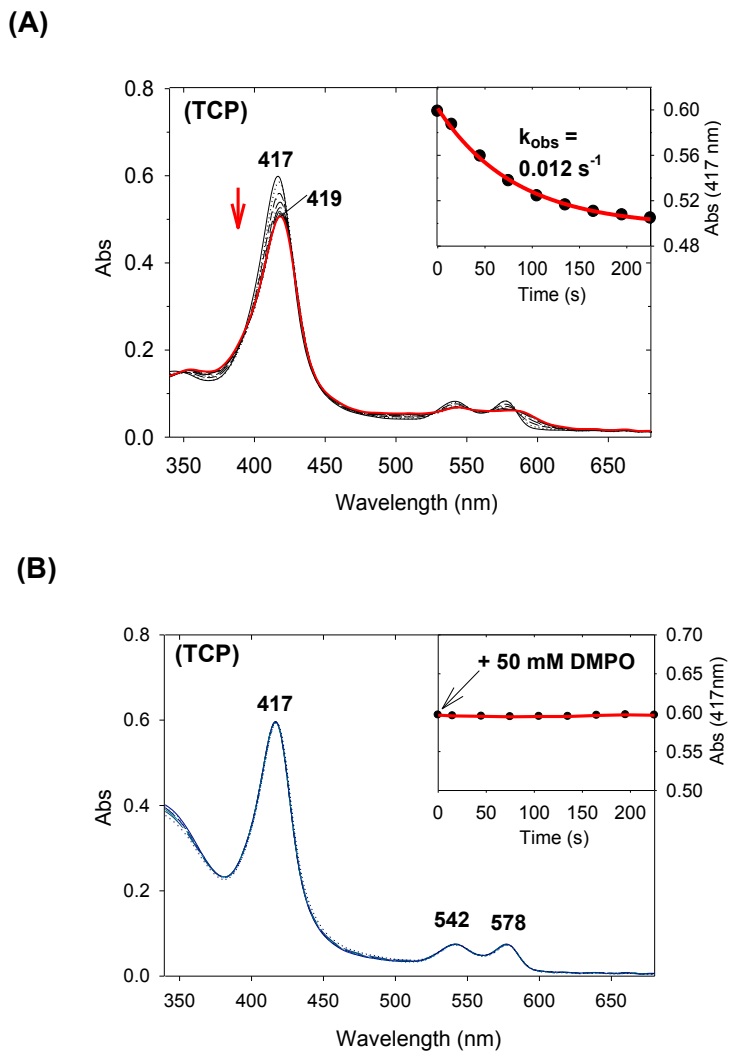


**Figure 3.9.** UV-visible spectroscopic monitoring upon addition of 25 μM $H_2O_2$ to the mixture of 5 μM oxy-DHP and 5 μM TCP in the (A) absence or (B) presence of 50 mM DMPO (0 - 225 s). The insets show the plots of absorbance at 417 nm as a function of time for both panels. In panel A inset, apparent first-order rate constant that is calculated from an exponential fit (red solid line) is shown. In panel B inset, a straight red line is drawn over the data points.

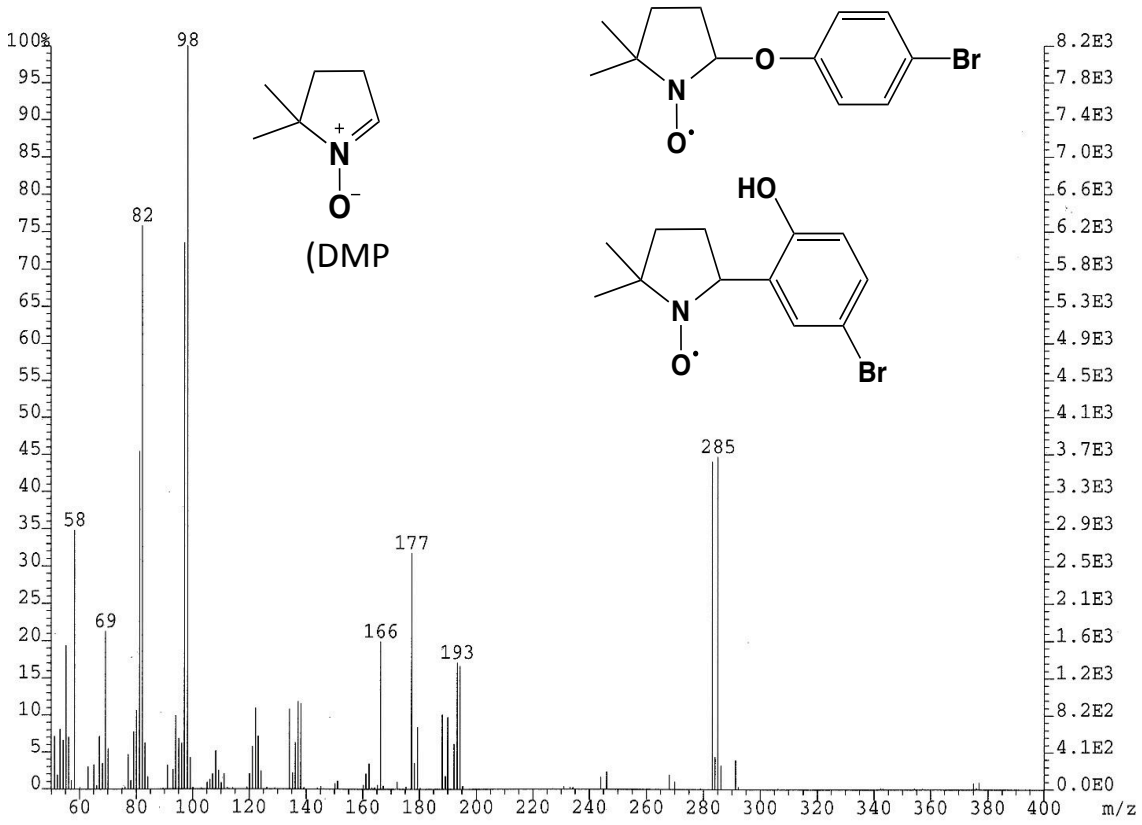


**Figure 3.10.** Mass spectrum of the 4-BP-DMPO adduct product extracted with ethyl acetate after the reaction of ferryl DHP (50 μM) and 4-BP (300 μM) in the presence of DMPO (50 mM). Ferryl DHP was generated by adding 300 μM $H_2O_2$ to ferric DHP (50 μM). The structure of DMPO and two candidates for the likely 4-BP-DMPO adduct structures are shown.

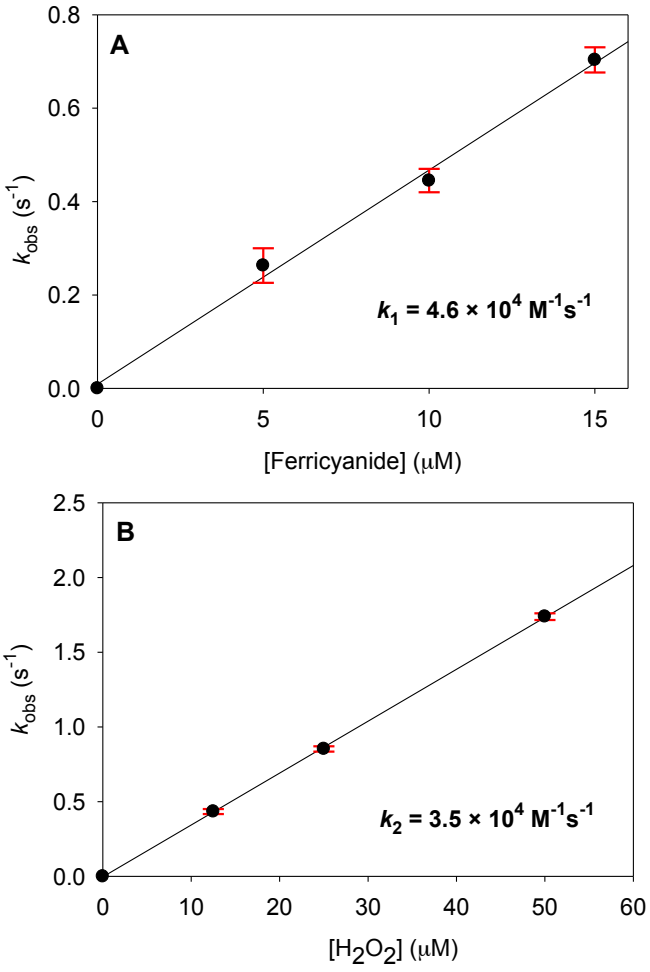


**Figure 3.11.** Measurements for the bimolecular rate constants $k_1$ and $k_2$ in Table 2. (A) Plot of $k_{obs}$ (apparent first-order rate constants) vs. [ferricyanide] for reaction of oxy-DHP with ferricyanide. (B) Plot of $k_{obs}$ vs. [$H_2O_2$] for reaction of ferric DHP with $H_2O_2$. The $k_{obs}$ values (solid circles) were calculated from exponential fits for time-dependent absorbance changes at 417 nm and 406 nm upon mixing (A) 5 μM oxy-DHP with 5, 10 and 15 μM potassium ferricyanide and (B) 5 μM ferric DHP with 12.5, 25 and 50 μM $H_2O_2$ on a stopped-flow spectrophotometer in 0.1 M potassium phosphate buffer, pH 7.0, at 4 °C. $k_1$ and $k_2$ were determined by calculating the slopes of the linear correlation as shown in solid lines in panel A and panel B, respectively.

PART II

CHAPTER 4

Introduction to Part II:

H93G myoglobin cavity mutant as spectroscopic model of cytochrome P450

**Heme-iron coordination models**

Heme-iron coordination modeling has been a subject of interest for decades. It provides valuable information for identifying newly found heme proteins and better understanding their structure-function relationships. Earlier attempts to generate heme coordination models has included the total synthesis of the porphyrins with the desired ligands attached [1-4]. Although this approach resulted in several good mimics of native heme protein active sites, the synthesis is challenging and problematic in yielding homogenous complexes.

Another method for preparing heme models has been the use of site-directed mutagenesis on native heme proteins. Myoglobin (Mb) is a relatively small (~15 kDa) and simple heme protein that has been proved to be an ideal scaffold for protein engineering. Numerous engineered Mbs have been created with improved native function ($O_2$ binding) or artificial enzymatic activities [5-8]. Mb has also been employed for the preparation of heme models. Directly replacing the proximal His of Mb by Cys or Tyr successfully generates models for P450 and catalase, respectively [9, 10]. However, only a quite limited number of models can be prepared by this method due to the structural constraints and folding problems found for some mutants. In 1994, Barrick established a novel approach to prepare heme models using a H93G Mb cavity mutant. The mutant replaces the proximal $His^{93}$ with a small Gly, leaving a proximal cavity for the binding of exogenous ligand to the heme (Figure 4.1). This simple yet creative approach has very little limitations in generating desired heme-coordination complexes compared with previous synthetic methods and immediately boosts the size of the heme modeling library.

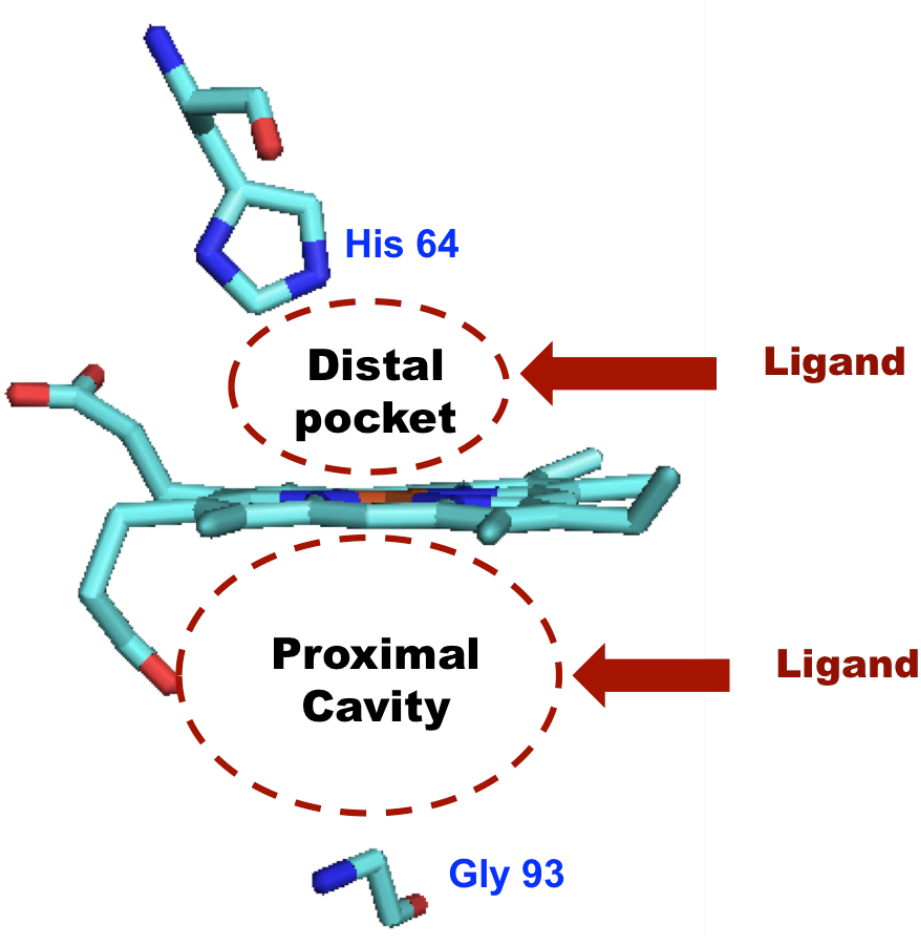


**Figure 4.1.** A schematic representation for the active site of H93G Mb showing the proximal cavity and the distal pocket where the exogenous ligands bind.

Our lab has contributed a large array of heme coordination models as mimics of native heme proteins with various proximal ligations [11]. For example, the imidazole adducts of H93G Mb structurally mimics His-ligated heme proteins such as peroxidases; the alkylamine adducts of H93G Mb spectroscopically resemble the Lys-ligated heme proteins such as CO oxidation activator (CooA). The H93G Mb adducts can also be studied in different iron oxidation states with addition of desired distal probing ligands such as CO, NO or $O_2$. All the prepared heme models have been characterized by both UV-visible (UV-Vis) absorption and magnetic circular dichoism (MCD) spectroscopy. MCD is highly useful as a fingerprinting technique in identifying the heme coordination structures because it provides both positive and negative signals (and cross-over points) as compared with only the positive features of the UV-Vis absorption spectroscopy. Taking advantage of the versatile protein scaffold and the powerful spectroscopic technique, we have established a large protein-based heme coordination library that contributes valuable knowledge on structure-function relationships of heme proteins.

**Cytochrome P450**

Cytochrome P450 (P450) is a large family of heme-containing monooxygenase enzymes that catalyze the insertion of one oxygen atom of $O_2$ to organic substrates (Eq. 4.1) [12]. The name comes from the unique absorption peak at 450 nm in the ferrous-CO state of the enzyme. P450 can be found throughout the biological kingdom with important functions such as detoxification of xenobiotics and synthesis of signaling molecules (e.g. hormones).

$$R_3C\text{-}H + O_2 + 2H^+ + 2e^- \rightarrow R_3C\text{-}OH + H_2O \quad (4.1)$$

The first solved structure of P450 is that of P450-CAM (CYP 101), a soluble protein isolated from a bacteria *pseudomonas putida* (Figure 4.2) [13]. The protein has a molecular mass of ~ 45 kDa consisting of a single polypeptide in an overall triangular shape (panel A). The heme cofactor is deeply buried inside with a conserved proximal cysteine residue that covalently tethers the heme to the protein backbone (panel B). The anionic Cys ligated to the heme iron provide a strong electron push that facilitats O-O bond cleavage to form the Cpd I of P450, which is the "active oxygen" intermediate that actually oxidizes hydrocarbon substrates [14]. Figure 4.3 schematically illustrates the whole catalytic cycle of P450 starting from a $H_2O$-bound six-coordinate low-spin ferric resting state (1). Upon substrate binding, the enzyme loses the distal $H_2O$ ligand yielding a five-coordinated high-spin species (2) which is readily reduced by one electron [provided by NADH through an electron-donor iron-sulfur protein putidaredoxin (Pd)] to ferrous state (3). The deoxyferrous P450 then bind $O_2$ to form the oxyferrous species (4), which is in resonance with a ferric superoxide complex (5). One electron transferred from NADH (via Pd) followed by protonation yield the ferric-hydroperoxide (7). The next step is the O-O bond heterolysis facilitated by the proximal "thiolate-push" discussed above. The resulting active species Cpd I (8) can oxidize inert hydrocarbon substrate camphor and return to the resting state. The maintenance of the proximal thiolate ligation to the heme iron is crucial for P450 to function.

**Models for Cytochrome P450**

It has been found that proximal heme environment is critical in stabilizing the heme-thiolate ligation [15]. In Figure 4.4, the proximal $Cys^{357}$ is in a H-bond network with the

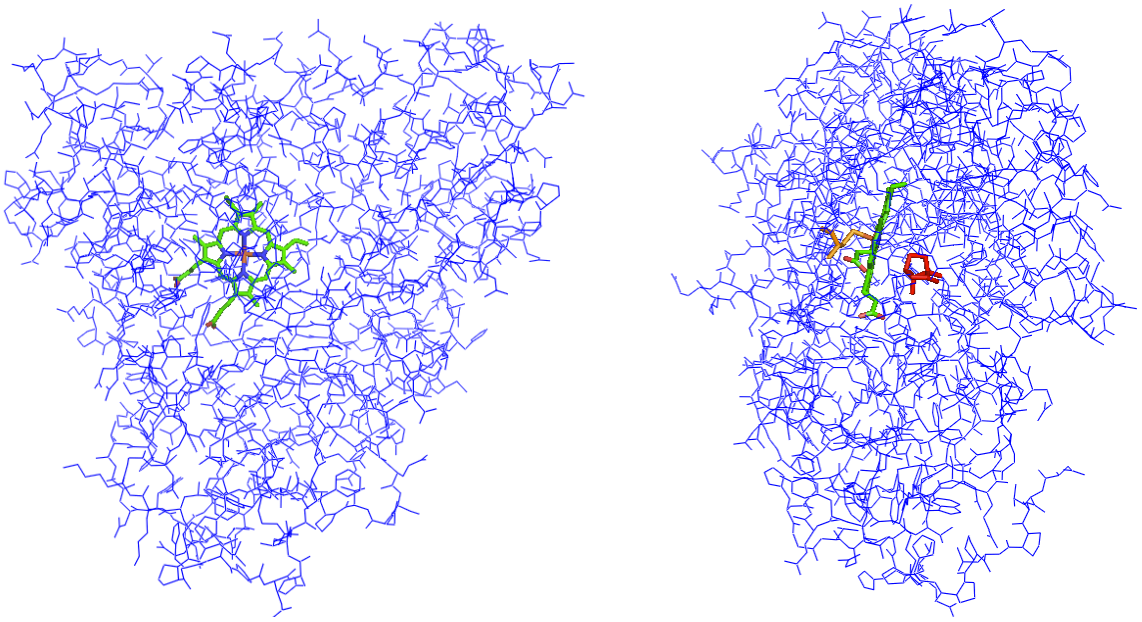


**Figure 4.2.** Front (A) and side (B) views of the structure of P450-CAM from *pseudomonas putida* (pdb accessing code: 2CPP) [13]. Heme prosthetic group is colored in green. Panel B shows substrate camphor molecule in red and the proximal cysteine residue in yellow.

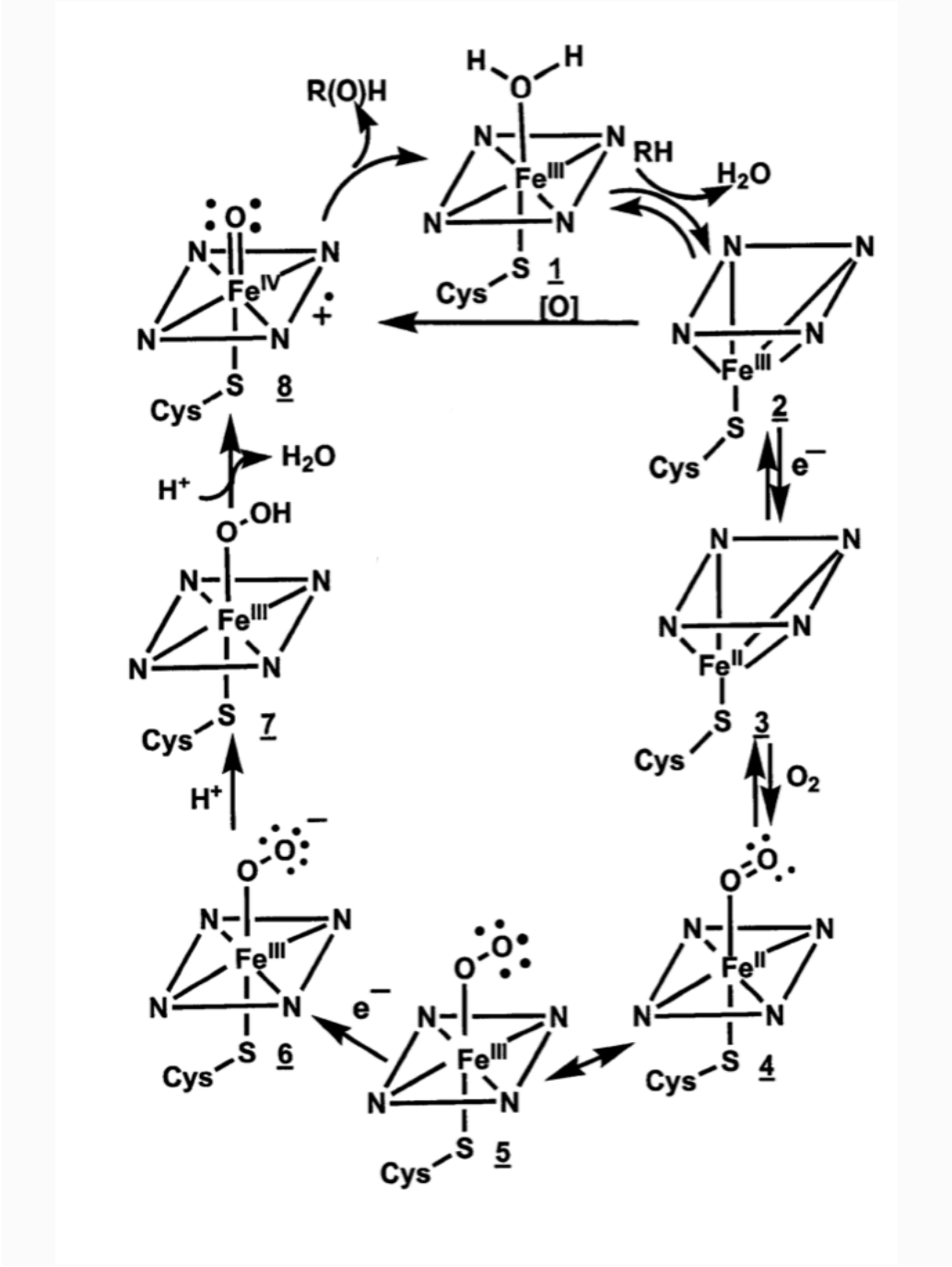


**Figure 4.3.** Reaction cycle for cytochrome P450 showing the core intermediates (adapted from reference [12]).

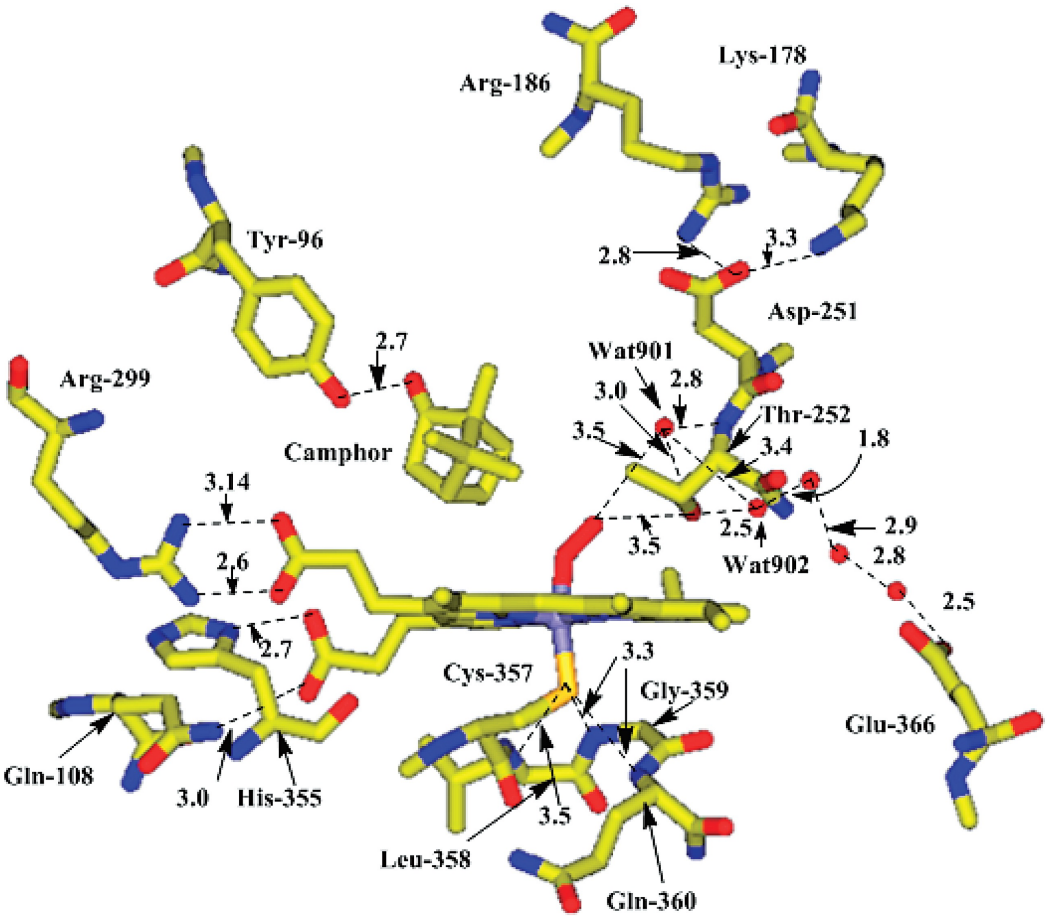


**Figure 4.4** Active site of cytochrome P450-CAM (CYP101) (taken from reference [16]). A possible proton delivery network involving a series of hydrogen bonded water molecules (the middle part of the right hand side) [31] is also shown (Protein Data Bank code: 1DZ8).

peptide carbonyl oxygen atoms of several adjacent residues such as $Leu^{358}$, $Gly^{359}$ and $Gln^{360}$. It has been of great interest to build a stable cysteinate-ligated heme structure in other heme proteins systems. Early attempts used the approach of site-directed mutagenesis. H93C human myoglobin, in which proximial His was replaced by Cys, exhibits spectroscopic features that resemble those of ferric P450 as well as significantly enhanced peroxidation activity [9]. However, upon reduction, the spectrum of ferrous H93C Mb looked quite different from the native ferrous P450, implying the loss of proximal thiolate ligation. In another study, the H175C/D235L yeast cytochrome c peroxidase (CcP) double mutant was prepared with the proximal His mutated to Cys and the nearby Asp replaced by Leu [17]. The purpose of replacing an anionic (i.e. carboxylate) Asp235 residue with a nonpolar neutral amino acid Leu in conjunction with His175Cys mutation is to help stabilize the negatively charged cysteinate ligation to heme iron that favors a hydrogen bond donor rather than hydrogen bond acceptor such as Asp. Unfortunately, the MCD spectra of this mutant also only resembled that of P450 in the ferric but not the ferrous state.

Our lab has been using H93G Mb as a scaffold to prepare models for P450 [18, 19]. Titrations of exogenous ligand-free ferric H93G Mb with an extensive series of thiols successfully generated mimics for ferric P450 with similar spectroscopic features. However, as the previous studies on human Mb and CcP, attempts to reduce the iron to ferrous state while retaining the thiolate ligand were unsuccessful. The five-coordinate adducts of ferrous H93G Mb with neutral thiol or thioether gave a MCD spectra that were similar in general pattern to that of five-coordinate imidazole-ligated ferrous WT Mb but quite distinct from that of thiolate-ligated deoxyferrous P450 (Figure 4.3) [18]. This

result suggested that the proximal cysteine thiolate might be protonated to yield a neutral thiol upon reduction of the heme iron to ferrous state.

The difficulty in establishing a stable cysteinate-ligated ferrous heme complex like that in ferrous P450 is proposed to be due to weakening of the Fe-S bond that is stable in the ferric state (overall charge on the heme iron = 0), but becomes unstable upon reduction of the iron (overall charge = -1). Thus, to create a spectroscopic model for ferrous P450, an alternative approach would be to use a neutral ligand(s) with donor properties similar to the cysteinate thiolate ligand. Alkyl phosphines are neutral ligands that have been previously shown to have donor properties similar to thiolates in P450 and related systems [20] and will be the focus of studies with H93G Mb reported herein.

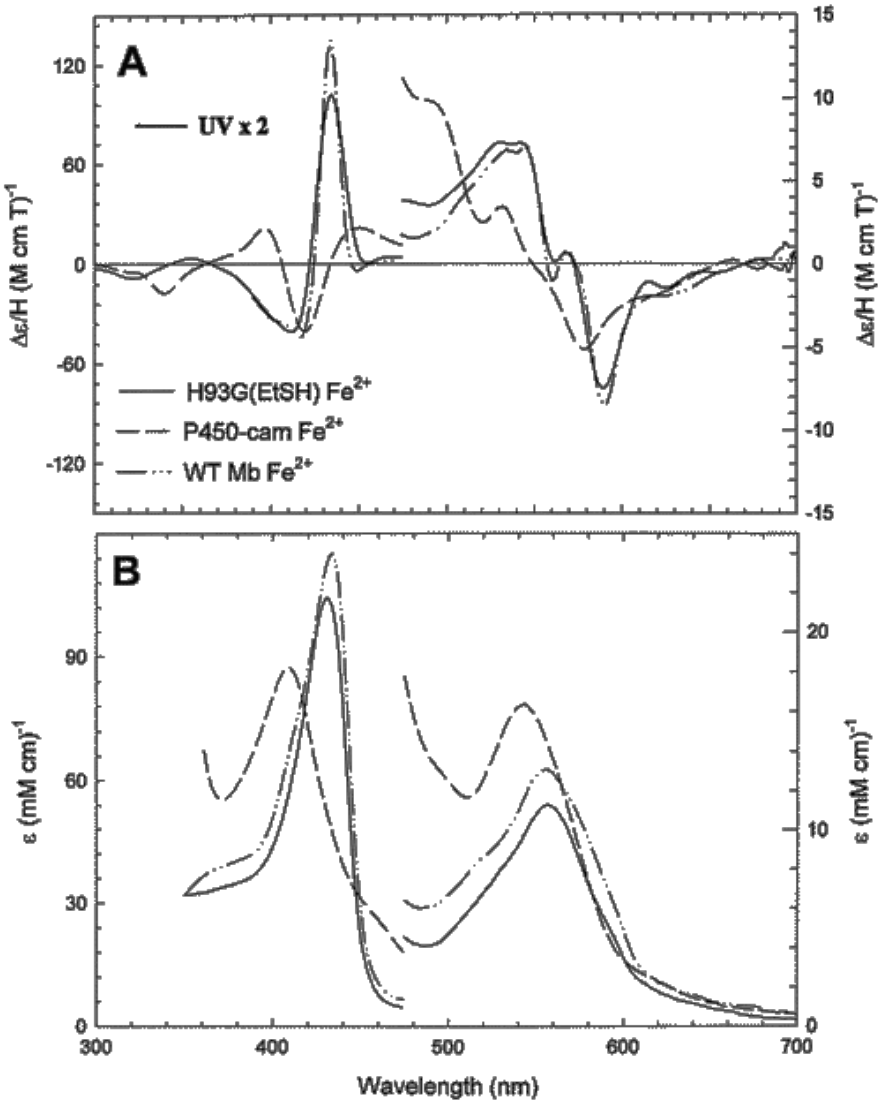


**Figure 4.5** Overlaid MCD (A) and UV-Vis (B) spectra of ferrous H93G(EtSH) complex (solid line), deoxyferrous cytochrome P450-CAM (dashed line) and deoxyferrous myoglobin (dash-dotted line) at pH 7.0 (taken from reference [18]).

**REFERENCES**


[1] C. Chang, T. Traylor, Proc. Natl. Acad. Sci. 70 (1973) 2647-2650.

[2] J.P. Collman, Acc. Chem. Res. 10 (1977) 265-272.

[3] G.E. Wuenschell, C. Tetreau, D. Lavalette, C.A. Reed, J. Am. Chem. Soc. 114 (1992) 3346-3355.

[4] T. Traylor, Acc. Chem. Res. 14 (1981) 102-109.

[5] S.-i. Ozaki, T. Matsui, M.P. Roach, Y. Watanabe, Coord. Chem. Rev. 198 (2000) 39-59.

[6] T. Hayashi, Y. Hisaeda, Acc. Chem. Res. 35 (2002) 35-43.

[7] T. Ueno, Angewandte Chemie International Edition 49 (2010) 3868-3869.

[8] V. Köhler, T.R. Ward, ChemBioChem 11 (2010) 1049-1051.

[9] S. Adachi, S. Nagano, K. Ishimori, Y. Watanabe, I. Morishima, T. Egawa, T. Kitagawa, R. Makino, Biochemistry 32 (1993) 241-252.

[10] K.D. Egeberg, B.A. Springer, S.A. Martinis, S.G. Sligar, D. Morikis, P.M. Champion, Biochemistry 29 (1990) 9783-9791.

[11] J. Du, M. Sono, J.H. Dawson, J. Porphyr. Phthalocya. 15 (2011) 29-38.

[12] M. Sono, M.P. Roach, E.D. Coulter, J.H. Dawson, Chem. Rev. 96 (1996) 2841-2888.

[13] T.L. Poulos, B.C. Finzel, A.J. Howard, J. Mol. Biol. 195 (1987) 687-700.

[14] A.E. pond, Ledbetter, A.P., Sono, M., Goodin, D.B., Dawson, J.H., Handbook on elctron Transfer Publisher: New York 56-104.

[15] S. Yoshioka, S. Takahashi, K. Ishimori, I. Morishima, J. Inorg. Biochem. 81 (2000) 141-151.

[16] R. Perera, Sono, M., Dawson, J. H., Met. Ions Life Sci. 3 (2007) 319–359.

[17] J.A. Sigman, A.E. Pond, J.H. Dawson, Y. Lu, Biochemistry 38 (1999) 11122-11129.

[18] M.P. Roach, A.E. Pond, M.R. Thomas, S.G. Boxer, J.H. Dawson, J. Am. Chem. Soc.121 (1999) 12088-12093.

[19] R. Perera, M. Sono, J.A. Sigman, T.D. Pfister, Y. Lu, J.H. Dawson, Proc. Natl. Acad. Sci. 100 (2003) 3641-3646.

[20] M. Sono, J.H. Dawson and L. P. Hager, Inorg. Chem. 24 (1985) 4339-4343.

# CHAPTER 5

## Mono- and bis-phosphine-ligated H93G myoglobin: Spectral models for ferrous-phosphine and ferrous-CO cytochrome P450[3]

[3] Sun, S., Sono, M., and Dawson, J. H. (2013) *J. Inorg. Biochem.* 127, 238-245. Preprinted here with permission of publisher.

**ABSTRACT**

To further investigate the properties of phosphines as structural and functional probes of heme proteins, mono- and bis-phosphine [tris(hydroxymethyl)phosphine, THMP] adducts of H93G myoglobin (Mb) have been prepared by stepwise THMP titrations of exogenous ligand-free ferric and ferrous H93G Mb, respectively. Bubbling with CO or stepwise titration with imidazole (Im) of the bis-THMP-ligated ferrous protein generated a mixed ligand (THMP/CO or THMP/Im, respectively) ferrous complexes. Stable oxyferrous H93G(THMP) Mb was formed at -40 °C by bubbling the mono-THMP-Fe(II) protein with $O_2$. A THMP-ligated ferryl H93G Mb moiety has been partially formed upon addition of $H_2O_2$ to the ferric mono-THMP adduct. All the species prepared above have been characterized with UV-visible (UV-Vis) absorption and magnetic circular dichroism (MCD) spectroscopy in this study. The six-coordinate ferrous bis-phosphine and mono-phosphine/CO complexes of H93G Mb exhibit characteristic spectral features (red-shifted Soret/unique-shaped MCD visible bands and hyperporphyrin spectra, respectively) that only have been seen for the analogous phosphine or CO-complexes of thiolate-ligated heme proteins such as cytochrome P450 (P450) and *C. fumago* chloroperoxidase (CPO). However, such resemblance is not seen in phosphine-ligated ferric H93G Mb even though phosphine-bound ferric P450 and CPO display hyperporphyrin spectra. In fact, bis-THMP-bound ferric H93G Mb exhibits MCD and UV-Vis absorption spectra that are similar to those of bis-amine- and bis-thioether-ligated H93G Mb complexes. This study also further demonstrates the utility of the H93G cavity mutant for preparing novel heme iron coordination structures.

## INTRODUCTION

It is well-known that the functions of heme-containing enzymes largely depend on the coordination structures of the iron center [1, 2]. Investigations of the iron oxidation and spin state, the amino acids coordinated to the heme iron and the influence of the surrounding protein environment provide key information to understand the mechanisms of actions of the native heme enzymes [3-5]. To thoroughly study the structures and the functions of the diverse heme enzymes, numerous heme iron model systems have been developed. Among these approaches, the use of H93G myoglobin (Mb) cavity mutant, pioneered by Barrick [6], provides a convenient way to generate heme coordination models. The proximal cavity in H93G Mb, formed by replacing the His ligand with a smaller non-coordinating Gly, allows exogenous ligands to enter into the active heme center of Mb. Our laboratory has successfully prepared several model heme complexes of defined structure using H93G Mb, such as H93G Mb imidazole (Im), alkylthiolate and carboxylate adducts as mimics of native Mb, cytochrome P450 (P450) and oxyanion-bound heme proteins, respectively [7-13]. The H93G Mb adducts with a phosphorus-donor ligand, however, have not been reported yet. Although phosphorus-donor ligands, such as phosphines, are not found in native heme proteins, they have been extensively used as structural and functional probes of hemoprotein active sites [14-19]. Compared to CO, phosphines are more versatile in that they can serve as distal ligands to both ferrous and ferric iron of hemoproteins.

In particular, we have shown that phosphine-ligated ferric P450 and *C. fumago* chloroperoxidase (CPO), with a thiolate/phosphine ligand set, exhibit the rarely observed unusually red-shifted Soret absorption bands that are characteristic of hyperporphyrins

[16], previously reported for thiolate-ligated ferric P450 and CPO with a bis-thiolate ligand set [20]. This suggested that phosphines have very similar donor properties to thiolate ligands and thus that heme adducts with proximal phosphine ligation might be spectroscopic mimics of P450. Further, since phosphines are neutral ligands and it has so far not been possible to bind anionic ligands such as thiolates to ferrous or ferryl H93G Mb [13] to make H93G models for those P450 states, it seemed plausible that neutral phosphines might serve as surrogate thiolates for the generation of ferrous and ferryl H93G adducts with spectral properties resembling those of ferrous and ferryl P450. In pursuit of that goal, we have in this study carried out a thorough spectroscopic investigation of H93G Mb phosphine complexes in the ferric, ferrous and ferryl states. Successful generation of the first H93G Mb spectral models for ferrous P450 and CPO will be described. The data reported herein also further expand the already extensive H93G Mb heme coordination model library.

## MATERIALS AND METHODS

*Materials.*

Sperm whale H93G Mb was expressed and purified in the presence of 10 mM Im as previously described [6, 9]. Im, tris(hydroxymethyl)phosphine (THMP), hydrogen peroxide and sodium dithionite were obtained from Sigma/Aldrich. CO and $O_2$ gases were purchased from Natural Air Product.

*Sample preparation.*

Imidazole was removed from the proximal cavity of H93G Mb by means of heme extraction and reconstitution with hemin [8]. Concentrations of ferric and ferrous H93G

Mb samples were calculated based on $\varepsilon_{406}$ = 112 $mM^{-1}$ $cm^{-1}$ in potassium phosphate buffer at pH 7.0, 4 °C, which was determined using the pyridine hemochromogen method [12, 21]. Complete oxidation of the protein heme iron is accomplished by addition of a few crystals of potassium ferricyanide (Fluka) followed by gel-filtration column chromatography. THMP and imidazole stock solutions were prepared by dissolving the solid in ethanol and water respectively.

For the THMP titration experiments, incremental amounts of aliquots from stock solutions of 1 mM to 0.5 M THMP in ethanol were added to exogenous ligand-free ferric H93G Mb (~25 μM) or ferrous H93G Mb(~3 μM). Comparable amounts of ethanol did not produce observable spectral changes. $K_d$ values were determined from hyperbolic regression fits of ligand saturation plots. All the titration experiments were conducted at pH 7.0 and 4 °C. The complete reduction of ferric H93G Mb to deoxyferrous state was achieved by adding solid sodium dithionite to degassed protein solutions. Bubbling CO to the bis-THMP-bound ferrous H93G Mb generated the ferrous-CO derivative. For imidazole titrations of bis-THMP-bound ferrous H93G Mb that had been prepared by dithionite-reduction of the bis-THMP complex of ferric H93G Mb, a 2 M imidazole stock solution (pH adjusted to 7.0) was used. The ferrous-$O_2$ complex was generated at -40 °C (in a mixed solvent, see below) in a chest freezer by addition of minimal sodium dithionite solution to an extensively degassed ferric protein sample containing 0.5 mM THMP followed by thorough bubbling with cold $O_2$. The ferryl derivative was generated from ferric H93G(THMP) Mb by adding 2.0 equivalents of $H_2O_2$ (relative to the H93G Mb concentration).

*Spectroscopic techniques.*

UV-visible (UV-Vis) absorption spectra were recorded with a Cary 400 spectrophotometer interfaced to a Dell PC. Magnetic circular dichroism (MCD) spectra were measured with a magnetic field strength of 1.41 T by using a JASCO J815 spectropolarimeter equipped with a JASCO MCD-1B electromagnet and interfaced with a Gateway PC through a JASCO IF-815-2 interface unit. Data acquisition and manipulation were carried out as previously described [9]. EPR spectra were measured with a Bruker EMXplus CW X-band EPR spectrometer using the following conditions: microwave frequency, around 9.4000 GHz; microwave power, 0.2 mW (4.5 K) or 10 mW (15 K); modulation amplitude, 5.0 G; and modulation frequency, 100.0 kHz. UV-Vis absorption spectra and MCD spectra were obtained in 100 mM potassium phosphate buffer (pH = 7.0) at 4 °C or in a cryosolvent of glycerol/0.1 M phosphate (70:30 vol/vol) buffer at -40 °C and EPR spectra were obtained in 100 mM bicine {2-[bis(2-hydroxyethyl)amino]acetic acid} buffer (pH = 7.5) at 4.5 K or 15 K.

## RESULTS AND DISCUSSION

*THMP binding to exogenous ligand-free ferric H93G Mb [ferric H93G(-L) Mb]and spectroscopic characterization of the resulting complexes.*

Stepwise additions of THMP to ferric H93G(-L) Mb produced spectral changes in the Soret and visible regions with two clear sets of isosbestic points during the titration (Fig. 1). This indicates that there are two phases throughout the ligand binding reaction. In the first phase (Fig. 1A), adding low concentrations (0 - 0.12 mM) of THMP to the exogenous ligand-free ferric H93G Mb led to the formation of the mono-THMP coordinated species with THMP binding to the proximal side of the heme and involved a

decrease in intensity of the Soret peak and an increase in absorbance around 577 nm. The assumption that THMP binds first to the proximal side of the heme in exodenous ligand-free H93G Mb (H93G(-L) Mb) is based on our previous study on imidazole (Im) binding to ferric and ferrous H93G(-L) Mb [12]. The preference for the proximal side for such relatively large ligands (Im, THMP) is the result of the influence by steric hindrance by the distal His-64. With further addition of THMP, a bis-THMP ferric H93G Mb with a second THMP binding to the distal side of the heme was gradually formed in the second phase. The Soret abosorption band is red-shifted from 406 nm to 415 nm. New UV-Vis spectral features appear in the visible region that are typical of low-spin ferric heme complexes consisting of two peaks around ~540 and ~560 nm that develop accompanying the appearance of a second set of isosbestic points (Fig. 1B).

The titration data were analyzed using a simple biomolecular association scheme and the plots of absorbance change vs. ligand concentration were analyzed by a regression fit of a saturation plot (difference absorbance change vs. THMP concentration) to a hyperbolic curve (Fig. 5.11, insets). The dissociation constant ($K_{d1}$) for THMP binding to ferric H93G(-L) Mb is ~0.11mM and the $K_{d2}$ for THMP binding to mono-THMP-bound H93G Mb is 5.0 mM (Fig. 5.1, A and B insets, respectively). The THMP saturation is not reached with ~10.6 mM ligand added for the second THMP binding due to the insufficient phosphine concentration added (saturation: ~ 10.6 / (10.6 + 5.0) = ~0.68). Higher concentrations of the phosphine were not used because of the slow autoreduction of the protein as evidenced by a gradual appearance of an absorption peak at ~450 nm (Fig. 1B). Note that it was a purpose of this study to obtain $K_d$ values to confirm formation of homogeneous (i.e., ligand-saturated) complexes, but not necessarily

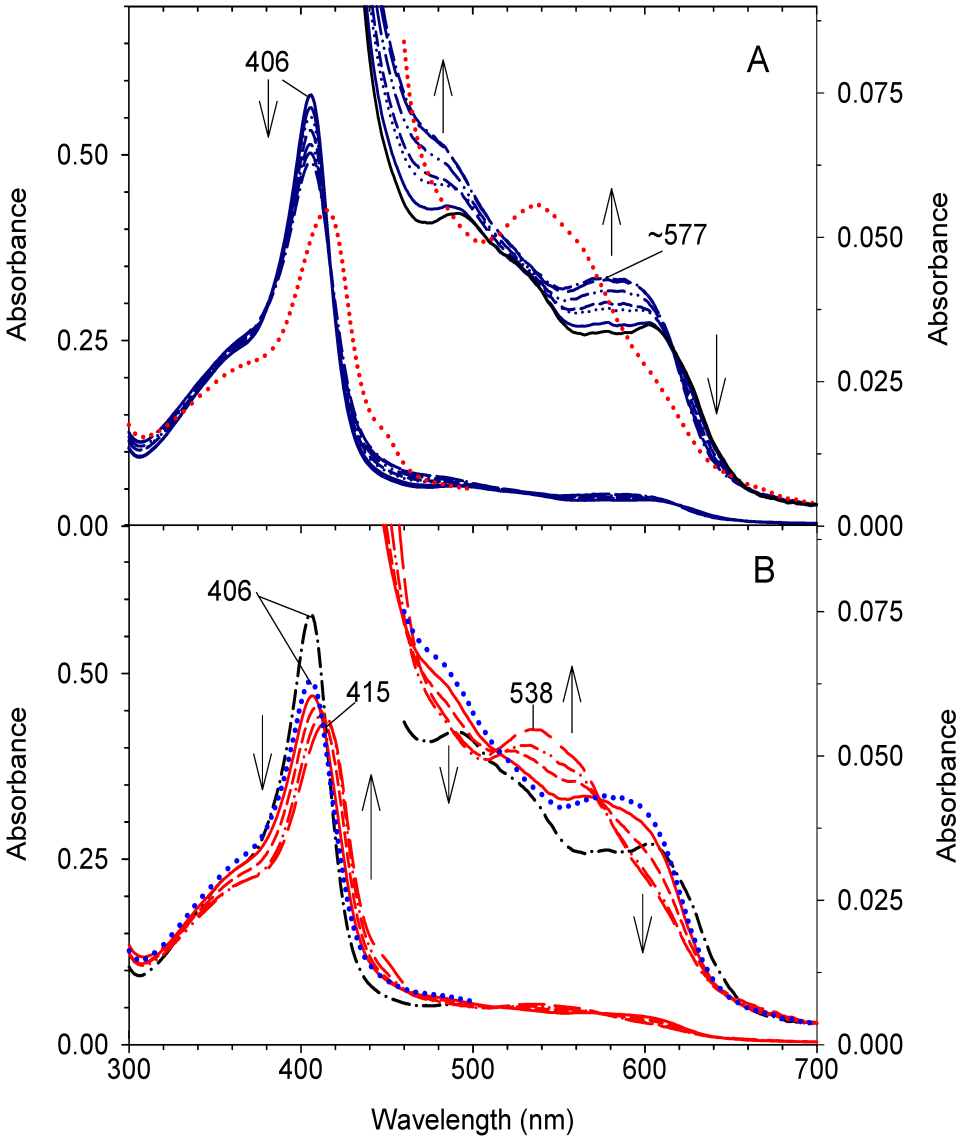


**Figure 5.1.** UV-Vis absorption spectral changes upon titration of ferric H93G(-L) Mb (25 μM in a 0.2-cm cuvette) with THMP in 0.1 M potassium phosphate buffer, pH =7.0, at 4 °C. (a) Spectral change in the first phase on addition of 0.027, 0.053, 0,11, 0.24, 0.50, 1.02 mM THMP. The dotted line represents the last spectra in the second phase on addition of 10.61 mM THMP as shown in figure (b). (b) Spectra change in the second phase on addition of 1.02, 1.67, 2.97, 5.54, 10.61 mM THMP. The dash-dotted line represents the starting spectra of exogenous ferric H93G(-L) Mb and the dotted line represents the last spectra in the first phase as shown in figure (a). The vertical arrows indicate the directions of absorbance changes.

to obtain the values with statistic uncertainties. Nevertheless, reproducibility of the values was estimated to be within +/- 10%.

Fig. 5.2 displays the UV-Vis absorption and MCD spectra of ferric H93G(-L) Mb (dotted line) and ferric H93G(mono-THMP) Mb (solid line) at pH 7.0. Their overall MCD band patterns are quite similar. For further comparison, previously published spectra of mono-Im (dot-dashed line) and mono-THT (tetrahydrothiophene) complexes (dashed line) of ferric H93G Mb [9, 22] are also overlaid in Fig. 5.2. As assigned previously, ferric H93G(-L) Mb at pH 7 is a mixture of six-coordinated bis-water-bound species and five-coordinate hydroxide adduct with the latter species being predominant at pH 7.0 and exhibits a UV-Vis absorption spectrum with a Soret peak at 406 nm and a charge transfer band at about 600 nm [22, 23]. Although the Soret region (350 - 450 nm) MCD and UV-Vis spectral features of all these heme species are similar to each other, their spectral line shapes in the visible region (450 - 670 nm) can be classified into two patterns. The high spin charge-transfer visible absorption band at ~605 nm of the ferric H93G(-L) Mb shifted to blue (shorter wavelength) upon ligation of THMP and THT, while the Im complex shows a distinctly red-shifted band at ~630 nm. The corresponding MCD band (trough) intensities and patterns for the two groups are also clearly distinguishable. The red-shifted weak MCD trough (~635 nm) and mostly negative feature (560 - 670 nm) for the Im adduct are characteristic of a six-coordinate nitrogen-donor-Fe(III) heme-$OH_2$ coordination mode. In contrast, more intense MCD features that are both negative (troughs) and positive (peaks) in this region appear to be attributable to a five-coordinate high spin heme as described above for H93G(-L) Mb and established for mono-thioether-ligated heme (based on resonance Raman evidence [24]). Thus, the

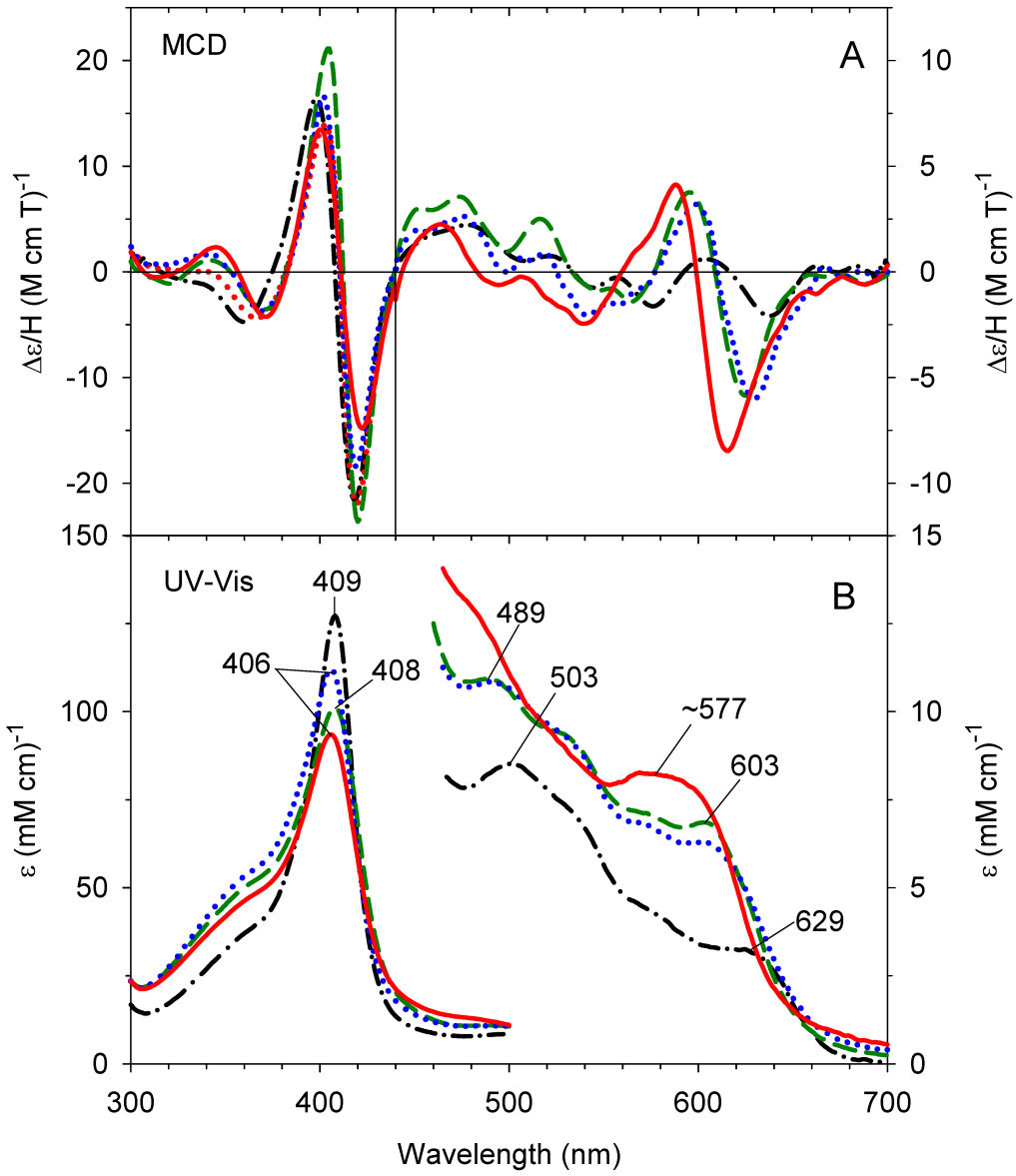


**Figure 5.2.** (Top) MCD and (bottom) UV-Vis absorption spectra of ferric H93G(THMP) Mb (solid line, 1.03 mM THMP) overlaid with the spectra of ferric exogenous ferric H93G(THT) Mb (dashed line, 21 mM THT), ferric H93G(Im) Mb (dash-dotted line, 1 mM Im) and ferric exogenous ligand free H93G Mb (dotted line) in 0.1 M potassium phosphate buffer, pH 7.0, at 4°C. The latter three spectra are replotted from Ref. [22].

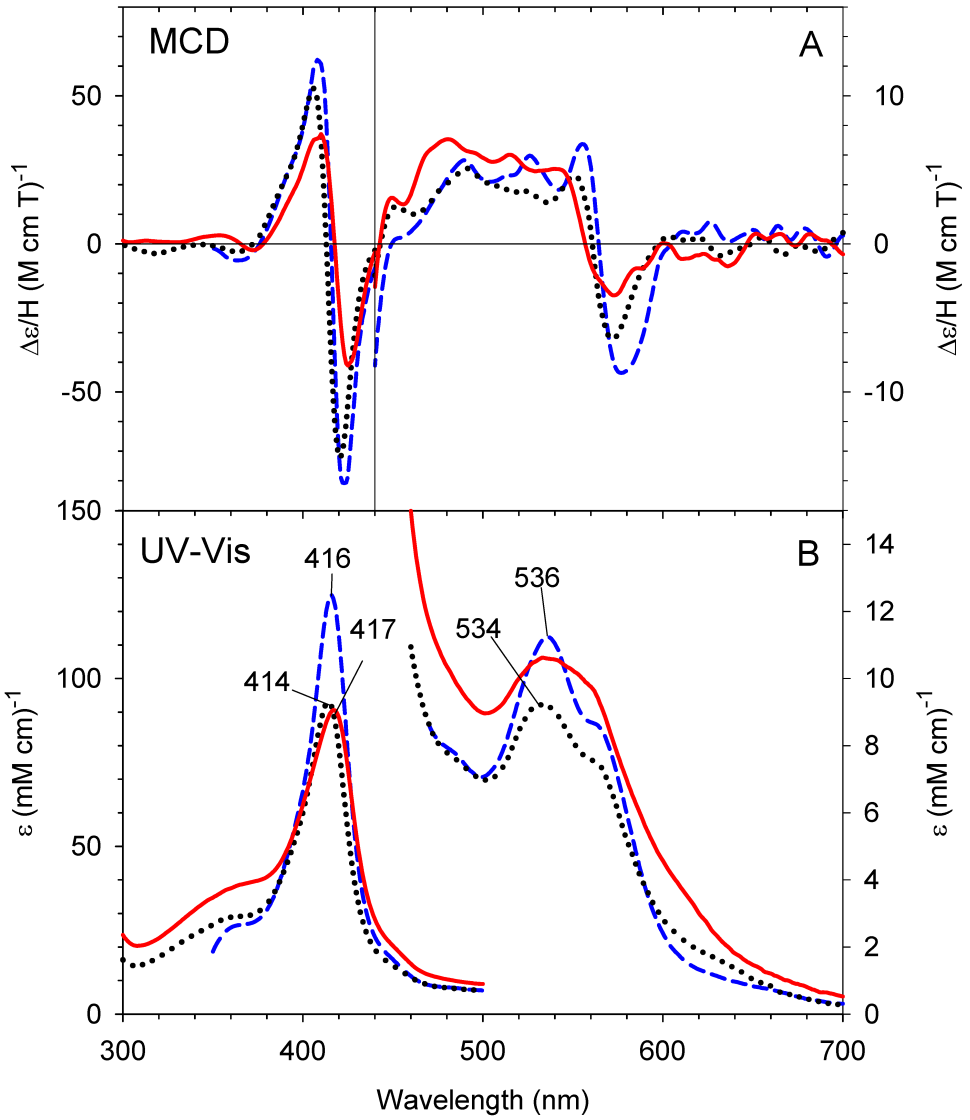


**Figure 5.3.** (Top) MCD and (bottom) UV-Vis absorption spectra of ferric H93G(bis-THMP) Mb (solid line, 17.6 mM THMP), ferric H93G(bis-Im) Mb (dashed line) in 0.1 M potassium phosphate buffer, pH 7.0, at 4 °C and ferric H93G (bis-THT) Mb (dotted line) in 0.1 M potassium phosphate, pH 5.0. The spectra for ferric H93G(bis-Im) Mb and ferric H93G (bis-THT) Mb are replotted from Refs. [12] and [22], respectively.

mono-THMP adduct of H93G Mb is likely to be also five-coordinate (*vide infra*, the EPR and Conclusions sections). Fig. 5.3 reveals that the UV-Vis and MCD spectra of ferric H93G(bis-THMP) Mb adduct that was prepared by addition of 34 mM THMP to ferric H93G(-L) Mb at once to minimize autoreduction, have band patterns that are broadly similar to those of the previously reported ferric bis-Im H93G Mb as well as the ferric bis-thioether (THT) H93G complexes [22] and related bis-Met-ligated heme protein or heme-carrier mutants [24, 25].

*THMP binding to ferrous H93G(-L) Mb and spectroscopic characterization of the resulting complexes.*

Titration of ferrous H93G(-L) Mb with THMP yields mono-THMP-bound ferrous H93G Mb with the $K_d$ value of 1.5μM (Fig. 5.12). Comparison of the UV-Vis and MCD spectra of this ferrous H93G(THMP) species to those of the previously reported ferrous H93G(Im) Mb [12] shows a close similarity except for a small blue shift of ~2 nm in Soret region for the THMP complex (Fig. 5.4).

Reduction of the ferric bis-THMP H93G Mb with dithionite yielded the corresponding ferrous bis-THMP complex. The overall UV-Vis and MCD spectra of this adduct (Soret peak at 451 nm and a main band at 546 nm with a shoulder at ~575 nm) resemble those of the phosphine adducts of cysteinate-ligated ferrous P450-CAM and CPO except for some blue-shifts for the H93G Mb adduct (Fig. 5.5). In contrast, as previously reported, phosphine-bound ferrous Mb has quite different spectroscopic features with the Soret peak at 436 and two visible region peaks at 535 and 568 nm ([14], this study). This is because Mb has a neutral histidine as its proximal ligand, while in ferrous P450-CAM or CPO, the proximal ligands is a negatively charged cysteinate. The

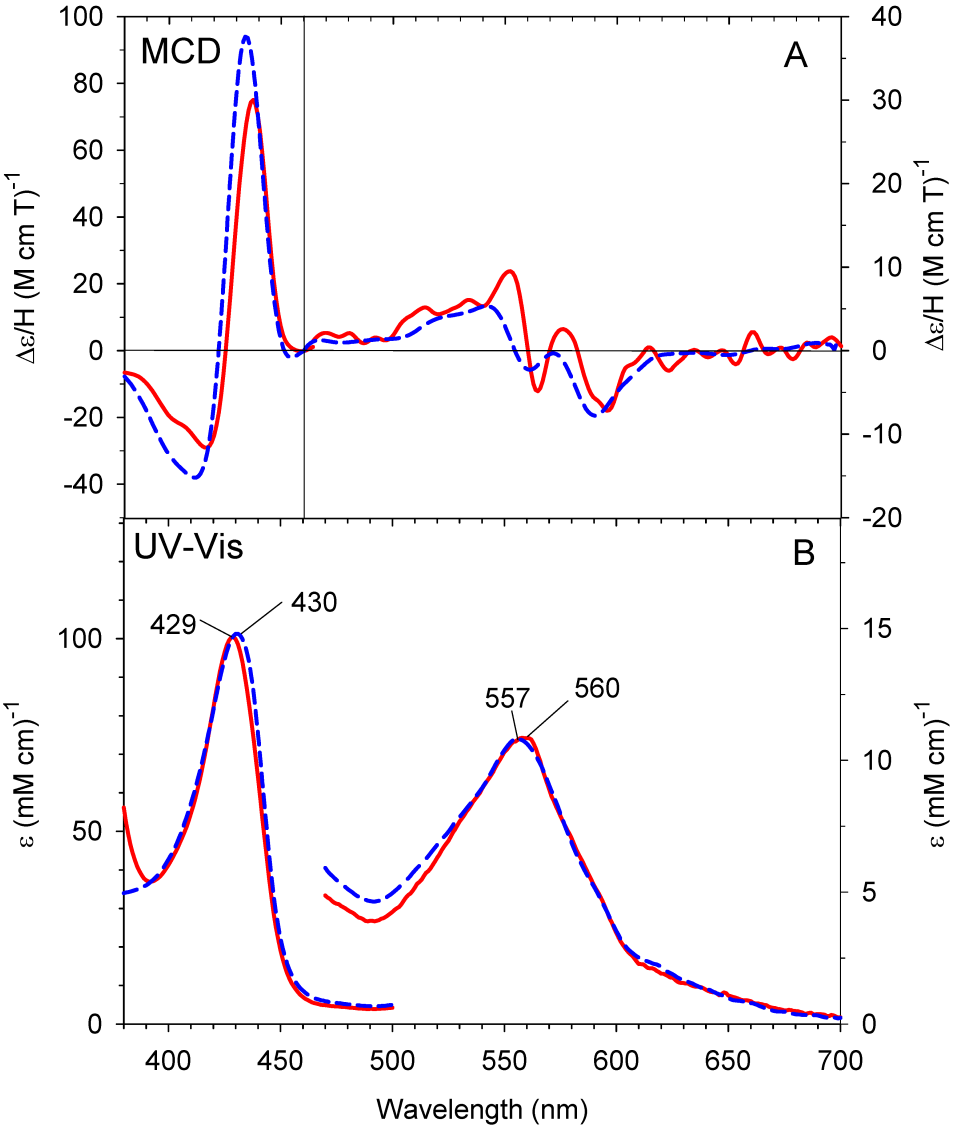


**Figure 5.4.** (Top) MCD and (bottom) UV-Vis absorption spectra of ferrous H93G(THMP) Mb (solid line, 250 μM THMP) compared with ferrous H93G(Im) Mb (dashed line, 2 mM Im) in 0.1M postassium phosphate buffer, pH 7.0, at 4 °C. The spectra for ferrous H93G(Im) Mb are replotted from Ref. [12].

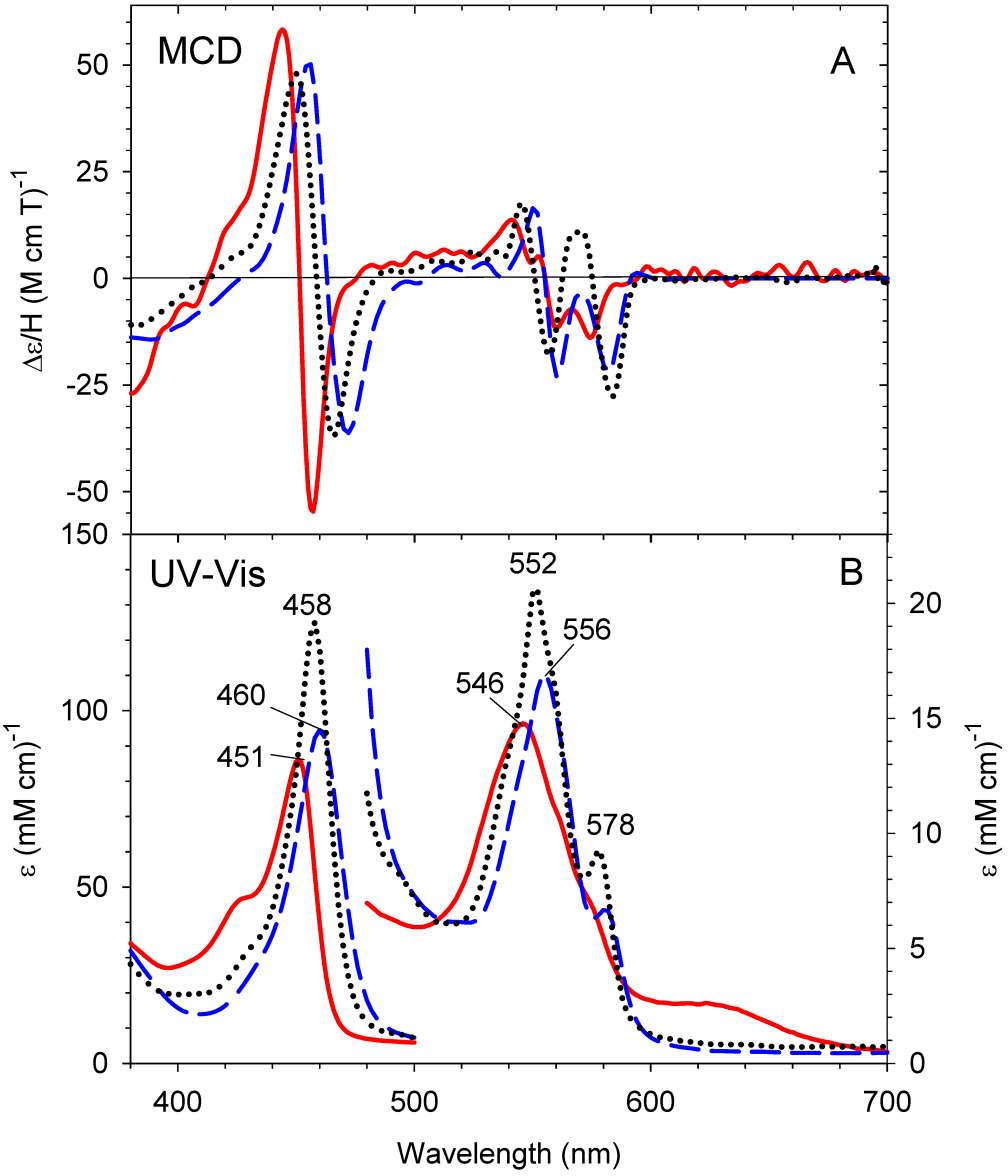


**Figure 5.5.** (Top) MCD and (bottom) UV-Vis absorption spectra of ferrous H93G(bis-THMP) Mb (solid line, 34 mM mM THMP), bis-(hydroxymethyl)methyl phosphine (BHMMP)-bound ferrous P450-CAM (dashed line) in 0.1 M potassium phosphate buffer, pH 7.0, at 4 °C and bis- BHMMP-bound ferrous CPO (dotted line) in 0.1 M potassium phosphate buffer, pH 6.3. The spectra for phosphine-bound ferrous P450-CAM and CPO were replotted from Ref. [16].

similarity of theferrous H93G(bis-THMP) complex to the phosphine adducts of ferrous P450-CAM as well as CPO is noteworthy. However, the derivative-shaped MCD Soret band of ferrous H93G(bis-THMP) Mb is 10 and 6 nm blue-shifted compared to those features in the spectra of the corresponding ferrous P450-CAM and CPO phosphine complexes, respectively. This is likely due to the differences in the donor properties (bis-phosphine vs. phosphine/thiolate) of the two axial donor ligands.

*CO, $O_2$ and Im complexes of THMP-ligated ferrous H93G Mb.*

Treatment of ferrous H93G(bis-THMP) Mb with CO yielded a stable ferrous-CO-H93G(THMP) Mb adduct that is again spectrally similar to parallel ferrous CO-P450-CAM and CPO with Soret maximum absorption at 437 nm and a main visible region band at 546 nm (Fig. 5.6). In contrast, ferrous-CO Mb exhibits a Soret band at 423 and two visible bands at 542 and 579 nm [26].

Titrating the bis-THMP-bound ferrous H93G Mb with Im caused the Soret absorption peak to shift from 451 nm to 432 nm and the main visible peak at 546 nm to split into two peaks at 534 nm and 564 nm (Fig. 5.13). The occurrence of clear single set of isosbestic points during the spectra change as well as the good fit of the plot of peak-to-trough absorbance in the difference spectra (data not shown) vs. Im concentration to the regression hyperbolic saturation (Fig. 5.13, inset) indicate a conversion from ferrous bis-THMP-bound H93G Mb to a novel THMP/Im mixed ligand-coordinated ferrous H93G derivative upon replacement of one of the two THMP ligand with Im. Further addition of Im to this THMP/Im mixed ligand complex of ferrous H93G Mb resulted in formation of bis-Im-bound adduct whose spectra are identical to those reported previously [12] (data not shown). Fig. 5.7 compares the MCD and UV-Vis spectra of the

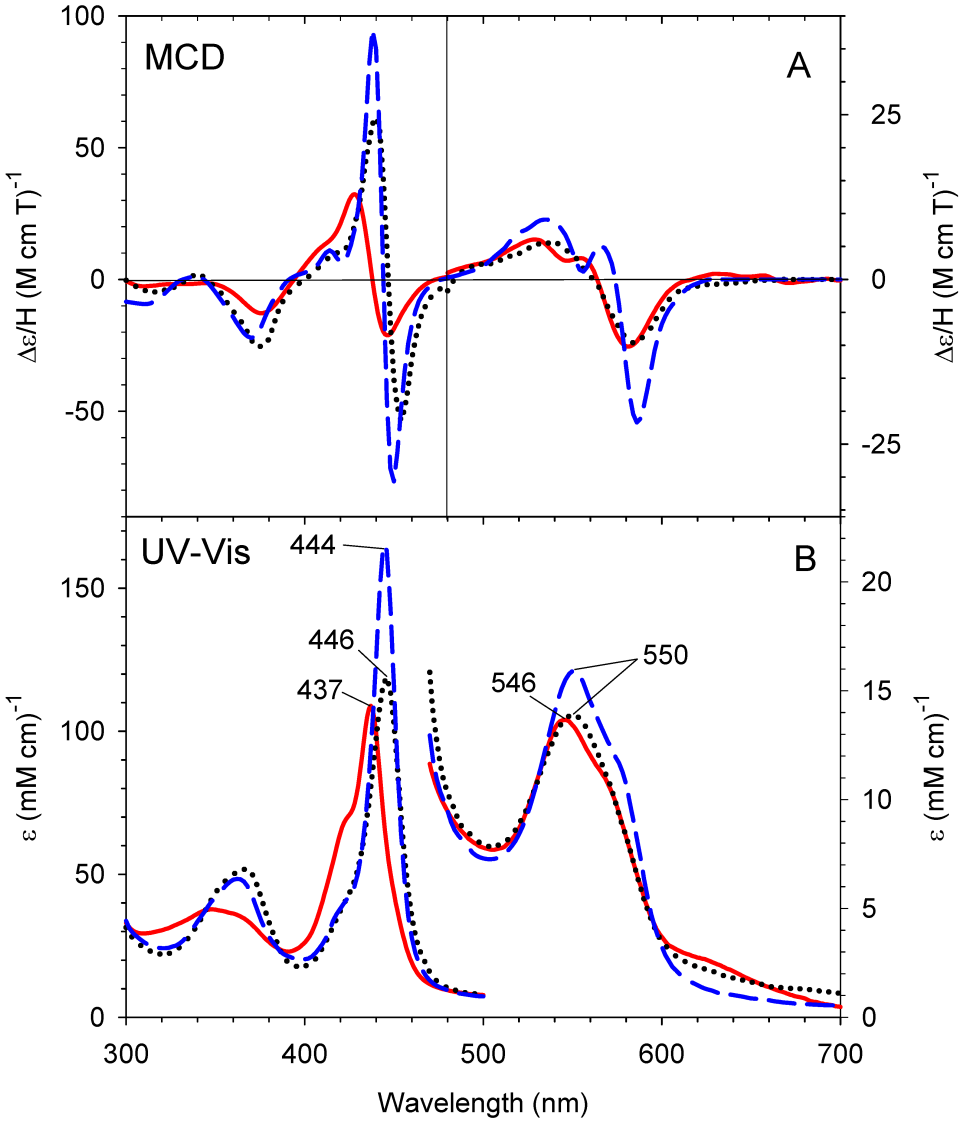


**Figure 5.6.** (Top) MCD and (bottom) UV-Vis absorption spectra of ferrous-CO H93G(THMP) Mb (solid line, 34 mM THMP), ferrous-CO P450-CAM (dashed line) in 0.1 M potassium phosphate buffer, pH = 7.0, at 4 °C and ferrous-CO CPO (dotted line) in 0.1 M potassium phosphate buffer, pH = 6.0, 4 °C. The spectra of ferrous-CO P450-CAM and CPO were replotted from Ref. [28].

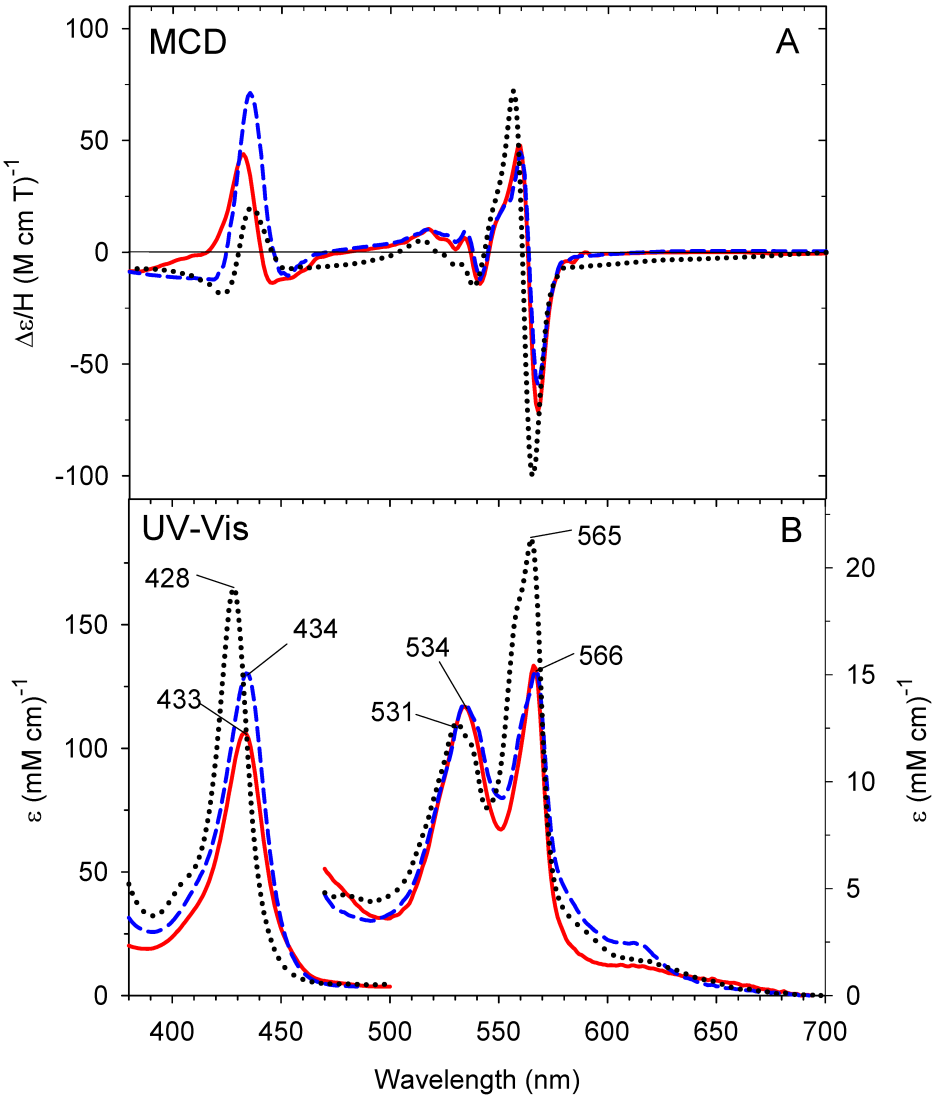


**Figure 5.7.** (Top) MCD and (bottom) UV-Vis absorption spectra of THMP/Im mixed ligand-bound H93G Mb (solid line, 50 mM THMP, 400 mM Im), THMP-bound ferrous sperm whale Mb (dashed line, 66 mM THMP) and bis-Im-bound ferrous H93G Mb (dotted line, 4 M Im) in 0.1M postassium phosphate buffer, pH 7.0. The spectra of the bis-Im-bound H93G Mb complex, recorded in this work, are essentially identical to those reported previously Ref. [12].

mono-THMP/mono-Im mixed ligand complex of ferrous H93G Mb (solid line) with those of THMP-bound ferrous sperm whale Mb (dashed line) that was prepared in this study. A close match of the spectra, especially in the visible region of the MCD spectra, supports the conclusion that both spcecies have the same coordination mode of the heme center.

Fig. 5.8 illustrates the MCD and UV-Vis spectra of the THMP-ligated oxyferrous H93G Mb (solind line) stabilized at -40 °C. Corresponding spectra of THT/$O_2$ complex of ferrous H93G Mb (dashed line), oxy-Mb (sperm whale, wild-type) (dotted line) and oxy-P450-CAM (dot-dashed line) that have previously been reported from our lab [10, 29] are overlaid for comparison. The oxyferrous H93G(THMP) Mb exhibits MCD and UV-Vis spectral features that are quite similar to those of wild-type oxyferrous Mb in both line shape and intensity, but not like those of oxy-P450-CAM, which shows relatively weak overall MCD band intensities and a single visible absorption peak (554 nm).

These results may be attributed to the difference in the nature of CO and $O_2$ ligands, the former of which is a much better pi-acceptor. The differences between these two ligands are not prominent for their complexes with the thiolate-ligated heme protein P450 (or CPO) and both the CO and $O_2$ complexes exhibit a hyperporphyrin spectrum [30,31]. On the other hand, their (CO and $O_2$) difference seems to be- come evident when a trans ligand is a phosphine in their heme adducts (this study).

*Phosphine-ligated ferryl H93G Mb.*

Fig. 5.9A demonstrates that incubation of the ferric H93G(mono-THMP) Mb (30 μM at pH 7, 4 °C with 2 equiv. of hydrogen peroxide caused the Soret peak to shift from

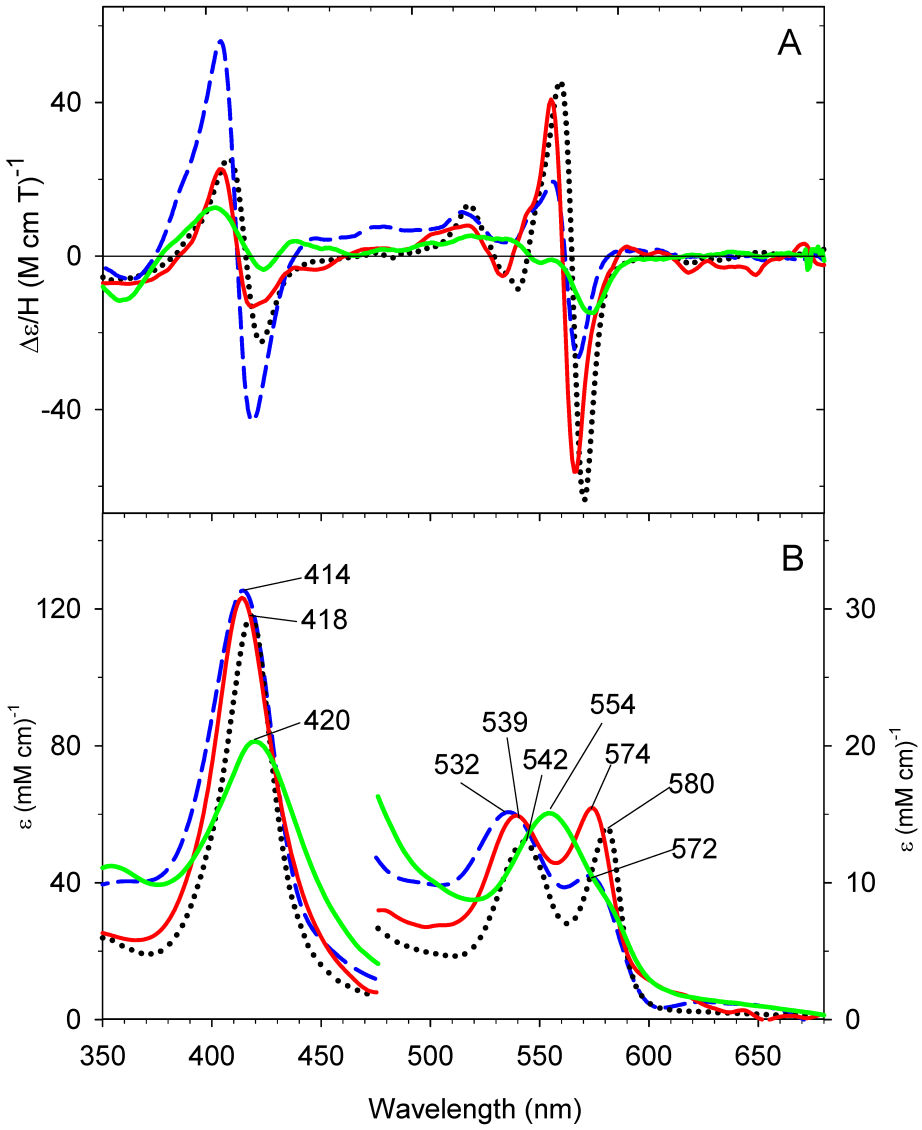


**Figure 5.8.** (Top) MCD and (bottom) UV-Vis absorption spectra of oxyferrous H93G(THMP) Mb (solid line, 0.5 mM THMP), oxyferrous H93G(THT) Mb (dashed line, 5 mM THT, replotted from [10]) at -40 $^{o}$C, oxyferrous wild-type Mb at -10 $^{o}$C (dotted line; replotted from [29]) and oxyferrous P450-CAM at -30 $^{o}$C (dash-dotted line; replotted from Ref. [29]).

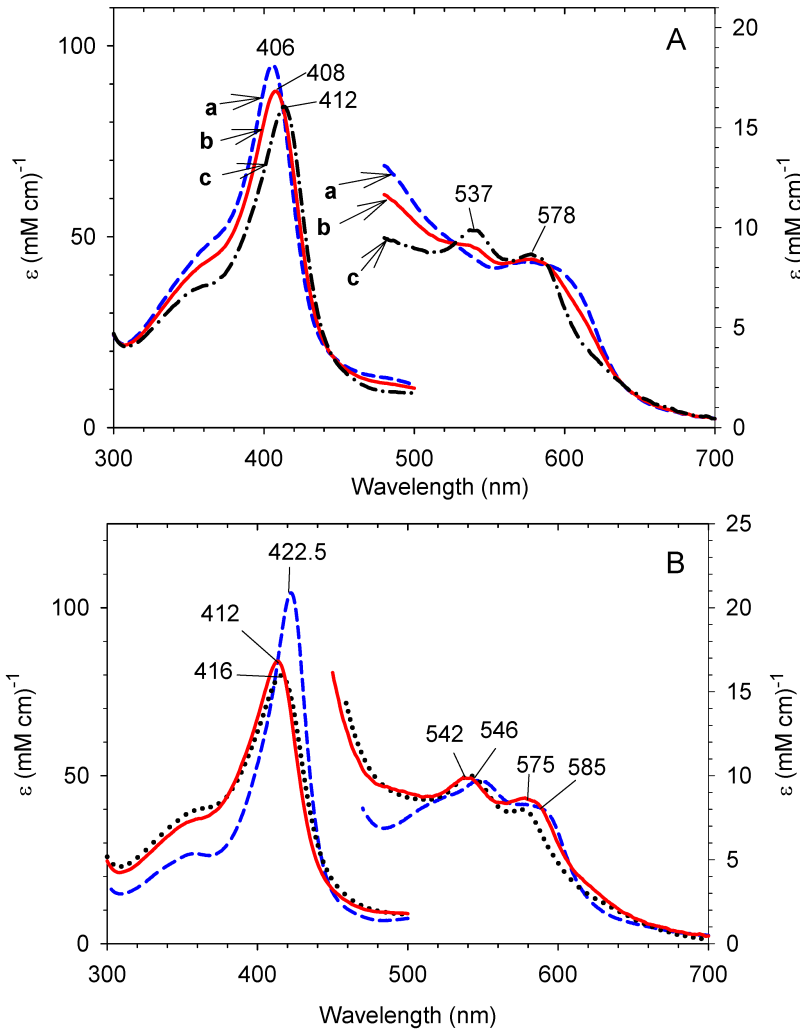


**Figure 5.9.** (Top) UV-Vis absorption spectra of ferric H93G(THMP) Mb (a) before (dashed line) and (b) after (solid line) addition of 36 μM $H_2O_2$ (recorded within 3 min after $H_2O_2$ addition) and (c) the extrapolated ferryl H93G(THMP) Mb spectrum (see text) (dash-dotted line) in 0.1M potassium phosphate buffer, pH 7.0, at 4 °C. The H93G Mb and THMP concentrations were 30 μM and 1.03 mM, respectively. (Bottom) UV-Vis absorption spectrum of the extrapolated ferryl THMP-bound H93G Mb (solid line) compared to the spectra of ferryl horse heart Mb (dashed line) and extrapolated ferryl THT-bound H93G Mb (dotted line). The spectra were recorded in 0.1 M potassium phosphate buffer at pH 7.0 at 4 °C. The spectrum of ferryl horse heart Mb was replotted from Ref. [32] and ferryl THT-bound H93G Mb from Ref. [22].

406 nm (spectrum a) to 408nm (spectrum b). The intensity of the charge transfer band at 603 for ferric H93G(THMP) Mb gradually decreases, while two new peaks at 537 and 578 nm appear. The spectral changes suggest that the ferric state is partially converted to a ferryl complex. However, unlike the case of mono-Im-bound ferric H93G Mb (see Fig. 5.3B, dot-dashed line) ([9] and this work), the 603 nm peak in the UV-Vis spectrum (spectrum a) did not completely disappear even after longer incubation time or treatment with higher concentration of $H_2O_2$. Given the expectation that the ferryl derivative would have no peak at 603 nm, it can be estimated that 40% of the ferric starting adduct converted to the ferryl derivative. Based on this estimation, the UV-Vis absorption spectrum of fully formed ferryl was calculated (Fig. 5.9A spectrum c). The extrapolated spectrum thus obtained has a Soret peak at 412 and two visible peaks at 537 and 578 nm. Compared to those of ferryl horse heart myoglobin and ferryl H93G(THT) Mb [22], the calculated spectrum of the ferryl H93G(THMP) Mb adduct shows quite similar band patterns (Fig. 5.9B) confirming that the extrapolation for the ferryl H93G(THMP) spectrum is reasonable. The lower intensity of the Soret absorption and the blue shift by 10 nm are likely due to the distinctions in the donor properties of the proximal axial ligands, phosphine vs. imidazole. The MCD spectrum for the ferryl complex of H93G(THMP) Mb is not available due to its relatively low stability at 4 °C presumably because the phosphine ligand in solution can serve as a reductant of the ferryl H93G Mb species. A phosphine-ligated ferryl heme complex has not been previously described.

*EPR characterization of mono- and bis-THMP-ligated ferric H93G Mb.*

Ferric H93G(-L) Mb exhibits two sets of broad rhombic high spin heme iron EPR signals at pH 7.5, 4.5 K [g-values: 6.32, ~5.65 and ~2.0 (1$^{st}$ set) and 6.08, ~5.85 and ~2.0

(2nd set)] (Fig. 5.10 a). This EPR spectral feature at pH 7.5 is similar to that at pH 10.0 for H93G(-L) Mb as examined in this study [g-values: ~6.56, ~5.42, 2.0 (1st set) and 6.15, 5.82, 2.0 (2nd set), spectrum not shown]. Similarly two sets of rhombic high spin EPR spectrum (6.89, 5.06, 1.92; 6.16, 5.84, ~2) have been observed for ferric heme complex of the H20A (His20Ala) mutant of HmuO (bacterial heme oxygenase) at 6 K and pH 10.0, where the heme has been shown to have a mono-hydroxide-ligated five-coordinate structure [33]. Upon addition of a low concentration (0.2 mM) of THMP to ferric H93G(-L) Mb at pH 7.5, much sharper and more intense high spin signals appeared (Fig. 5.10, b) that apparently consist of two sets of components, one of which is rhombic and has g-values (6.32, 5.65 and ~2.0) that are very similar to one of the two sets for the phosphine-free protein (Fig. 5.10, a). The other component showed a relatively small signal at g = 5.93. Further addition of THMP (total 10 mM) caused the rhombic signal (g = 6.32, 5.65) to diminish with the other signal (g = 5.93) intensity slightly increased (Fig. 5.10, c). Although formation of a low spin species is expected when 10 mM THMP is added to ferric H93G Mb (see Figs. 1b and 3), low spin EPR signals were only observed when temperature was raised to 15 K (Fig. 5.10, d) yielding a set of g-values at 2.97 and 2.26 (the third, smallest, g-value was not detectable). These values were similar to the corresponding low spin g-values of 3.05 and 2.22 of imidazole-bound ferric dehaloperoxidase from *Amphitrite ornata* [34, 35], a His-ligated heme protein, that was examined in the same series of experiments in this work.

To further analyze the two sets of the high spin signals (Fig. 5.10, b and c), attempts were made to deconvolute the overlapping spectra into two-component spectra. Somewhat unexpectedly, the rhombic signal was separated from the other one by simply

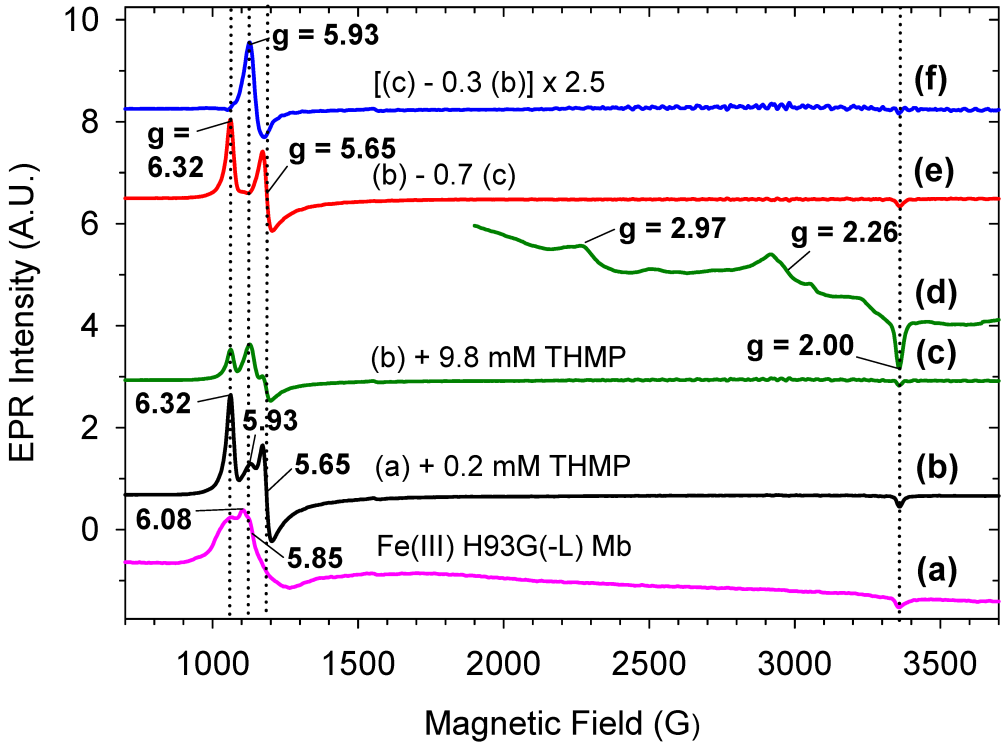


**Figure 5.10.** EPR spectra of Fe(III) H93G(-L) Mb (a), + 0.2 mM THMP (b), + 10 mM THMP (c and d) at 4.5 K (a – c) and 15 K (d). Spectra (e) and (f) are isolated (deconvolved) rhombic (e) and axial (f) high spin heme components of mono- (e) and bis-THMP-bound (f) Protein. The Y-axis positions for spectra a – f are arbitrarily offset for clarity. The relative signal intensities for b and c are proportional to their actual magnitudes, but the intensity for a has been enlarged by 7.5 times. See text for further descriptions.

subtracting 70% of spectrum (c) from spectrum (b) to generate spectrum (e) (Fig. 5.10e, dashed line). Conversely, the second signal was isolated by subtracting 30% of spectrum (b) from spectrum (c) (Fig. 5.10 f, dot-dashed line). These results demonstrate that the first set of signals decreased by a factor of ~3.3 (100/30), i.e., by ~ 70%, while the second set increased by ~1.4-fold (100/70) upon the increase in THMP concentration. Thus, the two sets of signals seen in spectrum (b) arise from two separate high spin heme species. The data also reveal that the g = 5.93 signal belongs to a high spin heme iron with axial symmetry (f). The rhombic heme may be assigned to the mono-THMP-bound (five-coordinate) H93G Mb. In an analogous case, mono-Met-ligated heme in the ferric H229A HtsA (a heme carrier protein) has been shown to contain a five-coordinate heme (based on resonance Raman evidence) and to exhibit a rhombic (along with an axial) high spin EPR spectrum [24]. Furthermore, the bis-Met-ligated low spin-type heme in R98C/H102M cytochrome *b*562 at pH 4.8 has exhibited a minor but sharp axial high spin signal (g = 5.9) together with the main low spin signal (g = 3.16, ~2.25) [25]. The authors attributed this signal (g = 5.9) to a probable artifact of freezing. The same explanation may be applicable to the present result with bis-THMP-ligated H93G Mb (Fig. 5.10, b and c). In fact the increase in the intensity of the g = 5.93 signal (by ~1.4 times) is significantly less than expected (~3.3-fold) if it is assigned as a high spin component of the bis-THMP adduct formation. Nevertheless, the likelihood that the g = 5.93 signal originated from the bis-THMP ligated H93G Mb heme cannot be totally dismissed. The presence of a small shoulder at ~615 nm in the UV-Vis absorption spectrum of this complex at 4 °C may suggest that it is not completely low spin. In summary, in this study we have obtained the rhombic EPR spectra of both high spin

mono-THMP-ligated and low spin bis-THMP-ligated ferric H93G Mb. To our knowledge, this represents the first EPR characterization of high and low spin ferric heme protein derivatives exclusively ligated by phosphines.

## CONCLUSIONS

Over the past four decades, numerous heme iron model complexes has been prepared and characterized in an effort to develop a better understanding of the mechanism of action of native heme-containing enzymes. A large variety of ligands have been investigated to generate complexes that mimic the active site of native hemoproteins [7-13]. However, phosphines, although used as probe ligands, have never been studied as proximal heme iron ligands. Phosphines bind to the distal binding site of heme proteins to yield mixed-ligand complexes that display characteristic spectroscopic features [30]. In this paper, a novel heme complex with phosphine as a proximal ligand has been generated and spectroscopically characterized. The generation and characterization of a large set of heme-phosphine complexes substantially expands the spectral database of heme coordination structures.

As shown in Scheme 1, ferric and ferrous mono- (e and c) and bis-phosphine ligated H93G Mb complexes (d and g) have been prepared by THMP titration of exogenous ligand-free H93G Mb (a and b). The ferric H93G(THMP) Mb adduct is assigned to be a five-coordinate species by analogy to the mono-Met-ligated H229A mutant of the HtsA heme carrier protein (whose wild-type counterpart has a His/Met-ligated six-coordinate structure heme) [24] as well as mono-THT adduct of H93G Mb [22] [footnote 1]. The lack of a distal side water axial ligand in the mono THMP- and THT-ligated ferric H93G Mb

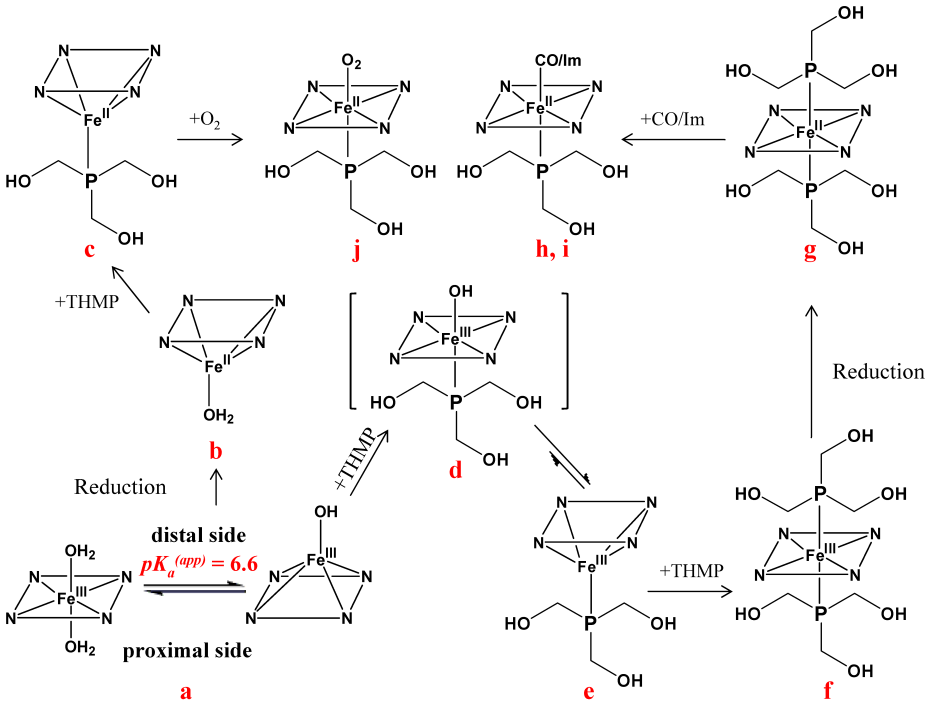


**Scheme 5.1.** Mono- and bis-THMP-ligated ferric and ferrous H93G Mb generated and examined in this work. Species d was not isolated but is proposed as an intermediate in the formation of e upon binding of mono-THMP to a, where a and e may be in equilibrium with e being a predominant species.

adducts, in contrast to the mono-Im/$H_2O$ six-coordinate complex [6, 9], is most likely due to non-optimal (too long) distances between the heme iron and the distal histidine (His-64) in the former two H93G Mbs. Proper distance are required for the distal His to form a hydrogen bond to hem iron-ligated water and thus to form a water-bound six-coordinate ferric heme complexes (for example, Mb (six-coordinate) vs. HRP (five-coordinate)). The ferric bis-THMP adduct exhibits spectral features similar to those of H93G Mb ligated with two identical neutral ligands such as bis-Im and bis-THT. The ferrous H93G(THMP) Mb has spectra that are nearly identical to those of ferrous H93G(Im) Mb.

Interestingly, the UV-Vis and MCD spectra of six-coordinate ferrous phosphine bound H93G Mb show similarities to those of corresponding P450-CAM and CPO derivatives: *i.e.,* ferrous H93G(bis-THMP) Mb is spectrally similar to ferrous phosphine-ligated P450-CAM and corresponding CPO while ferrous CO-H93G(THMP) (h) spectrally resembles ferrous CO-P450-CAM and ferrous CO-CPO. To our knowledge, this is the first reported non-thiolate-ligated heme model that exhibits spectral features comparable to those of thiolate-ligated hemoprotein complexes in the ferrous state. Since these unique spectral features were seen Cys/phosphine and Cys/CO complexes [27], but not for the Im/THMP (i) and Im (His)/CO adducts (e.g., ferrous-CO H93G(Im) Mb [6, 9]), such spectral uniqueness of the bis-THMP (g) and THMP/CO (h) derivatives of ferrous H93G Mb might be attributed to the difference(s) between these bases, Cys and THMP (alkylphosphine)] vs. Im as donor ligands. A most likely factor to explain such differences would be the much better nucleophilic (i.e., sigma-donor) nature of Cys thiolate and phosphines (phosphorous analog of amines) compared with Im (or amines).

Furthermore, a phosphine/Im mixed-ligand-bound H93G Mb adduct (i) that has been generated and spectroscopically characterized serves as a model of phosphine-bound sperm whale Mb. Ferryl H93G(THMP) Mb can be partially formed as previously reported for ferryl H93G (thioether, THT) Mb and their calculated UV-Vis spectra for homogenous ferryl species are quite similar. This is the first detailed study of the H93G Mb cavity mutant with phosphine as the axial ligand including the new ferrous-CO and ferrous-$O_2$ adducts and the results again demonstrate the capacity of the H93G Mb to serve as an extremely versatile scaffold for the preparation of a wide variety of heme coordination structures.

**ACKNOWLEDGEMENTS**

We thank Professors Steven G. Boxer for the H93G expression system, Michael T. Green for helpful discussions and Thomas Makris for assistance with the EPR measurements. This work was supported by the National Institutes of Health (GM 26730) and Research Corp. (to J.H.D.).

Footnote [1]: In a previous study on THT binding to ferric H93G(-L) Mb, we speculated that the mono-THT-bound protein is a six-coordinate species with THT and hydroxide as axial ligands [22]. However, since publication of that paper, we have become aware that an analogous mono-Met-ligated heme protein, H229A HtsA, with UV-Vis absorption and MCD spectra essentially identical to those of H93G(THT) Mb had been definitively characterized as a five-coordinate heme species using resonance Raman spectroscopy [24]. Thus, we now believe that the mono-THT-H93G Mb adduct also has a five-coordinate heme.

**REFERENCES**


[1] J.H. Dawson, Science, 240, 1988, 433-439.

[2] T.L. Poulos, J. Biol. Inorg. Chem. 1, 1996, 356-359.

[3] M. Perutz, H. Muirhead, J. Cox, L. Goaman, F. Mathews, E. McGandy, L. Webb, Nature, 219, 1968, 29-32.

[4] H.B. Dunford, Heme Peroxidase, Wiley-VCH, John Wiley and Sons, New York, 1999.

[5] P.R. Ortiz de Montellano (Ed.), Cytochrome P-450 Structure, Mechanism, and Biochemistry, Plenum Press, New York. 1986.

[6] D. Barrick, Biochemistry, 33, 1994, 6546-6554.

[7] J.H. Dawson, A.E. Pond, M.P. Roach, Biopolymers, 67, 2002, 200-206.

[8] M.P. Roach, A.E. Pond, M.R. Thomas, S.G. Boxer, J.H. Dawson, J. Am. Chem. Soc. 121, 1999, 12088-12093.

[9] A.E. Pond, M.P. Roach, M.R. Thomas, S.G. Boxer, J.H. Dawson, Inorg. Chem. 39, 2000, 6061-6066.

[10] R. Perera, M. Sono, J.A. Sigman, T.D. Pfister, Y. Lu, J.H. Dawson, Proc. Natl. Acad. Sci. USA. 100, 2003, 3641-3646.

[11] J. Qin, R. Perera, L.L. Lovelace, J.H. Dawson, L. Lebioda, Biochemistry, 45, 2006, 3170-3177.

[12] J. Du, M. Sono, J.H. Dawson, Spectroscopy, 22, 2008, 123-141.

[13] J. Du, M. Sono, J.H. Dawson, Coord. Chem. Rev. 255, 2011, 700-716.

[14] G. Simonneaux, Coord. Chem. Rev. 165, 1997, 447-474.

[15] A. Bondon, P. Petrinko, P. Sodano, G. Simonneaux, Biochim. Biophys. Acta. 872, 1986, 163-166.

[16] M. Sono, J.H. Dawson, L.P. Hager, Inorg. Chem. 24, 1985, 4339-4343.

[17] N. Legrand, A. Bondon, G. Simonneaux, Inorg. Chem. 35, 1996, 1627-1631.

[18] G. Simonneaux, A. Bondon, P. Sodano, Biochim. Biophys. Acta. 1038, 1990, 199-203.

[19] C. Brunel, A. Bondon, G. Simonneaux, Eur. J. Biochem. 214, 2005, 405-414.

[20] M. Sono, J. Dawson, L. Hager, J. Biol. Chem. 259, 1984, 13209-13216.

[21] K. Paul, H. Theorell, A. Akeson, Acta Chem. Scand, 7, 1953. 1284-1287.

[22] J. Du, M. Sono, J.H. Dawson, J. Porph. Phthal. 15, 2011, 29-38.

[23] A.E. Pond, M.P. Roach, M. Sono, A.H. Rux, S. Franzen, R. Hu, M.R. Thomas, A. Wilks, Y. Dou, M. Ikeda-Saito, Biochemistry, 38, 1999, 7601-7608.

[24] Y. Ran, M. Liu, H. Zhu, T.K. Nygaard, D.E. Brown, M. Fabian, D.M. Dooley, B. Lei, Biochemistry 49 (2010) 2834–2842.

[25] P.D. Barker, E.P. Nerou, M.R. Cheesman, A.J. Thomson, P. de Oliveira, H.A.O. Hill, Biochemistry 35 (1996) 13618–13626.

[26] M.P. Roach, Y.P. Chen, S.A. Woodin, D.E. Lincoln, C.R. Lovell, J.H. Dawson, Biochemistry 36 (1997) 2197–2202.

[27] J.H. Dawson, M. Sono, Chem. Rev. 87 (1987) 1255–1276.

[28] M. Sono, D.J. Stuehr, M. Ikeda-Saito, J.H. Dawson, J. Biol. Chem. 270 (1995) 19943–19948.

[29] M. Sono, K.S. Eble, J.H. Dawson, L.P. Hager, J. Biol. Chem. 260 (1985) 15530–15535.

[30] L.K. Hanson, S.G. Sligar, I.C. Gunsalus, Croat. Chem. Acta 49 (1977) 237–250.

[31] A. Waleh, J.R. Collins, G.H. Loew, M.C. Zemer, Int. J. Quant. Chem. 24 (1986) 1575–1589.

[32] E.D. Coulter, J. Cheek, A.P. Ledbetter, C.K. Chang, J.H. Dawson, Biochem. Biophys. Res. Commun. 279 (2000) 1011–1015.

[33] G.C. Chu, T. Yoshida, D.L. Rousseau, M. Ikeda-Saito, J. Am. Chem. Soc. 122 (2000)12612–12613.

[34] S. Franzen, M.K. Thompson, R.A. Ghiladi, Biochim. Biophys. Acta 2012 (1814) 578–588.

[35] F.P. Nicoletti, M.K. Thompson, B.D. Howes, S. Franzen, G. Smulevich, Biochemistry 49 (2010) 1903–1912.

**SUPPORTING INFORMATION**

**Figure 5.11.** Difference spectra of the THMP titrations of ferric H93G Mb. Insets show the hyperbolic regression fit (solid line) of saturation plots (closed circles) for THMP binding to (top) exogenous-free ferric H93G Mb and (bottom) mono-THMP-bound H93G Mb. Absorbance changes from the peak to trough in difference spectra ($\Delta\Delta A_{437\text{-}406}$ = $\Delta A_{437}$- $\Delta A_{406}$ , $\Delta\Delta A_{432\text{-}424}$ = $\Delta A_{432}$ - $\Delta A_{414}$) are plotted as a function of total THMP concentration.

**Figure 5.12.** UV-Vis spectral change on the titration of exogenous ligand free ferrous H93G Mb (3 μM in a 1 cm cuvette) with THMP in 0.1 M potassium phosphate buffer, pH 7.0, at 4°C. Vertical arrows indicate the directions of absorbance change upon addition of 0.78, 1.57, 3.92, 7.84, 15.69, 31.37 μM THMP. Hyperbolic saturation plot (solid circle) and its regression fit (solid line) of the titration data is shown in the inset where absorbance change at 429 nm is plotted as function of free (= total minus protein-bound) THMP concentration (0.39, 0.78, 1.73, 5.14, 12.82, 28.45 μM, respectively).

**Figure 5.13.** UV-Vis spectra change on the titration of bis-THMP-bound ferrous H93G Mb (50 mM THMP) with Im in 0.1 M potassium phosphate buffer, pH 7.0, at 4 °C. Vertical arrows indicate the directions of absorbance change upon addition of 2.25, 11.21, 22.30, 44.10, 86.30, 165.46 mM Im. Hyperbolic saturation plot (solid circle) and its regression fit (solid line) of the titration data are shown in the inset, where the peak-to-trough absorbance change in difference spectra (not shown) ($\Delta\Delta A_{433\text{-}454}$ = $\Delta A_{433}$ - $\Delta A_{454}$ ) is plotted as function of total Im concentration.

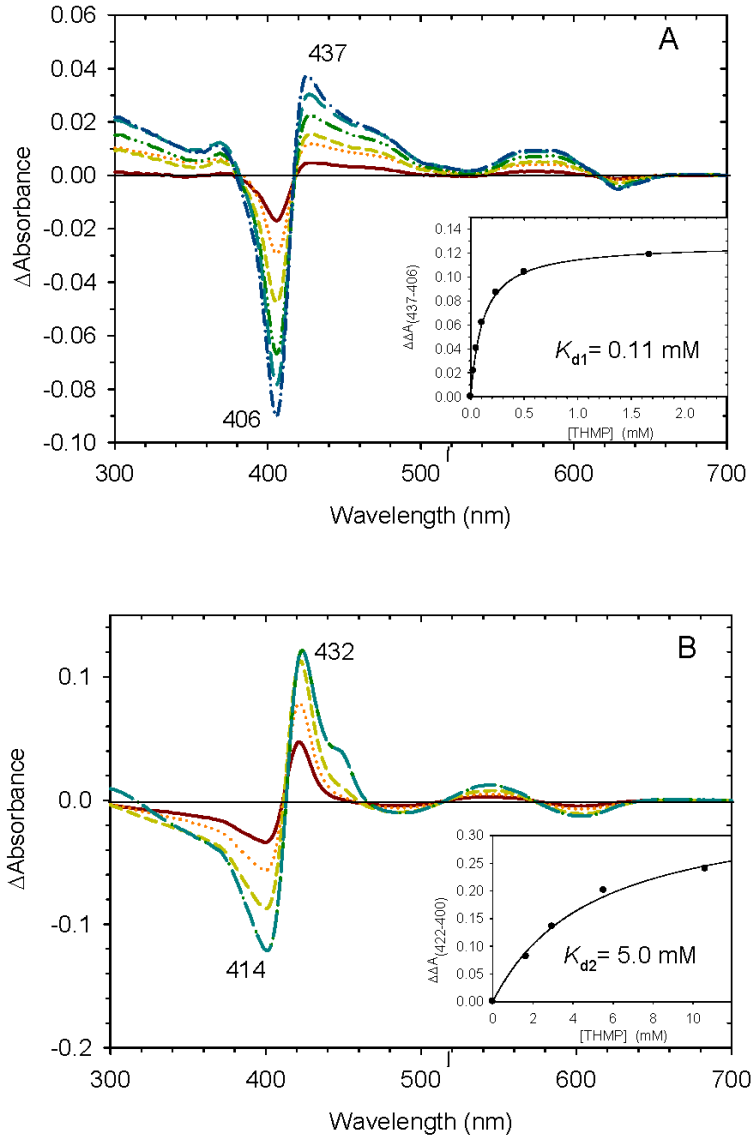


**Figure 5.11**

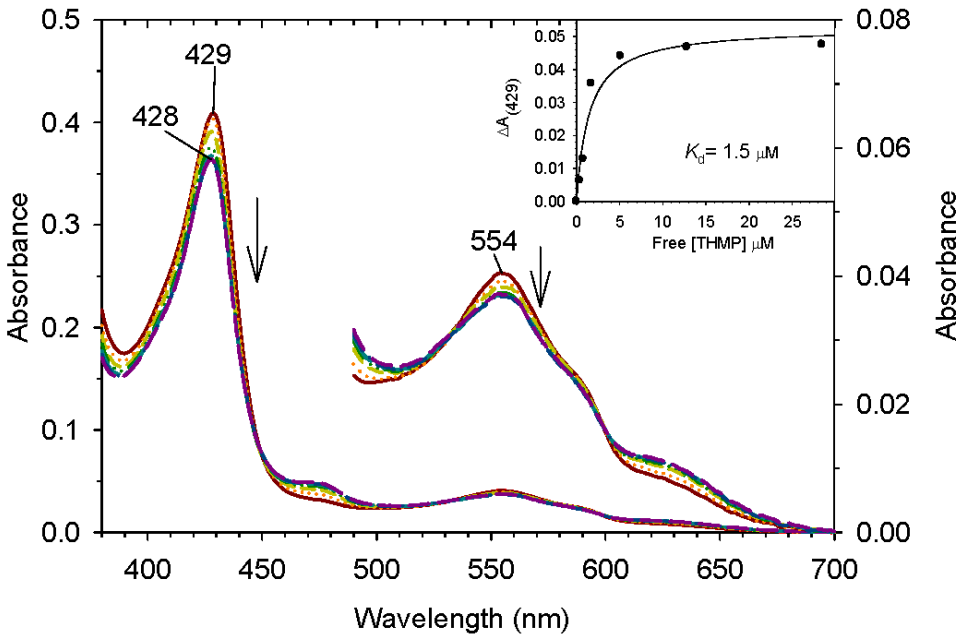


**Figure 5.12**

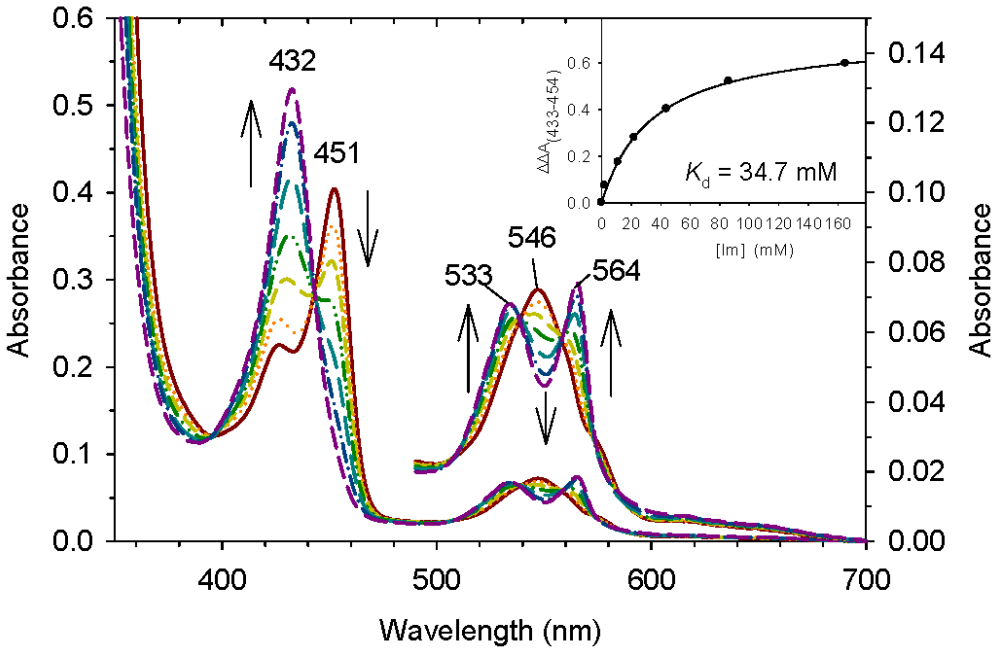


**Figure 5.13**

# APPENDIX A: COPYRIGHT PERMISSION

## COPYRIGHT PERMISSION FOR CHAPTER 2

This is a License Agreement between Shengfang Sun ("You") and Elsevier ("Elsevier") provided by Copyright Clearance Center ("CCC"). The license consists of your order details, the terms and conditions provided by Elsevier, and the payment terms and conditions.

**All payments must be made in full to CCC. For payment instructions, please see information listed at the bottom of this form.**

| | |
|---|---|
| Supplier | Elsevier Limited<br>The Boulevard,Langford Lane<br>Kidlington,Oxford,OX5 1GB,UK |
| Registered Company Number | 1982084 |
| Customer name | Shengfang Sun |
| Customer address | 631 Sumter St<br>COLUMBIA, SC 29201 |
| License number | 3406200646820 |
| License date | Jun 11, 2014 |
| Licensed content publisher | Elsevier |
| Licensed content publication | Archives of Biochemistry and Biophysics |
| Licensed content title | Influence of heme environment structure on dioxygen affinity for the dual function*Amphitrite ornata*hemoglobin/dehaloperoxidase. Insights into the evolutional structure–function adaptations |
| Licensed content author | Shengfang Sun,Masanori Sono,Chunxue Wang,Jing Du,Lukasz Lebioda,John H. Dawson |
| Licensed content date | 1 March 2014 |
| Licensed content volume number | 545 |
| Licensed content issue number | None |
| Number of pages | 8 |
| Start Page | 108 |
| End Page | 115 |
| Type of Use | reuse in a thesis/dissertation |
| Intended publisher of new work | other |
| Portion | full article |
| Format | electronic |
| Are you the author of this Elsevier article? | Yes |
| Will you be translating? | No |
| Title of your thesis/dissertation | INSIGHTS INTO THE EVOLUTIONAL ADAPTATIONS AND FUNCTIONAL SWITCHING MECHANISM IN DUAL FUNCTION HEMOGLOBIN/DEHALOPEROXIDASE (DHP) AND MODELING OF CYTOCHROME P450 ACTIVE SITE WITH H93G MYOGLOBIN CAVITY MUTANT |
| Expected completion date | Jul 2014 |
| Estimated size (number of pages) | 160 |
| Elsevier VAT number | GB 494 6272 12 |

# COPYRIGHT PERMISSION FOR CHAPTER 5

This is a License Agreement between Shengfang Sun ("You") and Elsevier ("Elsevier") provided by Copyright Clearance Center ("CCC"). The license consists of your order details, the terms and conditions provided by Elsevier, and the payment terms and conditions.

**All payments must be made in full to CCC. For payment instructions, please see information listed at the bottom of this form.**

| | |
|---|---|
| Supplier | Elsevier Limited<br>The Boulevard,Langford Lane<br>Kidlington,Oxford,OX5 1GB,UK |
| Registered Company Number | 1982084 |
| Customer name | Shengfang Sun |
| Customer address | 631 Sumter St<br>COLUMBIA, SC 29201 |
| License number | 3406200390415 |
| License date | Jun 11, 2014 |
| Licensed content publisher | Elsevier |
| Licensed content publication | Journal of Inorganic Biochemistry |
| Licensed content title | Mono- and bis-phosphine-ligated H93G myoglobin: Spectral models for ferrous-phosphine and ferrous-CO cytochrome P450 |
| Licensed content author | Shengfang Sun,Masanori Sono,John H. Dawson |
| Licensed content date | October 2013 |
| Licensed content volume number | 127 |
| Licensed content issue number | None |
| Number of pages | 8 |
| Start Page | 238 |
| End Page | 245 |
| Type of Use | reuse in a thesis/dissertation |
| Portion | full article |
| Format | electronic |
| Are you the author of this Elsevier article? | Yes |
| Will you be translating? | No |
| Title of your thesis/dissertation | INSIGHTS INTO THE EVOLUTIONAL ADAPTATIONS AND FUNCTIONAL SWITCHING MECHANISM IN DUAL FUNCTION HEMOGLOBIN/DEHALOPEROXIDASE (DHP) AND MODELING OF CYTOCHROME P450 ACTIVE SITE WITH H93G MYOGLOBIN CAVITY MUTANT |
| Expected completion date | Jul 2014 |
| Estimated size (number of pages) | 160 |
| Elsevier VAT number | GB 494 6272 12 |